National Library of Canada
Canadian Theses Service
Ottawa, Canada
K1A 0N4

Bibliothèque nationale du Canada
Services des thèses canadiennes

CANADIAN THESES

THÈSES CANADIENNES

NOTICE

The quality of this microfiche is heavily dependent upon the quality of the original thesis submitted for microfilming. Every effort has been made to ensure the highest quality of reproduction possible.

If pages are missing, contact the university which granted the degree.

Some pages may have indistinct print especially if the original pages were typed with a poor typewriter ribbon or if the university sent us an inferior photocopy.

Previously copyrighted materials (journal articles, published tests, etc.) are not filmed.

Reproduction in full or in part of this film is governed by the Canadian Copyright Act, R.S.C. 1970, c. C-30.

AVIS

La qualité de cette microfiche dépend grandement de la qualité de la thèse soumise au microfilmage. Nous avons tout fait pour assurer une qualité supérieure de reproduction.

S'il manque des pages, veuillez communiquer avec l'université qui a conféré le grade.

La qualité d'impression de certaines pages peut laisser à désirer, surtout si les pages originales ont été dactylographiées à l'aide d'un ruban usé ou si l'université nous a fait parvenir une photocopie de qualité inférieure.

Les documents qui font déjà l'objet d'un droit d'auteur (articles de revue, examens publiés, etc.) ne sont pas microfilmés.

La reproduction, même partielle, de ce microfilm est soumise à la Loi canadienne sur le droit d'auteur, SRC/1970, c. C-30.

THIS DISSERTATION
HAS BEEN MICROFILMED
EXACTLY AS RECEIVED

LA THÈSE A ÉTÉ
MICROFILMÉE TELLE QUE
NOUS L'AVONS REÇUE

Canada

NL-339 (r. 86/06)

THE UNIVERSITY OF ALBERTA

Characteristics of Pi 2 Type Geomagnetic Pulsations

by

B.G.R. Harrold

A THESIS

SUBMITTED TO THE FACULTY OF GRADUATE STUDIES AND RESEARCH

IN PARTIAL FULFILMENT OF THE REQUIREMENTS FOR THE DEGREE

OF Master of Science

Department of Physics

EDMONTON, ALBERTA

Spring, 1986

Permission has been granted to the National Library of Canada to microfilm this thesis and to lend or sell copies of the film.

The author (copyright owner) has reserved other publication rights, and neither the thesis nor extensive extracts from it may be printed or otherwise reproduced without his/her written permission.

L'autorisation a été accordée à la Bibliothèque nationale du Canada de microfilmer cette thèse et de prêter ou de vendre des exemplaires du film.

L'auteur (titulaire du droit d'auteur) se réserve les autres droits de publication; ni la thèse ni de longs extraits de celle-ci ne doivent être imprimés ou autrement reproduits sans son autorisation écrite.

ISBN 0-315-30221-6

American Geophysical Union
2000 Florida Avenue, N.W
Washington, D. C. 20009
Phone (202) 462-6903
TWX 710-822-9300

February 20, 1986

AGU Policy on Reproduction of Copyright Materials

AGU no longer requires that permission be obtained from AGU or the author(s) for the use of tables, figures, or short extracts of papers published in AGU journals or books, provided the source is appropriately cited for publication in scientific books and journals.

We recommend that the credit line read "authors, journal or book title, volume number, page number(s), year, copyright by the American Geophysical Union."

AGU Publications

DB:lh
Encl.

The American Geophysical Union encompasses the earth and space sciences
Geodesy, Seismology, Meteorology, Geomagnetism and Paleomagnetism
Oceanography, Hydrology, Volcanology, Geochemistry, and Petrology
Tectonophysics, Planetology, Solar-Planetary Relationships

Feb. 12, 1986

Journal of Geophysical Research
Space Physics
American Geophysical Union
2000 Florida Avenue, N.W.
Washington, D.C. 20009

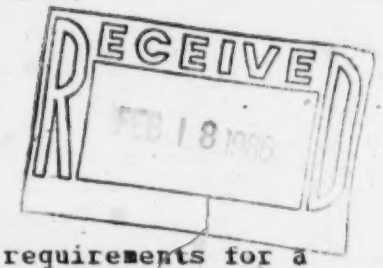

Dear Sir,

I am presently completing the requirements for a Master of Science degree through the University of Alberta (located in Edmonton, Alberta, Canada). In my thesis I would like to use several diagrams for which your journal holds the copyright. The purpose of this letter is to seek your permission to use these diagrams in my thesis. The diagrams in question are:
from:

Figure 1 from: Eastman, T.E., L.A. Frank, W.K. Lennartsson, The plasma sheet boundary layer, J. Geophys. Res., vol 89, p.1553, 1984.

Figures 8 and 9 from: McPherron, R.L., C.T. Russell, M.P. Aubry, Satelite studies of magnetospheric substorms on August 15, 1968, 9, Phenomenological model for substorms, J. Geophys. Res., vol 78, p. 3131, 1973.

Figures 3 and 5 from: Lester, M., W.J. Hughes, H.J. Singer, Polarization patterns of Pi 2 magnetic pulsations and the substorm current wedge, J. Geophys. Res., vol 88, p. 7958, 1983.

Figures 6 and 7 from: Samson, J.C., B.G. Harrold, Maps of the polarization characteristics of high latitude Pi 2's, J. Geophys. Res., vol 88, p. 5736, 1983.

Figure 4b from: Goertz, C.K., R.W. Boswell, Magnetosphere-ionosphere coupling, J. Geophys. Res., vol 84, p.7239, 1979.

Figures 1,2,3,4,5,6,8,9 from: Samson, J.C., B.G. Harrold, Characteristic time constants and velocities of high latitude Pi 2 s, J. Geophys. Res., vol 90, p. 12173, 1985.

I am seeking permission to use these figures in the following manner. The Public Archives division of the Government of Canada will microfilm my thesis (including

the aforementioned figures if you so consent) for the purpose of providing paper copies to individuals who request them (to a maximum of five copies per individual and under the condition that they not be used for commercial purposes).

As I am presently attending the University of Iowa, correspondence on this matter should be sent to:

Barry Harrold
c/o The Department of Physics and Astronomy
Van Allen Hall
The University of Iowa
Iowa City, Iowa 52242

Sincerely,

Barry Harrold

Barry Harrold

THE UNIVERSITY OF ALBERTA

RELEASE FORM

NAME OF AUTHOR — B.G.R. Harrold

TITLE OF THESIS Characteristics of Pi 2 Type Geomagnetic Pulsations

DEGREE FOR WHICH THESIS WAS PRESENTED Master of Science

YEAR THIS DEGREE GRANTED Spring, 1986

Permission is hereby granted to THE UNIVERSITY OF ALBERTA LIBRARY to reproduce single copies of this thesis and to lend or sell such copies for private, scholarly or scientific research purposes only.

The author reserves other publication rights, and neither the thesis nor extensive extracts from it may be printed or otherwise reproduced without the author's written permission.

(SIGNED) Barry Harrold

PERMANENT ADDRESS:

Box 538

Lamont, Alberta

T0B 2R0

DATED January 10, 1986

THE UNIVERSITY OF ALBERTA

FACULTY OF GRADUATE STUDIES AND RESEARCH

The undersigned certify that they have read, and recommend to the Faculty of Graduate Studies and Research, for acceptance, a thesis entitled Characteristics of Pi 2 Type Geomagnetic Pulsations submitted by B.G.R. Harrold in partial fulfilment of the requirements for the degree of Master of Science in Physics.

.....
Supervisor

.....

.....

.....

.....

Date..January..7,.1986.....

Abstract

The polarization and propagation characteristics of Pi 2 type geomagnetic pulsations are analyzed and compared to the predictions of existing theories. The observations at high latitude indicate a westward phase propagation of the Pi 2 waveform west of the center of the substorm current wedge and eastward phase propagation east of center. Measurement of the group velocity of the Pi 2 wave packet shows a similar pattern. The typical pulsation rise time observed at high latitudes is found to be comparable to that seen at mid-latitudes. Pulsation frequency shows a slight inverse variation with latitude near the substorm enhanced electrojet. The latitudinal dependence of Pi 2 power is examined using data from Samson and Harrold (1983). The high latitude horizontal polarization ellipse pattern found by Samson and Harrold (1983) is interpreted in light of the phase propagation measurements and the observed spatial distribution of Pi 2 power. It is shown that the phase propagation, power, and polarization ellipse patterns are consistent with an electric field of the form $\underline{E}(\underline{r},t) = (E_x(x),E_y(x),0)\exp(i(\lambda y+kz-\omega t))$.

Acknowledgements

I wish to thank Dr. J.C. Samson for his thought provoking comments and helpful suggestions on many aspects of this thesis. I also thank Professor G. Rostoker for his timely and insightful comments on plasma theory. Throughout most of this research, I have received financial support in the form of a Graduate Scholarship from the Natural Sciences and Engineering Research Council of Canada.

Table of Contents

Chapter	Page
I. Introduction	1
A. The Substorm	3
B. Pi2 Pulsations	5
C. The Transient Response Model	11
D. Resonant Field Line Model	18
E. Objectives	22
II. Method of Analysis	25
A. Background	25
B. Coordinate Systems	27
C. Selection Criteria	28
D. Time Series Analysis	33
III. Discussion of Results	44
A. Analysis of Day 281, 1978	45
B. Phase Delay	61
C. Envelope Parameters	70
D. Group Delay	73
E. Frequency	77
F. Power	85
G. Polarization Characteristics	90
H. Miscellaneous Interpretations	98
IV. Conclusions	101
V. Bibliography	103
VI. Appendix A	111

List of Tables

Table	Description	Page
1	Station Coordinates	29
2	Results of Analysis of Day 281, 1978	61
3	Events used in Phase study	62
4	Events used in Frequency study	79

List of Illustrations

Figure	Description	Page
1	Structure of the Magnetosphere. From Eastman et al., 1984.	2
2a	Substorm current system. From McPherron et al., 1973.	4
2b	Magnetic field perturbations observed on the ground due to the substorm current wedge. From McPherron et al., 1973.	4
3	Pi 2 pulsation in the interval 0555-0610 UT on March 14, 1978. The polarization ellipses are generated by plotting the H component verses the D component at successive time steps. The ellipticity is defined as the ratio of the minor axis to the major axis. The azimuth is defined as the orientation of the major axis. When no arrow is present the ellipticity is essentially linear. The azimuthal angles of these ellipses compare favourably with the model shown in Figure 2c. From Lester et al., 1983.	7
4	Observed ellipticity of the horizontal polarization ellipse at high latitude. Positive (negative) values correspond to counterclockwise (clockwise) polarization. Coordinates are relative to the latitude of the westward electrojet and the longitude of its center. From Samson and Harrold, 1983.	8
5	Observed azimuths of the horizontal polarization ellipse at high latitude. From Samson and Harrold, 1983.	8
6	Idealized magnetosphere for a uniform field. To connect with the actual quasi-dipolar field, in the tail of the magnetosphere, y points to the east, x points away from the earth. At the surface of the earth at high latitudes, z points into the earth and x points northward.	10
7a	A series of snapshots displaying the electric fields at different times. The dashed lines indicate 'equipotential'	

	contours. In the wave front $\nabla \times \underline{E}$ is not zero, and the magnetic field changes with time. For a low β plasma ($\beta = 8\pi nkT/B^2$). From Goertz and Boswell (1979).	14
7b	Field-aligned view of the propagating wave front of figure 7a.	14
8	The fields and currents associated with a propagating Alfvén wave interacting with the ionosphere with nonzero Hall conductivity. From Samson and Rostoker, 1983.	16
9	Map of Alberta and AFGL stations in centered dipole coordinates.	30
10	Simulated envelope of a Pi 2 pulsation. The statistical variance in the estimate of the value at the peak, yields a variance in the estimate of the 1/e time. We arbitrarily assume the variance is 5.	41
11a	High latitude data from the U of A array. (north-south component)	46
11b	High latitude data from the U of A array. (east-west component)	47
11c	High latitude data from the U of A array. (vertical component)	48
11d	Perturbation field at 11:04 Universal time for four U of A stations. The change of sign of the Z component and the minimum in the H component places the substorm electrojet near 65.5 degrees.	49
12a	Mid-latitude data from the AFGL array. (north-south component)	51
12b	Mid-latitude data from the AFGL array. (east-west component)	52
12c	Mid-latitude data from the AFGL array. (vertical component)	53
12d	Perturbation field at 11:04 Universal time for Vict, New, and Rpc. The curve represents an approximate fit to the D component data. The change of sign of the D component occurs to the west of the station coverage.	54

13a	High latitude filtered data from the U of A array.	55
13b	High latitude filtered data from the U of A array.	56
13c	High latitude filtered data from the U of A array.	57
14	High latitude pure state from U of A array.	58
15	High latitude envelope from U of A array.	59
16	High latitude frequency function from U of A array.	60
17	East-west phase delay obtained using the D component of the U of A array data.	63
18	East-west phase delay obtained using the H component of the U of A array data.	64
19	Ratio of the maximum amplitudes of the D and H components for all stations from the 16 events.	66
20	East-west phase delay obtained using the H component of the AFGL array data. From Samson, et al., 1985.	67
21	Contouring of the east-west component of the propagation vector k (radians/degree longitude) for the H component data. Shaded (clear) areas correspond to westward (eastward) regions of propagation.	67
22	Histogram of envelope rise times for 16 events.	71
23	Histogram of envelope fall times for 16 events.	71
24	Histogram of envelope widths for 16 events.	73
25	Measurement of the group delay obtained using the H component of the high latitude data from the U of A array.	74
26	Group delay obtained using the H component of the mid-latitude data from the AFGL array. From Samson, et al., 1985.	75
27	Estimated Pi 2 frequency plotted as a function of station location for each of	

	the 9 events.	80
28	A composite plot of the data from figure 27.	81
29	Pi 2 frequency plotted as a function of station location relative to the substorm enhanced electrojet.	82
30	The mean frequency of each event is subtracted from each station's frequency estimate and plotted relative to the position of the substorm enhanced electrojet.	83
31	Distribution of stations in substorm centered coordinates. The data are that of Samson and Harrold, 1983.	86
32	Spatial distribution of Pi 2 power which has been smoothed (about the array of points plotted) and normalized to the station in each event with the largest power.	86
33	Distribution of stations for the data of group 1.	88
34	Spatial distribution of power for the data of group 1.	88
35	Spatial distribution of stations for the data of group 2 plus the distribution of normalized power.	89
36	Currents associated with the "solenoid" structure near the arc. B sees effects from both upward and downward field aligned currents. A sees only the edge effects due to the downward field aligned current. Net effect is a change in sign of the D component perturbation. Ionospheric currents propagating westward yield a dc component + periodic component component in H. A and B have the "same" H component. Net result is a polarization reversal between A and B.	93
37	Illustration of how a reversal of the D component is associated with a reversal of the sense of polarization.	93
38a	Sketch of latitudinal power distribution of Pi 2.	95

38b	Sketch of sense of polarization.	95
38c	Self-consistent relationship among power, sense of polarization, and phase propagation predicted by data and equation I-15.	96
39	Correlation between the data of figure 21 and the prediction of figure 38c.	98
40a	A typical substorm perturbation field (simulated).	100
40b	Magnitude of the electric field for a propagating Alfvén wave.	100

I. Introduction

The earth's magnetic field has a dipolar configuration that is distorted by the dynamic pressure exerted on it by the solar wind. This interaction establishes a boundary (called the magnetopause) characterized by a velocity shear in the flow of the particles. This equilibrium configuration of this boundary is determined by balancing the solar wind dynamic pressure outside the magnetosphere to the magnetic field pressure inside. This complex interaction establishes a number of distinct regions in the earth's magnetosphere as shown in figure 1. These regions are characterized by particle type, energy, density, and direction of flow. While the explanation of the steady-state configuration of the magnetosphere is fairly well established, (Dungey, 1961; Beard, 1960; Spreiter et al., 1966) the same cannot be said of observed perturbations to this state. These perturbations, often caused by sudden changes in the solar wind parameters, are propagated as ultra-low frequency plasma waves in the magnetosphere.

This study concentrates on transient waves associated with a particular fluctuation called a geomagnetic substorm. Near the earth's surface, these waves appear as damped, quasi-sinusoidal oscillations superposed on the magnetic fields of the substorm expansive phase. These Pi 2 type pulsations, as they are called, range in period from 40 seconds to about 150 seconds and have a typical amplitude of 15 nT (at auroral latitudes). To establish how these

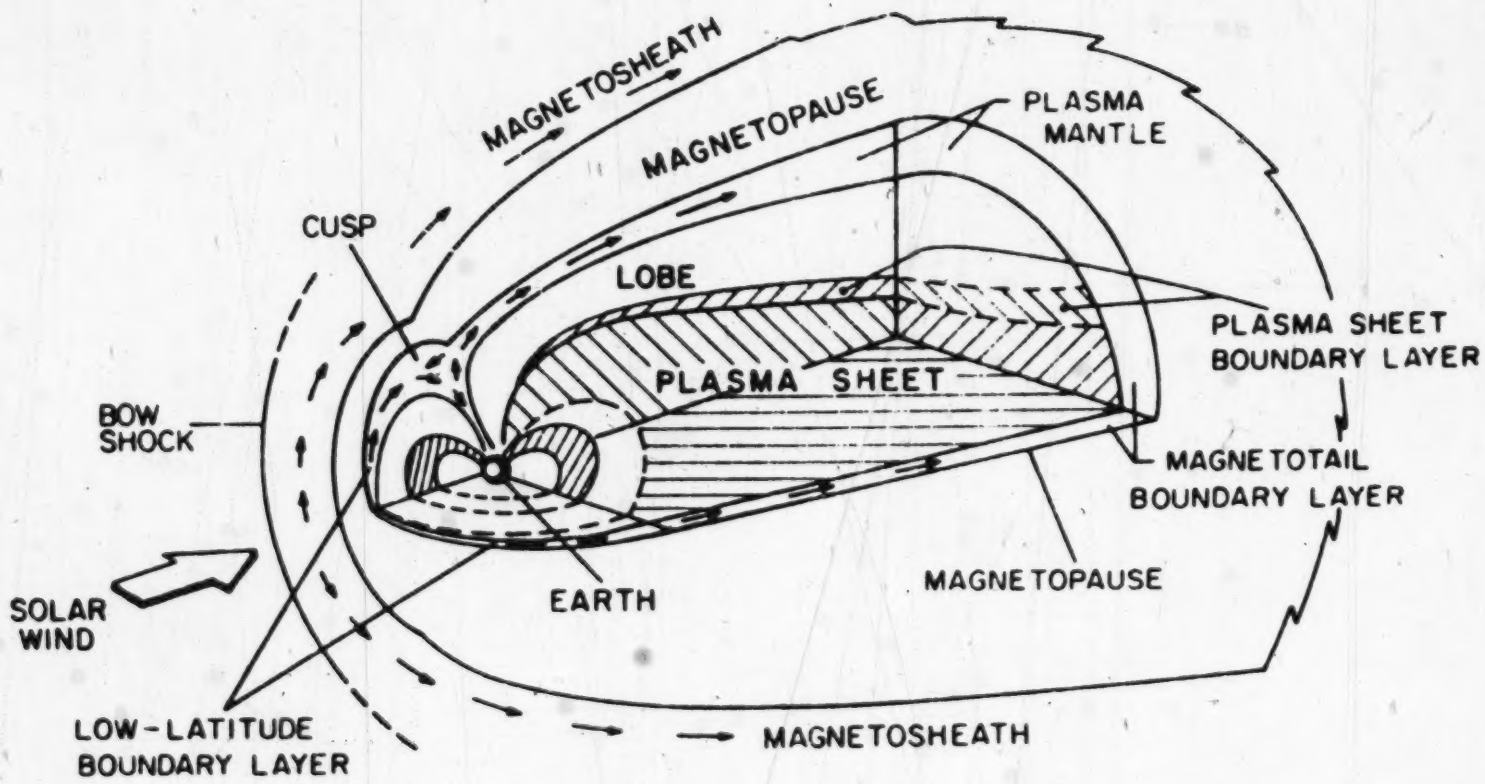

Figure 1: Structure of the Magnetosphere. From Eastman et al., 1984.

substorm associated pulsations fit into the overall structure of the magnetosphere, a brief description of the substorm is in order.

A. The Substorm

The expansive phase of the magnetospheric substorm is the magnetic manifestation of an abrupt transport of energy by field aligned currents extending from the plasma sheet near local midnight to the ionosphere (see figures 2a, 2b). Closure of these currents through the auroral ionosphere results in the conversion of solar wind energy to heat in the ionosphere. The close association of the substorm with Pi2 pulsations implies that understanding Pi2's will lead to a further understanding of the substorm.

Understanding the mechanisms of the substorm contributes to our understanding of the interaction between the earth's magnetic field, the magnetospheric plasma, and the solar wind. The basic theoretical techniques used to solve problems in space plasma physics are also used in other magnetoplasmas such as those found in fusion research and astrophysics. In particular since Pi 2's are related to some sort of periodic oscillation of the plasma and are closely related to accelerated electrons, determining the equations that adequately describe these waves could have important analogs in the field of fusion research in which plasma waves are used to heat a plasma to fusion temperature. The fact that there are still relatively few

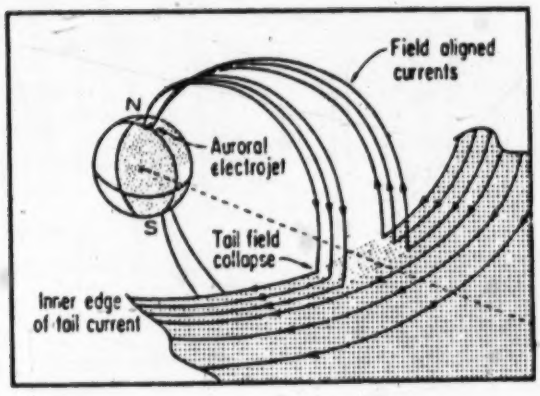

Figure 2a: Substorm current system. From McPherron et al., 1973.

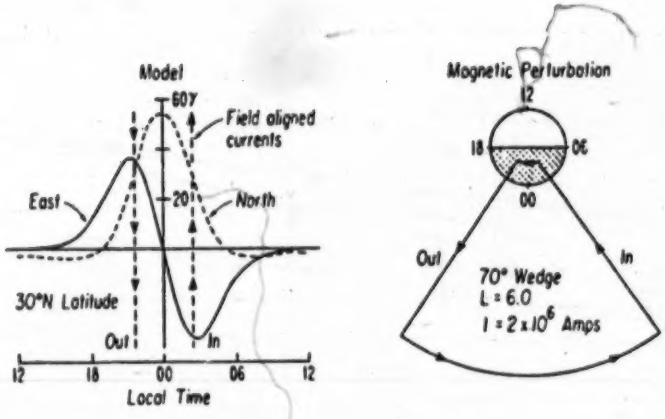

Figure 2b: Magnetic field perturbations observed on the ground due to the substorm current wedge. From McPherron et al., 1973.

analytic solutions to realistic problems in plasma physics is all the more reason to study the subject.

B. Pi2 Pulsations

Before we can study these pulsations we must first outline their distinguishing characteristics. We have already mentioned their characteristic frequencies and amplitudes, so we ask 'how do these quantities vary in space and time?'.

It has long been realized that the Pi 2 band power is localized in latitude and longitude (Jacobs and Sinno, 1960; Olson and Rostoker, 1975). Recently, a more exact location of the power maximum was determined to be just south of the substorm enhanced electrojet and east of the westward travelling surge (Samson and Rostoker, 1983). Furthermore, there is evidence that there is a secondary power maximum about 10 degrees latitude south of the electrojet, near the latitude that the plasmapause maps to (Stuart, 1974; Fukunishi, 1975; Stuart et al., 1979; Kuwashima and Saito, 1981). The variation of Pi 2 frequency with latitude has been studied by observing how the dominant frequency (i.e. the frequency corresponding to the most power at the most stations) for a given event varies with changes in the location of breakup region. It was found by Kuwashima and Saito (1981) that the dominant frequency decreases with increasing breakup latitude.

Measurements relating to the phase of the waves (east-west phase velocity, polarization ellipse of the horizontal perturbation magnetic field) have also been taken (Rostoker, 1967; Bjornsson et al., 1971; Fukunishi, 1975; Saito et al., 1976; Rostoker and Samson, 1981; Pashin et al., 1982; Lester et al., 1983, 1984; Samson and Rostoker, 1983; Samson and Harrold, 1983; Samson et al., 1985). Predominantly westward phase propagation has been observed at mid-latitudes. For a single event, the typical polarization ellipse pattern seen at mid-latitudes is shown in figure 3. At high latitudes the statistical pattern shown in figures 4 and 5 has been recorded.

Given this available empirical data, the question is can we obtain an accurate theoretical description of these pulsations by solving the pertinent equations? Which equations we use naturally depends on the physical properties of the magnetospheric plasma. The plasma that we are dealing with is very tenuous (densities of about 1 cm^{-3}). Because of these extremely low densities, we can treat the plasma as collisionless. Thus in analyzing the response of the plasma to applied fields, as a first approximation we can treat the response of a species of particles the same as a single particle response. Thus the force equation (in cgs units) for a species of particles k moving in fields $\underline{E}$ and $\underline{B}$ is:

$$m_k \frac{d\underline{v}_k}{dt} = q_k(\underline{E} + \underline{v}_k \times \underline{B}/c) \qquad \text{I-1}$$

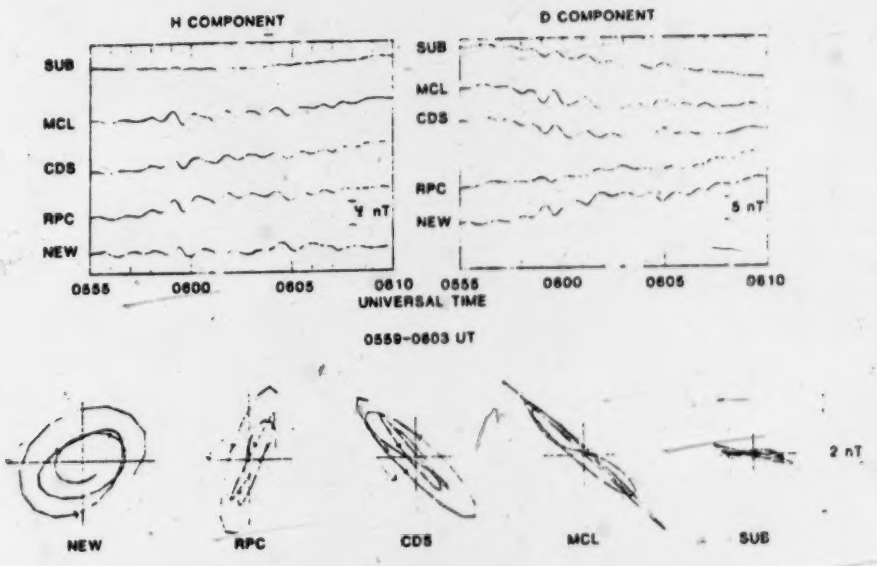

Figure 3: Pi 2 pulsation in the interval 0555-0610 UT on March 14, 1978. The polarization ellipses are generated by plotting the H component verses the D component at successive time steps. The ellipticity is defined as the ratio of the minor axis to the major axis. The azimuth is defined as the orientation of the major axis. When no arrow is present the ellipticity is essentially linear. The azimuthal angles of these ellipses compare favourably with the model shown in Figure 2c. From Lester et al., 1983.

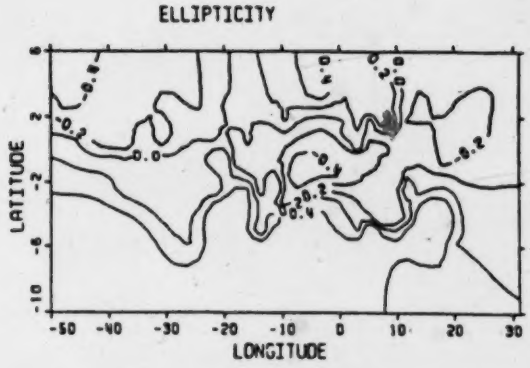

Figure 4: Observed ellipticity of the horizontal polarization ellipse at high latitude. Positive (negative) values correspond to counterclockwise (clockwise) polarization. Coordinates are relative to the latitude of the westward electrojet and the longitude of its center. From Samson and Harrold, 1983.

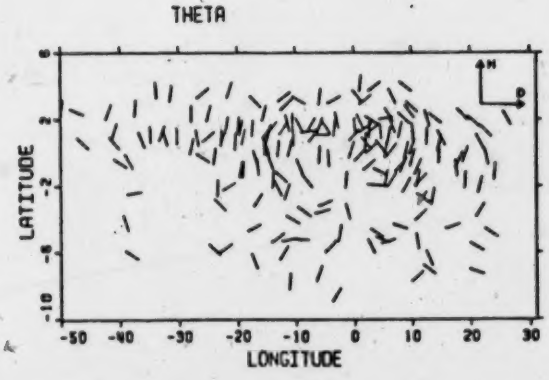

Figure 5: Observed azimuths of the horizontal polarization ellipse at high latitude. From Samson and Harrold, 1983.

The electric current produced by all species in the plasma is simply:

$$\underline{J} = \sum_k n_k q_k \underline{v}_k \qquad \text{I-2}$$

These two equations plus Maxwell's equations:

$$\nabla . \underline{B} = 0 \qquad \text{I-3}$$

$$\nabla . \underline{E} = 4\pi\rho \qquad \text{I-4}$$

$$\nabla \times \underline{E} = -c^{-1}\frac{\partial \underline{B}}{\partial t} \qquad \text{I-5}$$

$$\nabla \times \underline{B} = 4\pi c^{-1}\underline{J} + c^{-1}\frac{\partial \underline{E}}{\partial t} \qquad \text{I-6}$$

form the basic cold plasma equations.

In a uniform background magnetic field (see figure 6 for the geometry), these equations can be linearized (assuming small perturbations in the ambient fields) and an expression for the electric field can be obtained (see appendix A). The result is:

$$\nabla x \nabla x \underline{E} = K . \underline{E} / C^2 \qquad \text{I-7}$$

where $K = -\mathrm{diag}[(1+c^2/v^2)\partial^2/\partial t^2, (1+c^2/v^2)\partial^2/\partial t^2, (\partial^2/\partial t^2+\Pi^2)]$ and $\Pi^2 = 4\pi(n_i q_i^2/m_i + n_e e^2/m_e)$. Π is called the plasma frequency and v is the Alfvén speed.

Using this equation, models describing the Pi 2 pulsations can be derived. To this point there have been two principal models which have become popular: the Transient Response Model and the MHD Resonance Model.

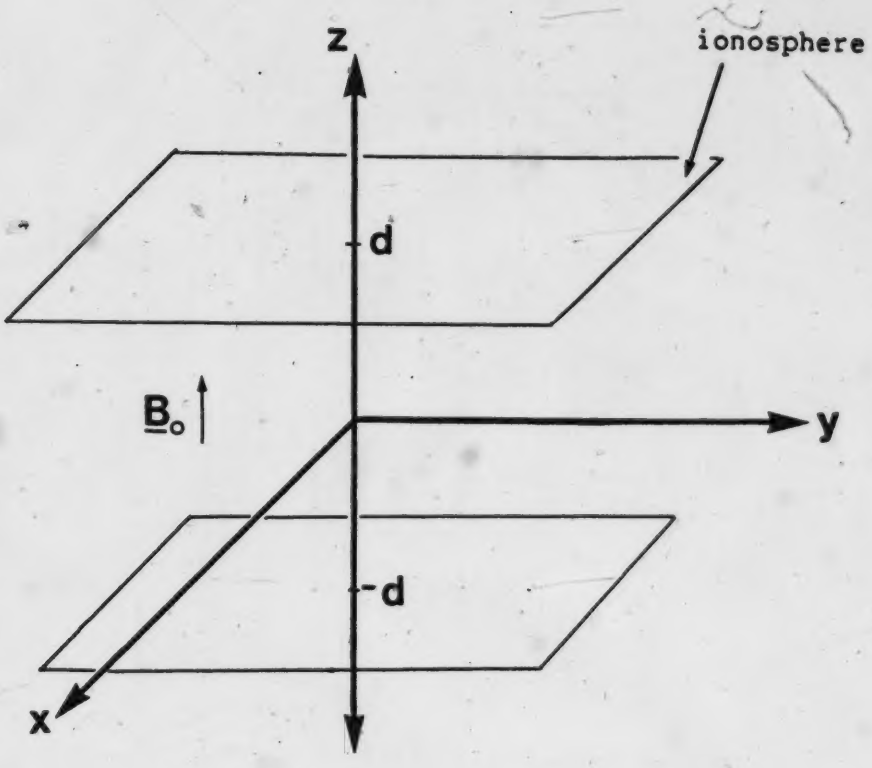

Figure 6: Idealized magnetosphere for a uniform field. To connect with the actual quasi-dipolar field, in the tail of the magnetosphere, y points to the east, x points away from the earth. At the surface of the earth at high latitudes, z points into the earth and x points northward.

C. The Transient Response Model

The essential phenomenological features of the transient response model for Pi 2 pulsations are outlined below. Due to processes not yet well understood, but possibly due to magnetic reconnection, there is a change in the convective flow in the plasma sheet in the magnetotail. It suffices to say that if this change develops sufficiently rapidly, we can treat subsequent developments as an initial value problem. Associated with this change is a decrease in the transverse electric field in this region (Kan et al., 1982). The crosstail current associated with this electric field also experiences a localized variation (Nishida, 1979). Current continuity requirements result in the establishment of field aligned currents at the boundary of the inhomogeneity. This pulse of current leads to transverse perturbations in the ambient magnetic field and is thus called a transverse or shear Alfvén wave. This wave propagates along the highly conducting magnetic field at the Alfvén speed. The development of this this current system was first described by McPherron et al. (1973).

The interaction of this pulse with the ionosphere is the crucial ingredient in the establishment of quasi-sinusiodal oscillations. Because the ionosphere - magnetosphere interface represents a plasma density and field aligned conductivity discontinuity, incident plasma waves will be reflected. The reflection coefficient relating the an incident Alfvén wave field $\underline{E}_i(\underline{r},t)$ to the reflected

wave field $\underline{E}_2(\underline{r},t)$ was derived by Scholer (1970) to be approximately:

$$R = \frac{\Sigma_m - \Sigma_o}{\Sigma_m + \Sigma_o}$$

where $\Sigma_m = c^2/(4\pi v)$ (v = Alfvén speed = $B_o/(4\pi\rho)^{1/2}$) and Σ_o is the height integrated Pederson conductivity. The observed oscillations arise due to subsequent reflections of the pulse between the ionosphere and the source region or the ionosphere in the opposite hemisphere (Goertz and Boswell, 1979; Kan et al., 1982; Samson, 1982; Baumjohann and Glassmeier, 1984). The question as to whether the returning pulse reflects from the source or the opposite ionosphere depends on how the ambient magnetic field configuration changes as a result of the substorm. Some authors (Samson (1982) for example) advocate that the field lines threading the source region change from a tail-like to a dipolar configuration. This would lead to reflections of the pulse between the northern and southern auroral ionospheres. On the other hand, Kan et al. (1982) and Goertz and Boswell (1979) advocate a source region which maintains an enhanced electric field and thus a pulse incident on this region will be reflected (reflection coefficient = -1). In either case, this pulse will be damped out as its electric fields generate ionospheric currents which dissipate Joule heat.

The above qualitative description of the transient response model can be quantified using equation I-7. Goertz and Boswell (1979) showed that a useful solution to equation

I-7 can be obtained by reducing the problem to 2 dimensions: $\partial/\partial y = 0$ and $E_y = 0$. The x and z components of the equation become (c.f. equations 13 and 16b of Goertz and Boswell(1979)):

$$\frac{\partial^2 E_z}{\partial x \partial z} - \frac{\partial^2 E_x}{\partial z^2} = -(1/c^2+1/v^2)\ \frac{\partial^2 E_x}{\partial t^2} \qquad \text{I-8}$$

$$\frac{\partial^2 E_x}{\partial z \partial x} - \frac{\partial^2 E_z}{\partial x^2} = -(\Pi^2 + \frac{\partial^2}{\partial t^2})E_z \qquad \text{I-9}$$

where Π is the plasma frequency.

These two equations plus the initial conditions ($E_x(x,z,t=0)$ and $\partial E_x(x,z,t=0)/\partial t$) and boundary conditions at the source region (z=0) and at the ionospheres ($z=\pm d$) completely specify the problem. The boundary condition at the source corresponds to a localized increase in E_x. The ionospheric boundary condition is (see Goertz and Boswell, 1979):

$$(\frac{\partial E_x}{\partial z} + 4\pi\Sigma_o c^{-2}\frac{\partial E_x}{\partial t})\Big|_{z=+-d} = 0 \qquad \text{I-10}$$

where Σ_o is the height integrated Pederson conductivity of the ionosphere.

The essential features of the solution are illustrated in figure 7a. Observe the pulse of upward field aligned current propagating toward the ionosphere at $t=z/v$, and its subsequent reflection at the ionosphere. Figure 7b illustrates a field aligned view of the propagating wave.

There are three important effects which must be taken into account in order to apply this model to the geomagnetic field. The first is that we must map it to a quasi-dipolar

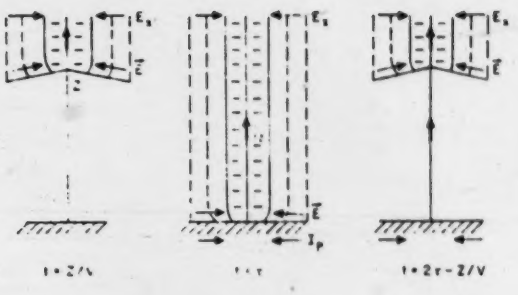

Figure 7a: A series of snapshots displaying the electric fields at different times. The dashed lines indicate 'equipotential' contours. In the wave front $\nabla \times \underline{E}$ is not zero, and the magnetic field changes with time. For a low β plasma ($\beta = 8\pi nkT/B_o^2$). From Goertz and Boswell (1979).

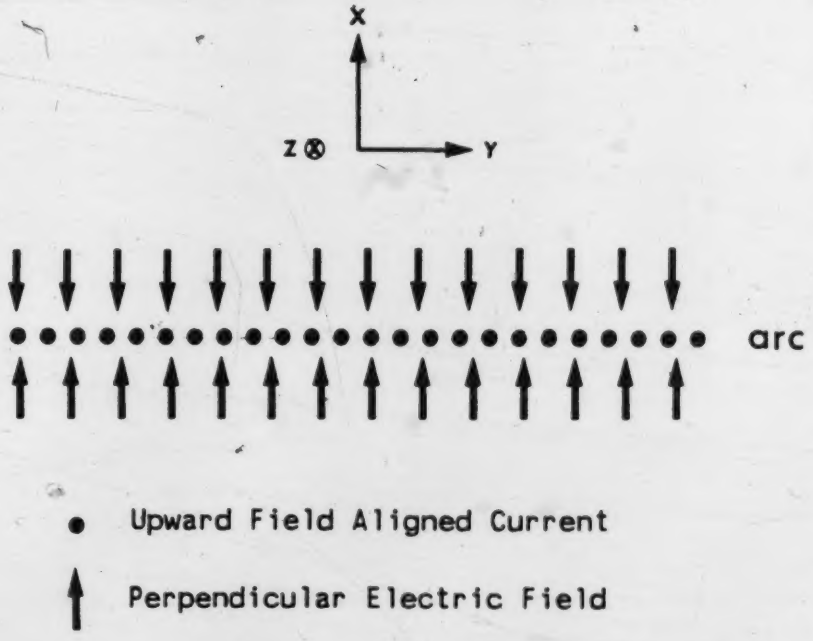

Figure 7b: Field-aligned view of the propagating wave front of figure 7a.

configuration. This is done in a qualitative manner. The mapping procedure indictates that the source region is the plasma sheet in the magnetotail.

The second effect concerns the nature of the ionospheric conductivity. The ionosphere has a high Hall conductivity. This means that north-south electric fields incident on the ionsophere generate east-west Hall currents. These ionospheric Hall currents close through upward field aligned currents in the arc and downward field aligned currents far to the east and west of the arc.

The third effect is that the ionspheric conductivies (Pederson and Hall) are not uniform. In fact, the conductivity decreases sharply at the equatorward and poleward boundaries of the auroral oval (Horwitz et al., 1978). Thus ionospheric currents flowing within the auroral oval tend to generate field aligned closure currents at these boundaries.

The model current system qualitatively taking into account these effects is shown in figure 8. The currents system consisting of ionospheric Pederson currents flowing into the arc, upward field aligned current within the arc, plasma sheet closure currents (not shown) and downward field aligned current[1] on the poleward boundary of the auroral oval forms an approximate solenoid-like current system. The same can be said of the currents flowing in the region south of the arc but north of the equatorward border of the

---

[1]Note that the downward field aligned current is not latitudinally localized.

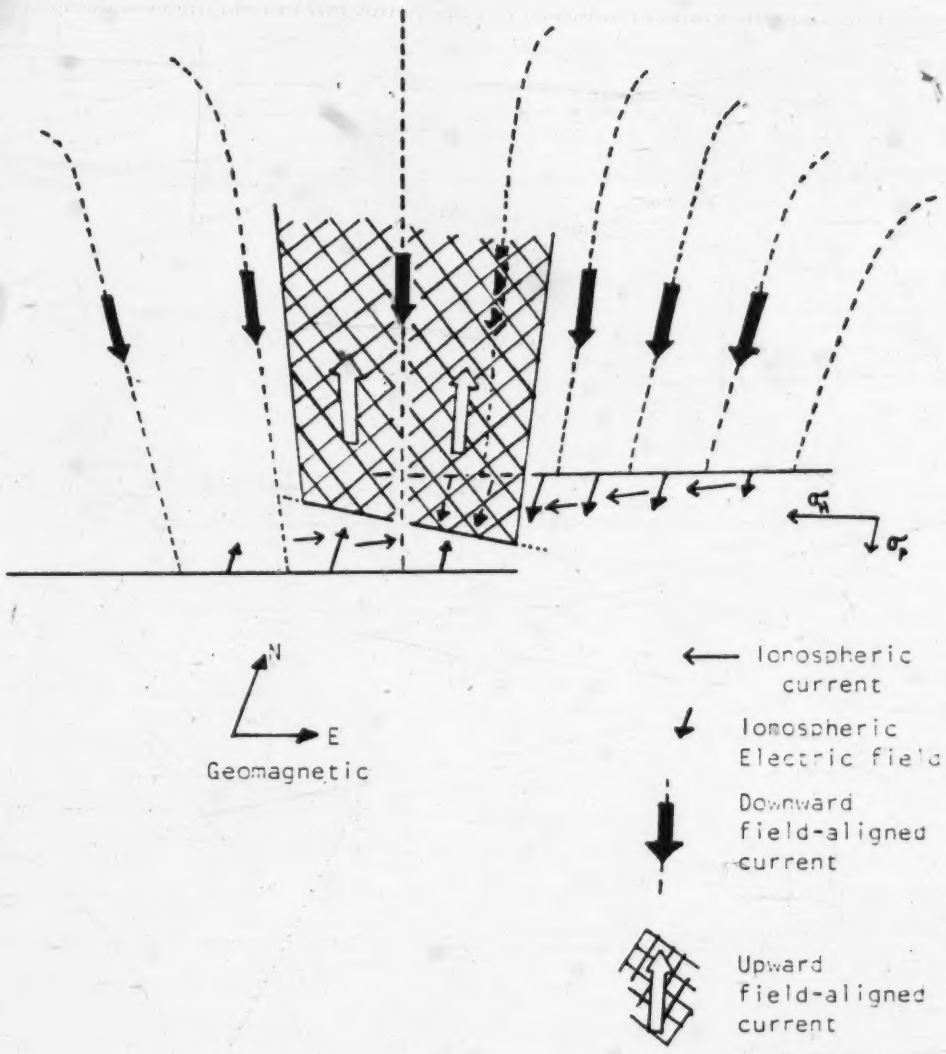

Figure 8: The fields and currents associated with a propagating Alfvèn wave interacting with the ionosphere with nonzero Hall conductivity. (From Samson and Rostoker, 1983)

auroral oval. At midlatitudes (50 - 60 °N Geomagnetic), the integrated effect of the field-aligned currents associated with these solenoid-like structures is very small compared to the magnetic signatures of the field-aligned Hall closure current system. There are two reasons for this. The first is that the ionospheric Hall conductivity is 3 to 4 times the ionospheric Pederson conductivity. Thus, the Hall closure currents are larger and produce stronger magnetic fields than the Pederson closure current system. The second reason is that outside the "solenoid" (i.e. south of the equatorward border of the auroral oval) the magnetic field due to the downward field-aligned current is directed opposite to that of the upward field aligned current and thus cancel one another out. We are now in a position to use the model to make predictions.

From the geometry of the quasi-dipolar magnetic field, one such prediction is that the observed period of the pulsation will increase with increasing breakup latitude (i.e. the latitude that the source region maps into). This is evident if, after many reflections, the transient response becomes a resonance phenomena. The period of the pulsation train is predicted to be 4T (where T is the one way Alfvén travel time from the source to the ionosphere. From Kan et al., 1982; Baumjohann and Glassmeier, 1984). Since T is roughly proportional to the length of the field line threading the source region (located in the equatorial plane of the plasma sheet (Kan et al., 1982)), it is the

fact that (for a dipolar field) field lines intersecting the ionosphere at higher latitudes are longer which leads to the above prediction. A quantitative verification of this was made by Kuwashima and Saito (1981) (although the data also fit the predictions of (their) resonant model).

A second important prediction of this model concerns the gradients in the magnetic fields. Near the highly (latitudinally) localized upward field-aligned current (i.e. near the arc), large gradients in the D component (y component) of the magnetic field may be expected. At either end of the arc, gradients in the H component (x component) are expected. Large gradients are also expected at the poleward and equatorward boundaries of the auroral oval. As mentioned previously, outside the auroral oval, the magnetic fields of the solenoid-like structures decrease dramatically and thus large gradients are expected in all three components of the (perturbation) magnetic field. This concludes our outline of the main features of the transient response model of Pi 2 pulsations and a description of the resonant model is now in order.

D. Resonant Field Line Model

The resonant field line model for Pi 2 pulsations was first proposed by Atkinson (1966) and has received much support (Saito, 1969; Saito and Sakurai, 1970; Raspopov et al., 1972; Saito et al., 1976; Kuwashima, 1978; Kuwashima and Saito, 1980, 1981). The source of the pulsations is

assumed to be a plasma inhomogeneity located in the plasma sheet of the magnetotail. As in the previous model the reason for the development of such an inhomogeneity is beyond the scope of this study. Once again, due to current continuity requirements at the boundaries of this inhomogeneity, a transverse Alfvén wave is launched along the magnetic field. Considering this current pulse to be a superposition of many spectral components, and the north and south auroral ionospheres to be the reflecting boundaries, then only those spectral components that have wavelengths that are integral multiples of the field line length will survive. That is, modes of propagation that have wavelengths which are not integral fractions of twice the length of the field line will be strongly damped. Hence standing waves are set up in the "cavity" bounded by the ionospheres. Thus in this model, the Pi 2 pulsations are portrayed as eigenoscillations of local field lines passing through the source region.

Once again, the previous qualitative description can be quantified using equation I-7. Following the method outlined by Nishida (1978), the electric field is assumed to be of the form:

$$\underline{E} = (E_x(x), E_y(x), 0)\exp(i\{\lambda y + kz - \omega t\}) \qquad \text{I-11}$$

From the form of this electric field, it is apparent that provision has been made for east-west (y direction) and field aligned (z direction) wave propagation. Note also that

an $\exp(-i\omega t)$ time dependence has been employed. In this regime, the properties of the magnetosphere determines the allowed values of k, namely, that the wavelength $(2\pi/k)$ will be an integral fraction of 4d. Substituting equation I-11 into equation I-7 and ignoring the effect of displacement currents (i.e. $1+c^2/v^2 \simeq c^2/v^2$) yields:

$$(\omega^2/v^2 - k^2)E_x = i(\frac{dE_y}{dx} - i\lambda E_x) \qquad \text{I-12}$$

$$(\omega^2/v^2 - k^2)E_y = -\frac{d}{dx}(\frac{dE_y}{dx} - i\lambda E_x) \qquad \text{I-13}$$

The equation for the z component can be obtained from I-12 and I-13 and thus has not been shown (i.e. d/dx(I-12) + $i\lambda$(I-13)). Eliminating E_x from these equations yields (c.f. equation 118, p. 193 of Nishida, 1978):

$$\frac{d^2E_y}{dx^2} - \frac{\lambda^2}{(K^2-k^2)(K^2-k^2-\lambda^2)}\frac{dK^2}{dx}\frac{dE_y}{dx} + (K^2-k^2-\lambda^2)E_y = 0 \qquad \text{I-14}$$

where $K^2 = \omega^2/v^2$. Note that it has been assumed that v is dependent on x (i.e. the density is not uniform). Nishida (1978) pointed out that this equation reduces to the dispersion equation for the fast mode hydromagnetic wave if $\lambda = 0$ or $dK^2/dx = 0$ (homogeneous medium). For an inhomogeneous medium and $\lambda \neq 0$, equation I-14 has a singularity at $K^2 = k^2$. This means that the resonant frequency kv matches the frequency of the source (ω).

Even without going into the details of the solution to I-14, some useful predictions of this model can be made. The first prediction is that the fundamental period of the oscillations will be twice the one way Alfvén travel time

between the north and south ionospheres (Kuwashima and Saito, 1981). Assuming that earth's magnetosphere is symmetric about the equatorial plane, it is predicted that the pulsation period will increase with increasing breakup latitude.

The predicted polarization characteristics of the resonant field line model were first calculated by Hasegawa and Chen (1974) and Southwood (1974). These characteristics can be determined by using equations I-5, I-11, and I-12. Equations I-5 and I-11 imply that the perturbation magnetic field $\underline{b}$ is related to $\underline{E}$ by: $b_y/b_x = -E_x/E_y$. Thus by equation I-12:

$$b_y/b_x = \frac{-i\lambda}{(K^2-k^2-\lambda^2)} \frac{dE_y}{dx} \frac{1}{E_y} \qquad \text{I-15}$$

It was pointed out by Nishida (1978) that the above equation is not restricted to the resonant field line model since it was derived only on the basis of the form of the electric field and not on the assumption that k be integral multiples of $2\pi/(4d)$. Nevertheless, since the time dependence is $\exp(-i\omega t)$, for $\mathrm{Im}(b_y/b_x)$ positive (negative) the polarization is counterclockwise (clockwise) as viewed along $\underline{B}_0$. This equation predicts polarization reversals in regions where $d(\ln E_y)/dx$ changes sign and where λ changes sign (Southwood, 1974). In regions where $K^2-k^2-\lambda^2 < 0$ (for $\omega \simeq .06$ rad/sec, $v_A \simeq 500$ km/sec, and $\lambda \simeq 6\times10^{-8}$ km^{-1}(from Samson et al., 1985) $K<\lambda$), and where clockwise (counterclockwise) polarization is observed, $\lambda d(\ln E_y)/dx$ is

predicted to be greater (less) than zero. Given the polarization map of figure 4, and measurements of λ and $d(\ln E_y)/dx$ in in the auroral region, verification of this prediction is possible.

E. Objectives

The goal of this study is to determine the magnetic field structure of the Pi2. In order to do this, I shall use ground-based magnetometer data from the University of Alberta array (see Rostoker and Hughes (1979) for a description of this array) in an effort to calculate various parameters that describe these pulsations. These parameters include frequency, effective phase velocity, effective group velocity, envelope rise time and fall time, and power distribution. On the basis of these measurements, I shall attempt to substantiate or refute the proposed theoretical models.

While there have been many studies on the characteristics of Pi 2 pulsations, I shall attempt to improve or expand on the results of these studies in the following ways. First of all, the data considered will partly include stations in the auroral oval. Phase studies by Lester et al. (1983,1984) and Samson et al.(1985) have only considered stations predominantly south of this oval in the mid - latitude range. In order to fully understand these pulsations it is desireable to map their measurable characteristics over as large an area as possible. Hence the

high latitude measurements will be an important addition to the propagation information that already exists on Pi2's.

Secondly I shall re-analyze the data of Samson et al. (1985) in light of my recent work on the estimated error involved in the Hilbert transform technique. Such an analysis is an important aspect of any research and thus will be a worthwhile exercise.

Thirdly, I shall present a study of the latitudinal dependence of the observed Pi2 frequencies. Most of the past studies of this dependence have looked at the peak in the power spectra to assign a frequency associated with the Pi2 (at a given station) whereas I shall assign it in the time domain using the Hilbert transform. This analysis will also differ from previous studies as a result of the filtering technique employed. It is believed that the pure state filter (see Samson (1983) for a thorough description of this filter) will make the trends more evident.

In the interest of completeness I also intend to discuss the phase data in light of previous studies of polarization data by Rostoker(1967), Fukunishi (1975), Kuwashima (1978), Baranshkiy et al. (1978), Kuwashima and Saito (1981), Pashin et al.(1982), Samson (1982), Samson and Harrold (1983), Samson and Rostoker (1983), Lester et al. (1983,1984), and Sakurai and McPherron (1983). Although an excellent review of the polarization studies is given by Baumjohann and Glassmeier (1984), it lacks the synthesis with the high latitude phase velocity calculations which may

provide important new insights.

II. Method of Analysis

The method of analysis can be subdivided into three separate procedures. We begin with (1) discussing techniques used in previous studies, (2) outlining the selection criteria for the events, (3) move on to our choice of coordinate systems and (4) finally discuss the mathematics of our time series analysis.

A. Background

Empirical studies on this subject can generally be categorized as statistical in nature or as single event studies. The latter variety are useful in emphasizing features that are unique to a particular event and thus may or may not depict the features common to most Pi2's. Because the statistical studies generally highlight the common features and mask out the unique ones, I have chosen to employ this type of study for my analysis. There remains two principal question to address: how to calculate the phase, frequency, and envelope information and which is the best coordinate system in which to plot the data.

The analysis of the time series themselves has generally employed band pass filtering and calculation of the dominant frequency by the peak in the power spectra. The phase information has usually been calculated in the frequency domain using a spectral technique outlined by Green (1976). This technique is adequate when the phenomena do not involve finite group velocities. If an envelope

contains only a few pulsations then it is desireable to use the technique given in Samson et al. (1985).

This technique differs from the technique used by Green in two important ways. It employs a higher degree of filtering by applying a pure state filter (Samson, 1983) and secondly, uses a Hilbert transform to extract the phase, frequency and envelope information from the pure state. The advantage in using the pure state filter is that the contribution of the unpolarized (isotropic) noise to the signal is substantially reduced. This is particularly important in the analysis of data from high latitudes which usually contains substantial electrojet noise. With the lower noise level it is expected that any statistical trends will be more clearly elucidated. An advantage to employing the Hilbert transform over the spectral technique is that estimation of the frequency is not dependent on the digitizaion interval. Pi2 frequencies that lie between two multiples of the fundamental frequency will have phase estimates that will be more error prone. (although this can be partially alleviated by "padding" the ends of the time series with zeroes - a rather artificial manipulation). The second advantage is that the envelope can contain as few as one oscillation and still give reasonably accurate phase estimates- the spectral technique could not be used for such a pulsation. Finally, it was shown by Samson et al. (1985) that the spectral technique mixes phase and group velocities. This is not desireable at high latitudes where

it is expected that group velocities will be finite and hence the spectral technique will not accurately estimate the phase velocity.

B. Coordinate Systems

We now turn to the question of which coordinate system to use to plot the calculated information. Earlier studies (Bjornsson et al., 1971) predominantly used a local time based coordinate system coupled with geomagnetic latitude. The next advance was to adjust the location of the observation station to be relative to the latitudinal location of the substorm breakup. Rostoker(1972) employed this system with good success. Lester et al. (1983,1984), for example, used a coordinate system centered on the location of the center of the substorm wedge current system. Samson and Rostoker (1983) used a similar system, but a slightly different technique was employed to find this location. It was found that this last system yielded the most consistent results for Pi2 studies.

The use of such a coordinate system is justified as follows. It is well established that the substorm current wedge does not always develop on the same local time meridian, nor does the substorm enhanced electrojet always develop at the same latitude. Thus, any statistical study which examines the spatial variation of some quantity associated with the substorm should use a coordinate system which is invariant from one substorm event to the next. It

is believed that locating the stations relative to the center of the wedge current system forms one such invariant coordinate system.

The center of the wedge current system is determined by: the latitudinal point where the ΔZ excursion from the quiet time baseline (taken just before onset) is zero in its transition from $\Delta Z < 0$ to $\Delta Z > 0$ with increasing latitiude and the longitudinal point where the mid-latitude ΔD excursion from the quiet time baseline is zero in its transition from $\Delta D > 0$ to $\Delta D < 0$ with increasing eastward longitude (see figure 2b). As confirmation of this location, the ΔH component at high latitudes should be a minimum with respect to latitude and at midlatitudes ΔH should be a maximum with respect to longitude. The success with which Samson and Harrold (1983), Samson and Rostoker (1983) and Lester et al.(1983) applied this coordinate system is indicative that it is indeed the favored coordinate system for this analysis.

C. Selection Criteria

There are five criteria used in selecting the events of the phase analysis part (phase delay, group delay, rise and fall times) of this study. First of all, each event used in this study was required to have data available from at least three of the four stations in the east-west part of the U of A array (see table 1 and figure 9 for coordinates and locations of these stations). Use of only two stations may

Table 1: Station Coordinates

Station Name	Pneumonic	Centered Dipole Coordinates Latitude	Longitude
U of A array			
Providence	Prov	67.5	292.2
Hay River	Hayr	67.3	294.7
Fort Smith	Smit	67.3	300.1
Uranium City	Uran	67.5	304.7
Leduc	Ledu	60.6	303.0
Fort McMurray	Mcmu	64.3	303.6
Fort Chipewyan	Ftch	66.1	301.1
AFGL array			
Newport	New	55.2	299.3
Rapid City	Rpc	53.3	319.0
Camp Douglas	Cds	54.5	334.5
Mount Clemens	Mcl	53.6	343.9
Sudbury	Sub	53.6	358.4
EMR Stations			
Churchill	Chur	68.7	322.8
Great Whale River	Gwr	66.6	348.8
Baker Lake	Bake	73.8	317.1
Yellowknife	Yell	69.1	294.6
Victoria	Vict	54.3	294.2
Whiteshell	Whit	59.9	325.3
U.S. Standard Observatories			
Boulder	Boul	48.7	317.9
College	Coll	64.8	282.9
Fredericksburg	Fred	49.5	351.0
Sitka	Sitk	60.2	276.0

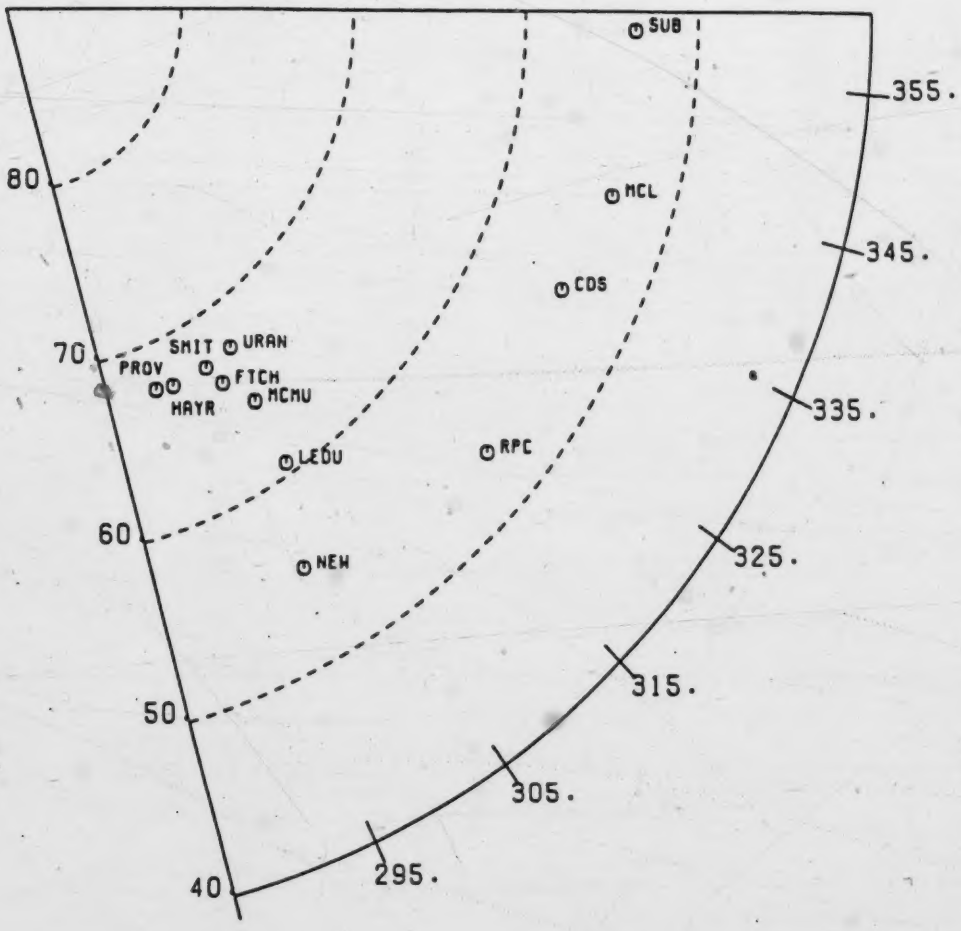

Figure 9: Map of Alberta and AFGL stations in centered dipole coordinates.

lead to an ambiguity in the phase difference between the stations whereas with three stations, a trend in the phase may be seen which eliminates this ambiguity. Secondly, each time series had to consist of at least 25 minutes of uninterrupted data, ending at the point where the Pi2 is completely damped out. This condition reduces the possibility of the data in the interval having a timing error. Thirdly, the Pi 2 as seen in the highpass filtered data had to have a high signal to noise ratio. This condition ensures that the filtered data actually is representative of the Pi2 pulsation and not some other superposed anomalous phenomena. It was found that the best filtering results were obtained when the amplitude of the pulsation was at least 20% of the amplitude of the enhanced electrojet. The difficulty in finding events satisfying this criteria necessitated the use of events which failed this test, but these events were in a minority. Fourthly the center of the wedge current system (as outlined above) had to be within the bounds of the available arrays (AFGL, U of A, U.S. Standard Observatories, EMR). This limited the longitudinal location of the center of the wedge current system to the range 275 to 358 degrees east (geomagnetic) and and the latitudinal location of the breakup to the range 60.6 to 69.1 degrees north (geomagnetic). Our choice of coordinate system made it necessary that the location of the main substorm current system be known.

Finally, it was observed that some Pi2 wave trains have frequencies that change after only a couple of pulsations (i.e. multiple Pi 2 events). Because of the difficulty of calculating phase differences over these transition points and because of the nature of the averaging method used in the phase difference calculation, it was desirable that the Pi2 wave train be relatively short - only having a few pulsations and at most only one transition point.

In addition to the aforementioned tests, the analysis of the latitudinal dependence of Pi 2 frequency required an additional selection criterion. This is because tests run using simulated data showed that the error involved in the frequency estimate varies with the magnitude of the substorm onset. It was observed that the estimated frequency was generally lower than the actual frequency of the test data and that the frequency difference increased with increasing electrojet intensification relative to Pi 2 amplitude. This fact was not of much concern in the phase analysis since only the stations in the east-west part of the array were used. Hence the stations would have similar electrojet intensification signatures and thus similar errors in the frequency estimate. However, the signature of an electrojet intensification decreases with increasing latitudinal distance from the electrojet. Thus,in analyzing the frequency dependence on latitude an additional criterion was needed so that all the points in the statistical base would have the same statistical significance.

The analysis with simulated data indicated that the error in the frequency estimate was less than 4% if the ratio of Pi2 amplitude to electrojet intensification in each component was greater than 0.4. Thus the specific criteria used in selecting events and which stations to use from each event was that the magnetic signature of the electrojet or field aligned current intensification as seen in any of the components be less than twice the amplitude of the Pi2 pulsation present.

D. Time Series Analysis

The time series are analyzed using the same technique as Samson et al. (1985) and the essential features of this method are outlined below (taken from Samson (1983) and Samson et al. (1985)). To each time series analyzed in this study a series of filters was applied in order to enhance the signal to noise ratio. The first of these filters was a high pass filter to eliminate low frequency trends (less than 3mHz). The second filter is used to extract the so called pure state via a method analagous to that used in quantum statistical mechanics to find the approximate wave function of a system.

The spectral density matrix ($S) is defined as the outer product of the Fourier transform of the 3-component time series with its hermitian adjoint. Our estimate of the density matrix ($\hat{S}$) is obtained by smoothing the outer product over a narrow frequency band centered on the desired

frequency:

$$\hat{\mathbf{S}}(k) = (2m+1)^{-1} \sum_{j=k-m}^{k+m} \underline{z}(j)\underline{z}^*(j) \qquad \text{II-1}$$

$$\underline{z}(j) = \sum_{t=0}^{n-1} \underline{X}(t)\exp(-2\pi ijt/n) \qquad \text{II-2}$$

where bold face type indicates a 3 x 3 matrix and 3 component vectors are denoted by "_". 2m+1 = width of spectral window used to smooth the data and $\underline{X}(t)$ is the 3 component time series (corresponding to data from one magnetometer) of length n.

We define the pure state by a vector $\underline{\nu}$ in unitary space. Then, for example, the pure state with maximum power is found from the equation:

$$\frac{\partial}{\partial \underline{\nu}} (\underline{\nu}^* \mathbf{S} \underline{\nu} / (\underline{\nu}^* \underline{\nu})) = 0 \qquad \text{II-3}$$

where $\underline{\nu}^* \mathbf{S} \underline{\nu} / \underline{\nu}^* \underline{\nu}$ = power in direction $\underline{\nu}$. The solution is thus:

$$\underline{\nu}^* \mathbf{S} = \lambda \underline{\nu}^* \qquad \text{II-4}$$

$$\lambda = \underline{\nu}^* \mathbf{S} \underline{\nu} / (\underline{\nu}^* \underline{\nu}) \qquad \text{II-5}$$

Hence the pure states correspond to the eigenvectors of S and the power maxima correspond to the eigenvalues. The (global) power maximum is thus the largest eigenvector. Furthermore since S can be expanded using the outer product of it eigenvectors we have:

$$\mathbf{S} = \sum_i \lambda_i \underline{\nu}_i \underline{\nu}_i^\dagger \qquad \text{II-6}$$

If S represents a polarized wave then all the power is in one direction $\underline{\nu}_o$ and hence S only has one unique

eigenvector:

$$S = \lambda_o \underline{\nu}_o \underline{\nu}_o^{\dagger} \qquad \text{II-7}$$

The difficulty is that S as calculated in equation II-1 does not represent a polarized wave, but contains some noise which we wish to get rid of before calculating the pure state vector. Thus, it is assumed that our signal contains a polarized wave plus uncorrelated noise: $\underline{z}(j) = a(j)\underline{u} + \underline{e}(j)$, where $\underline{u}$ = direction of polarization (which by definition of a polarized wave is largely independent of j), the a(j) are the Fourier amplitudes of our pure state, and $\underline{e}$ is the random noise.

To obtain the best estimates of a(j) and $\underline{u}$ we shall minimize the mean square error:

$$\xi[\ (\underline{z}(j)-\underline{e}(j)-a(j)\underline{u})^{*}\mathbf{E}^{-1}\ (\underline{z}(j)-\underline{e}(j)-a(j)\underline{u})] \qquad \text{II-8}$$

where ξ denotes the ensemble average over the spectral band of interest. The quantity **E** is equal to $\xi[\underline{e}(j)\underline{e}^{*}(j)]$ and is included to normalize the variances. It was shown by Samson (1983) that the optimal solutions for a(j) and $\underline{u}$ using this criteria are:

$$\underline{u} = \mathbf{E}^{(1/2)}\underline{\nu}_o \qquad \text{II-9}$$

$$a(j) = \underline{u}^{*}(\mathbf{E}^{-1} - \mathbf{S}^{-1})\underline{z}(j)/(\underline{u}^{*}\mathbf{E}^{-1}\underline{u}) \qquad \text{II-10}$$

where $\underline{\nu}_o$ is the eigenvector of S with the largest eigenvalue. If we assume that the noise is isotropic (i.e. **E=I**), then $\underline{u}$ and a(j) are completely specified. With a(j)

and $\underline{u}$ calculated, we inverse Fourier transform $a\underline{u}$ to obtain the filtered pure state time series. In practice, we use $\hat{S}$ (equation II-1) in place of S. Once we have obtained the pure state our next step is to extract the phase and amplititude information.

This information is obtained by: (1) a judicious choice of a mathematical model for the filtered pure state time series and (2) the Hilbert transform. (For a comprehensive discussion of the use of the Hilbert transform to obtain the amplitude and phase information see Goodman (1960).) The choice of the mathematical model is based on the observation that pure state Pi2 pulsations are very similar to damped sinusoids. Thus, using $X_i(t,\underline{x})$ to denote the filtered time series, we use the following mathematical model for each component:

$$X_i(t,\underline{x}) = a_i(t,\underline{x}) \cos(f_i(t,\underline{x})) \qquad \text{II-11}$$

where i denotes the H, D, and Z components of the magnetic field. The Hilbert transform Y(t) of a function X(t) is defined by:

$$\begin{aligned} Y(t) &= \pi^{-1} P\int ds\ X(s)/(s-t) \\ &= (2\pi)^{-1}\int X(\omega)\exp[i\omega(t+\pi/(2|\omega|))]d\omega \end{aligned} \qquad \text{II-12}$$

where P denotes the principal value and $X(\omega)$ is the Fourier transform of X(s) ($X(\omega) = \int X(s)\exp(-i\omega s)ds$). The integral in equation II-12 is replaced by a sum as the time series is of finite length. Hence the Hilbert transform of equation II-11

is:

$$Y_i(t,\underline{x}) = a_i(t,\underline{x}) \sin(f_i(t,\underline{x})) \qquad \text{II-13}$$

Subsequently we can easily obtain the amplitude and phase functions:

$$a_i(t,\underline{x}) = (X_i^2(t,\underline{x}) + Y_i^2(t,\underline{x}))^{1/2} \qquad \text{II-14}$$

$$f_i(t,\underline{x}) = \arctan(Y_i(t,\underline{x}) / X_i(t,\underline{x})) \qquad \text{II-15}$$

The phase and frequency information is extracted by assuming the source of these pulsations are travelling wave phenomena. Thus a_i and f_i will have the following forms:

$$a_i(t,\underline{x}) = a_i(\underline{v}_i.\underline{x}/v_i^2 - t) \qquad \text{II-16}$$

$$f_i(t,\underline{x}) = \underline{k}_i.\underline{x} - \omega_i t + \phi_i \qquad \text{II-17}$$

where $\underline{v}_i$ is the group velocity.

To look at the east-west component of the phase propagation, we used an east-west array of stations on a line of constant latitude. Using the ith component of the magnetic field, the phase difference between two stations (1,2) is:

$$f_i(t,\underline{x}(1)) - f_i(t,\underline{x}(2)) = \underline{k}_i.(\underline{x}(1) - \underline{x}(2))$$

where $\underline{x}(j)$ is the location of the jth station. Since the stations are on a line of constant latitude, $\underline{x}(1) - \underline{x}(2) = (y(1) - y(2))\underline{e}_y$, where $\underline{x} = (x,y,z)$. Thus:

$$k_{yi} = (f_i(t,\underline{x}(1)) - f_i(t,\underline{x}(2)))/(y(1) - y(2)) \qquad \text{II-18}$$

The frequency is estimated with the assumption that the phase varies linearly in time (equation II-17). Hence:

$$\omega_i = -\frac{\partial f_i(t,\underline{x})}{\partial t} \qquad \text{II-19}$$

This assumption was found to be valid in time intervals in which the amplitude function was greater than 37% ($=e^{-1}$) of its maximum value in the interval. The final frequency $\langle\omega_i\rangle$ used was averaged over the time interval in which the amplitude was greater than 50% of its maximum value:

$$\langle\omega_i\rangle = -(m+1)^{-1} \sum_{t=t1}^{t1+m} \frac{\partial f_i(t,\underline{x})}{\partial t} \qquad \text{II-20}$$

Note that in the above expression, we have used the fact that the data are digitized at 5 second intervals so that time can be labelled by the integer t. In the above expression, t1 is the time at which the pulsation amplitude is 50% of its maximum value (on the rising edge of of envelope) and m is the width of the envelope (from the t1 to its corresponding point on the falling edge of the envelope). The time derivative in II-20 was calculated using the finite difference:

$$\begin{aligned}\frac{\partial f_i(t,\underline{x})}{\partial t} &= \frac{\partial}{\partial t}\arctan(Y_i(t,\underline{x})/X_i(t,\underline{x})) \\ &= (X_i^2(t,\underline{x})+Y_i^2(t,\underline{x}))^{-1}[X_i(t,\underline{x})Y_i(t+1,\underline{x}) \\ &\quad - Y_i(t,\underline{x})X_i(t+1,\underline{x})]/T_s \qquad \text{II-21}\end{aligned}$$

where T_s = 5 second sampling interval.

In a similar manner, the final estimate of $\langle k_{y_i}\rangle$ consisted of time averaging expression II-18 for k_{y_i}.

Because of the possibility of finite group velocities, the interval over which k_{y_i} is averaged must be restricted to the time interval that the envelopes from the two stations overlap. This time interval was chosen to be centered on the average peak time (peak time = time of maximum amplitude of the pulsation) of the two stations. Its length was chosen to be 1/2 a period of oscillation of the Pi 2. Thus for a mean peak time at $t=t2+n'/2$ and an averaging interval n' (n'=nearest integer to $\pi/(<\omega_i>T_s)$), $<k_{y_i}>$ is:

$$<k_{y_i}> = (2n'+1)^{-1}(y(1)-y(2))^{-1}\sum_{t=t2}^{t2+n'}[f_i(t,\underline{x}(1))-f_i(t,\underline{x}(2))] \qquad \text{II-22}$$

Thus for the ith component of the magnetic perturbation field, the estimate of the east-west phase delay is $v_{o_i}^{-1} = <\omega_i>/<k_{y_i}>$.

The east-west group delay (v_i^{-1}) is calculated directly from the two envelopes of a pair of stations:

$$v_i^{-1} = \Delta t/(y(1) - y(2)) \qquad \text{II-23}$$

where Δt is the time shift between the two envelopes calculated from the times on each envelope that corresponds to 37% of the maximum amplitude on the rising edge of the envelope.

A discussion of the error in the estimates of phase and group delay must deal with a number of possible sources for the error. The first source concerns how well the time series from two stations are sychronized. We have sought to eliminate this source of error by employing selection

criteria in choosing the stations and events used in the analysis. A second source of error could arise from the filtering technique itself. While it is designed to reduce the noise to signal ratio, in doing so some of the signal is bound to be lost with the noise and some of the noise is bound to remain with the filtered signal. Evaluating this type of error is very difficult, as a result we will simply give estimates of its magnitude which take into account the manner in which the phase and group delays are estimated. A third possible source of error could arise from the proximity of the recording instrument to extraneous sources of magnetic fields such as magnetic anomolies within the earth, powerlines, etc. Since the installation of these instruments was part of a scientific effort designed explicitly to study auroral phenomena, these factors have been previously considered. Thus our main concern in the error estimates is the filtering technique.

Since the group delay is calculated from the time shift of comparable features of the envelopes from two stations, an estimate of the error in this time shift is sufficient to calculate the error in group delay. Figure 10 presents an envelope from simulated data; from this figure, it is apparent that slight deviations in the estimated value of the envelope near its peak will result in slight variations in the estimate of the location of the 1/e time (possible variations of about 5 seconds). Thus it is estimated that the error in the time shift between two stations is

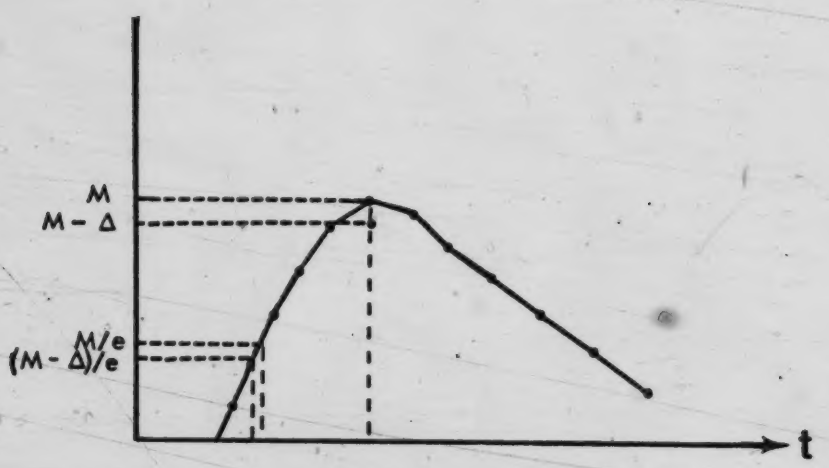

Figure 10: Simulated envelope of a Pi 2 pulsation. The statistical variance in the estimate of the value at the peak, yields a variance in the estimate of the 1/e time. We arbitrarily assume the variance is 5.

approximately 5 seconds. Hence the error in the group delay is: $\Delta v_i^{-1} = 5\text{sec} / (y(1)-y(2))$.

The estimate of the error in the phase delay was slightly more complicated. It was assumed that the only source of error in this measurement was in the estimate of the phase difference (not in the estimate of the frequency or station separation). With this in mind we have that:

$$\Delta v_{oi}^{-1} = \langle\omega_i\rangle^{-1}\Delta\langle k_{yi}\rangle \qquad \text{II-24}$$

The problem reduces to estimating the error in $\langle k_{yi}\rangle$. In order to do this, we note that $\langle k_{yi}\rangle$ is an time average over an interval of length $(n'+1)$. Thus we can treat $\langle k_{yi}\rangle$ as a linear function of $2(n'+1)$ variables $(f_i(t,\underline{x}(j)),$ $t=t2,\ldots t2+n',\ j=1,2)$. If we consider each of these variables to be a random variable and independent of one another, then the variance of $\langle k_{yi}\rangle$ is (see page 73, Jenkins and Watts, 1968):

$$\mathrm{Var}(\langle k_{yi}\rangle) = (2n'+2)^{-1}(y(1)-y(2))^{-2}\mathrm{Var}(f_i(t,\underline{x})) \qquad \text{II-25}$$

As an estimate of the variance of the phase, we assume that it varies inversely with the period of the pulsation:

$$\mathrm{Var}(f_i(t,\underline{x})) = (2\pi T_*/T)^2 \qquad \text{II-26}$$

where T is the period of oscillation $(2\pi/\langle\omega\rangle)$. Using the definition that $(\Delta\langle k_{yi}\rangle)^2 = \mathrm{Var}(\langle k_{yi}\rangle)$ and using equations II-24, II-25, and II-26 we have:

$$\Delta v_{oi}^{-1} = 5\text{sec}/[2(n'+1)]^{1/2}/(y(1)-y(2)) \qquad \text{II-27}$$

This completes the discussion of error associated with the phase and group delays. We now proceed with the actual analysis of the data.

III. Discussion of Results

The three component magnetometer data used in this study came from two main sources: 1) the University of Alberta array consisting of 7 stations located near the auroral oval, and 2) 5 mid-latitude stations from the AFGL array (for a description of these arrays see Rostoker (1982) and Lester et al. (1983)). In addition to these arrays, some data were also obtained from the Energy Mines and Resources (EMR) and U.S. Standard Observatories arrays. The list of these stations and their centered dipole coordinates is given in table 1 and some of the stations are plotted in figure 9. A word about the form and usage of the data is in order.

The EMR and U.S. Standard Observatory data were stored in an analog format on microfilm and photographs of these chart recordings were used to determine the latitudinal and longitudinal location of the wedge currents (see figure 2) for a few of the events. The AFGL data were recorded in a digitized format on magnetic tape and used 1) to determine the longitudinal location of the wedge currents and 2) to look at the spatial variation of Pi 2 frequency and phase delay. The U of A data were also recorded on magnetic tape in a digitized format and were used 1) to determine the latitudinal location of the substorm enhanced electrojet and 2) to look at the spatial variation of Pi 2 frequency, phase delay, envelope parameters, group delay, and power distribution. The digitized data used in this study had a

sampling rate of 5 seconds.

The data are presented as a statistical ensemble of the events used in this study. The advantage of the statistical presentation over an event by event presentation is that data trends are more readily discernible to the eye. An event by event analysis is advantageous when examining exceptional events that do not fit into the general pattern or for illustrating the important characteristics of a typical event. First of all I will work through the analysis procedure for a typical event and subsequently illustrate the statistical results for all of the events. I will then present a statistical study of frequency verses latitude. Finally, I will analyze the latitudinal dependence of Pi 2 power using data from Samson and Harrold (1983).

A. Analysis of Day 281, 1978

The event chosen on day 281,1978 has an onset at 11:02 UT as can be seen in figure 11. This figure depicts a magnetogram for the U of A array. For convenience, an arbitrary baseline has been removed from this data. The actual baseline from which the perturbation fields were calculated was taken at one minute before substorm onset (i.e. at about 11:01 UT). Thus at Providence, the H component baseline was 73 nT; at Hay River, the H component baseline was 65 nT, etc. The H and Z perturbation fields at Leduc, Fort McMurray, Fort Chipewyan, and Uranium City at 11:04 UT are plotted in figure 11d. On the basis of the

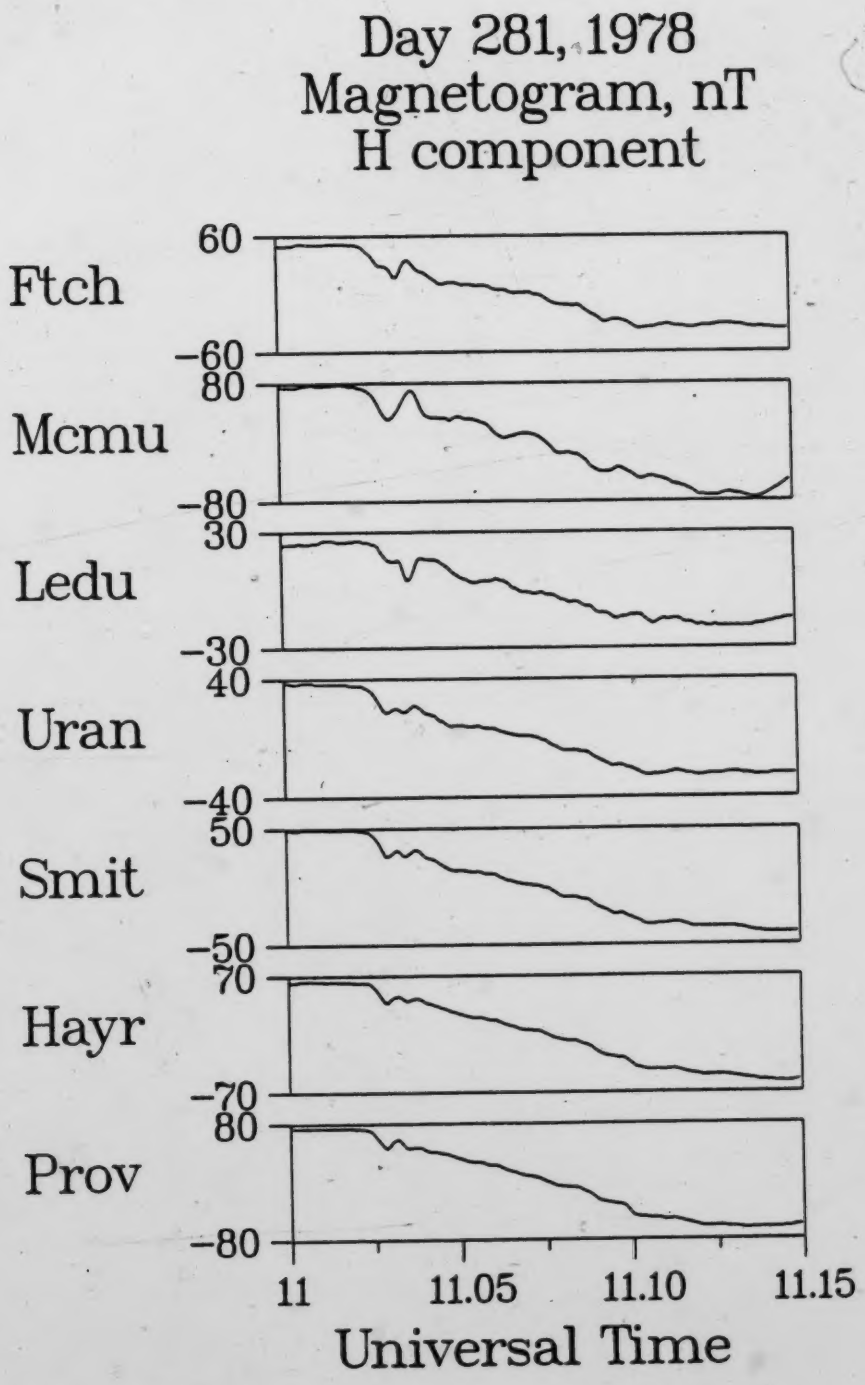

Figure 11a: High latitude data from the U of A array.
(north-south component)

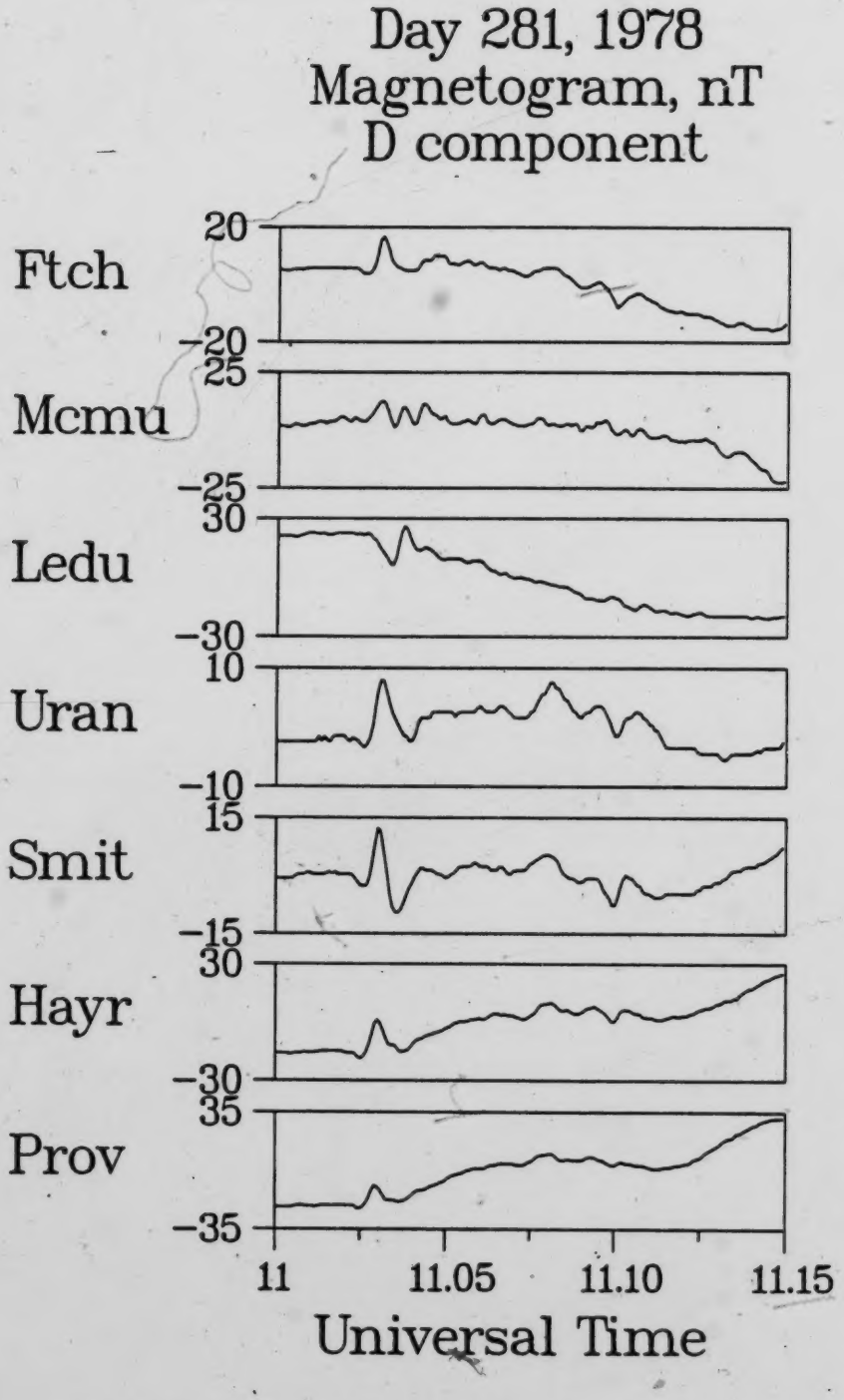

Figure 11b: High latitude data from the U of A array.
(east-west component)

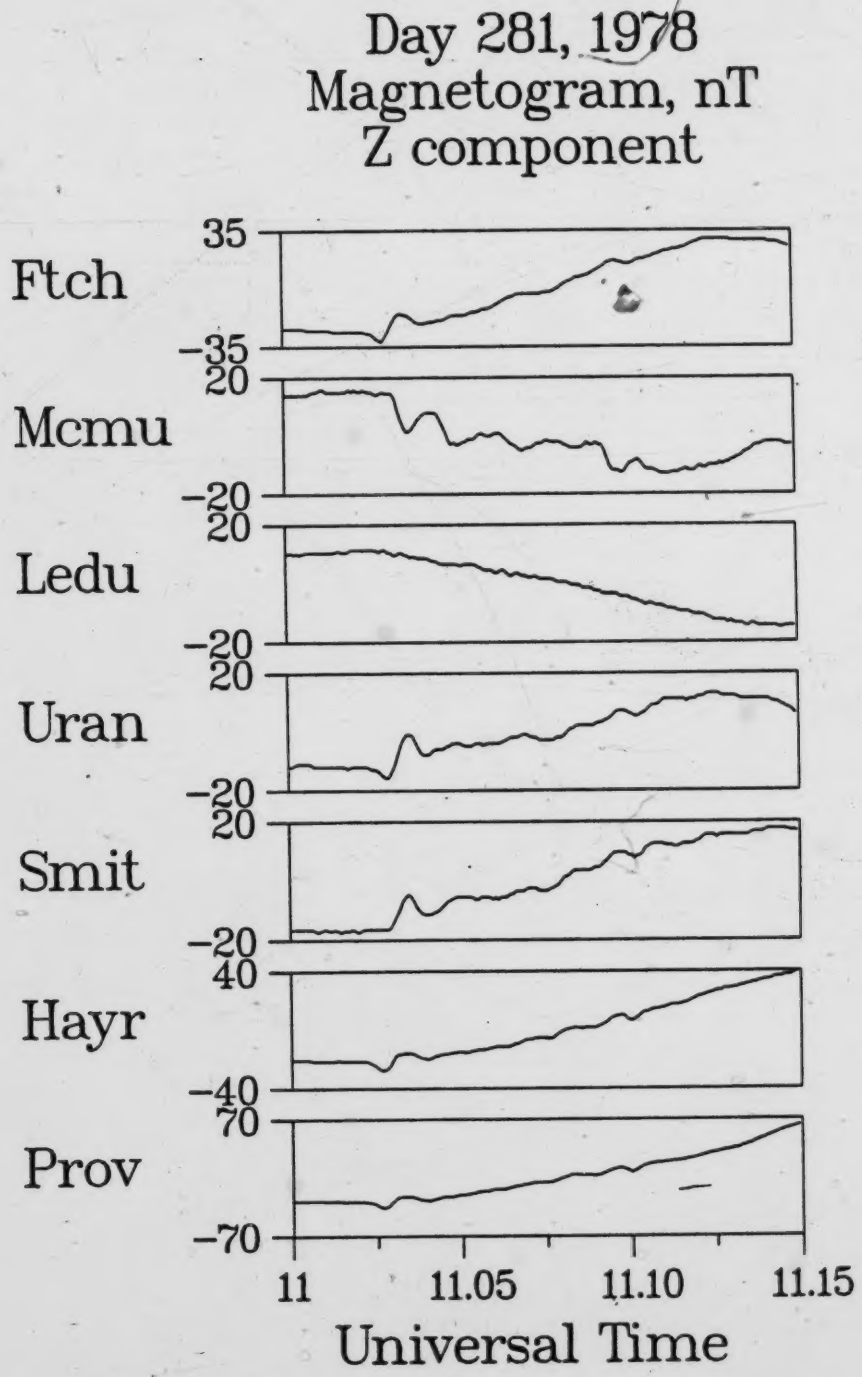

Figure 11c: High latitude data from the U of A array. (vertical component)

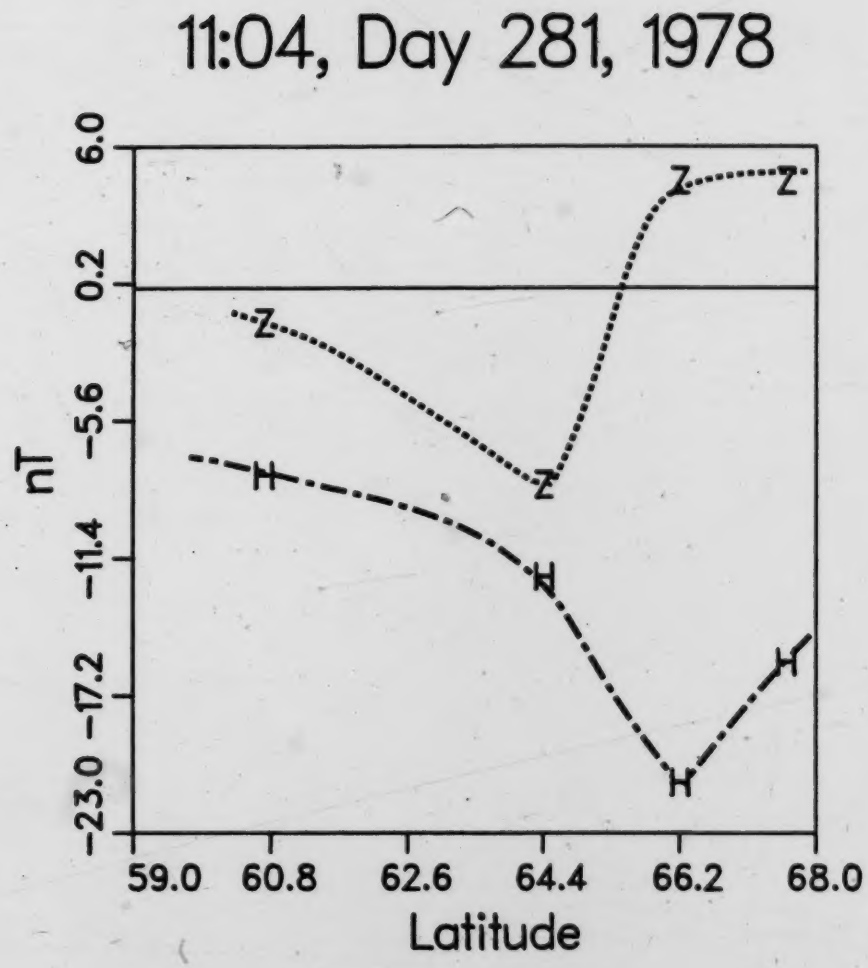

Figure 11d: Perturbation field at 11:04 Universal time for four U of A stations. The change of sign of the Z component and the minimum in the H component places the substorm electrojet near 65.5 degrees.

change in sign of ΔZ and the minimum in ΔH, the latitude of the center of the substorm enhanced electrojet was estimated to be 65.5 °N.

Figure 12 illustrates the AFGL array stations. Because of the data gap at Camp Douglas (Cds), this station was not used. The baselines for the calculation of the perturbation fields were estimated in the same manner as for the U of A array. The H and D perturbation fields from Rapid City, Newport, and Victoria (the magnetogram for Victoria was recorded on microfilm but is not shown) at 11:04 UT are plotted in figure 12d. Using the D component, the longitudinal location of the wedge current system was found to be west of the station coverage (i.e. less than about 290 degrees as indicated in figure 9). Had data been available from Sitka (276 ° longitude), a more accurate estimate of this position could have been made.

Using the filtering process outlined previousy,we obtain the highpass filtered data shown in figures 13a,b, and c and the H component of the 'pure state' pulsations shown in figure 14. Figures 15 and 16 show the amplitude and frequency (for the pure states) as functions of time. At first glance the frequency calculations appear to fluctuate wildly, however, during the time intervals that the amplitude function is near its maximum, the frequency function is fairly constant. With this in mind, we limited our use of frequencies to a time interval near the amplitude maximum. Table 2 show a condensed output from the analysis

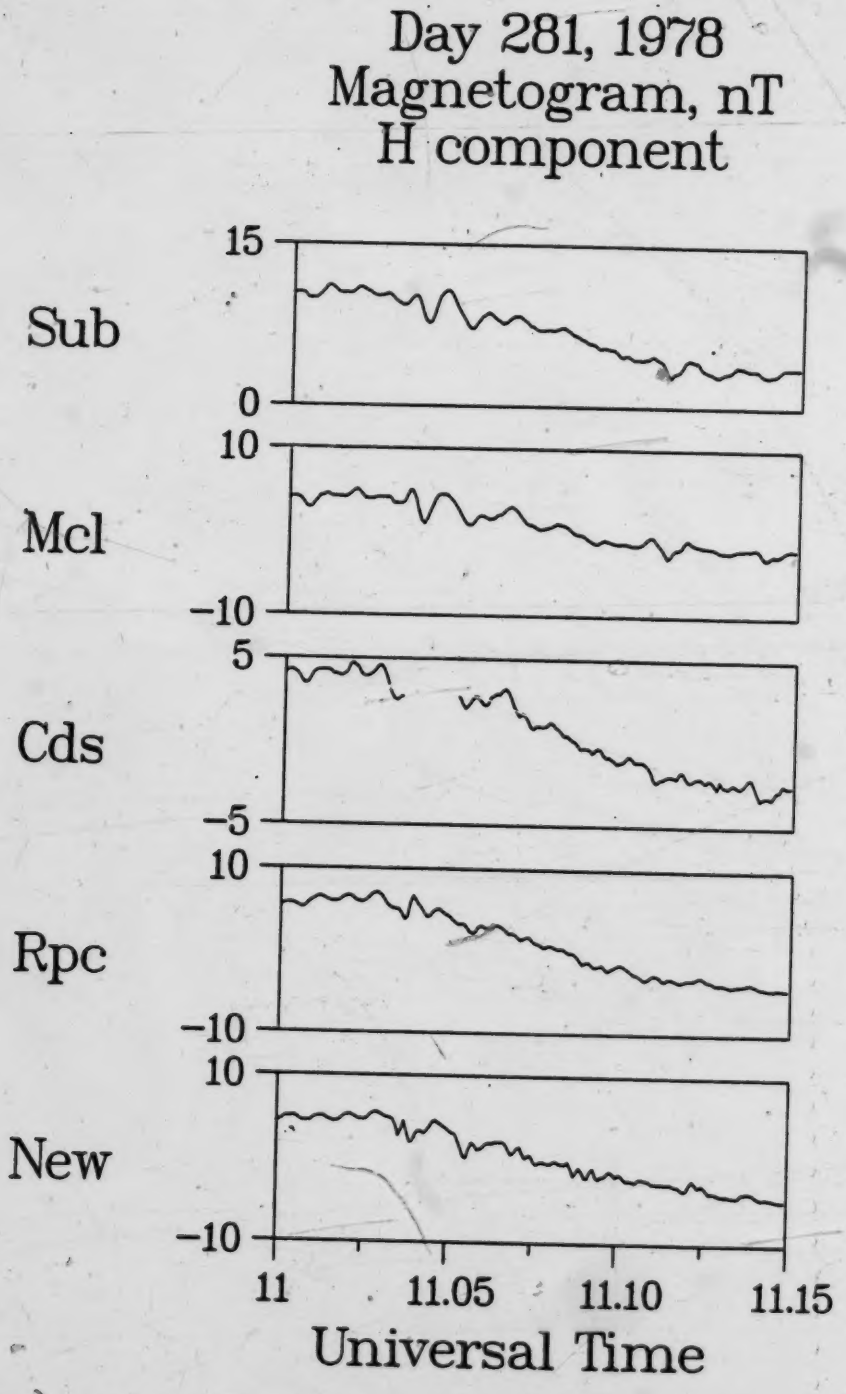

Figure 12a: Mid-latitude data from the AFGL array. (north-south component)

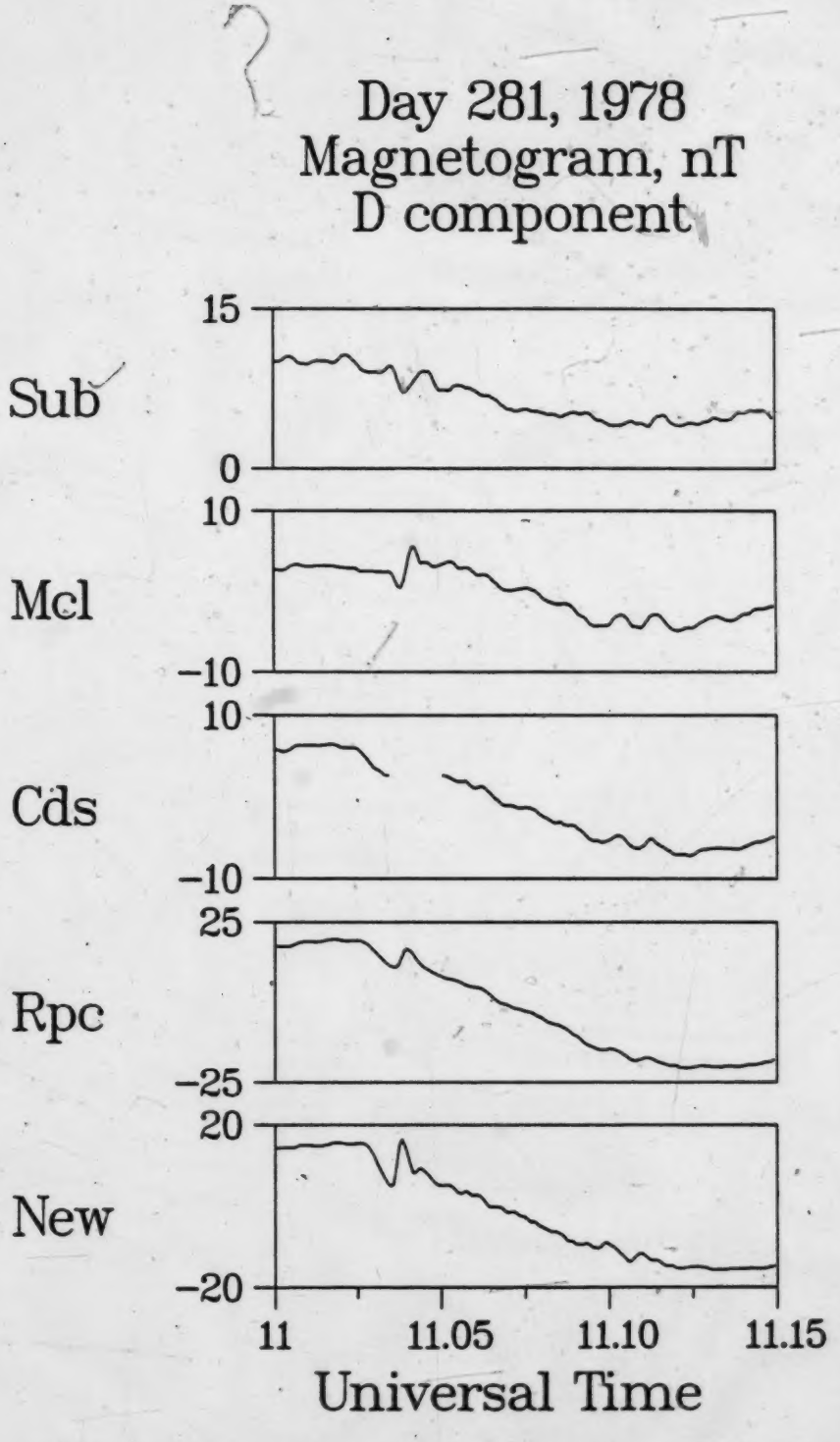

Figure 12b: Mid-latitude data from the AFGL array. (east-west component)

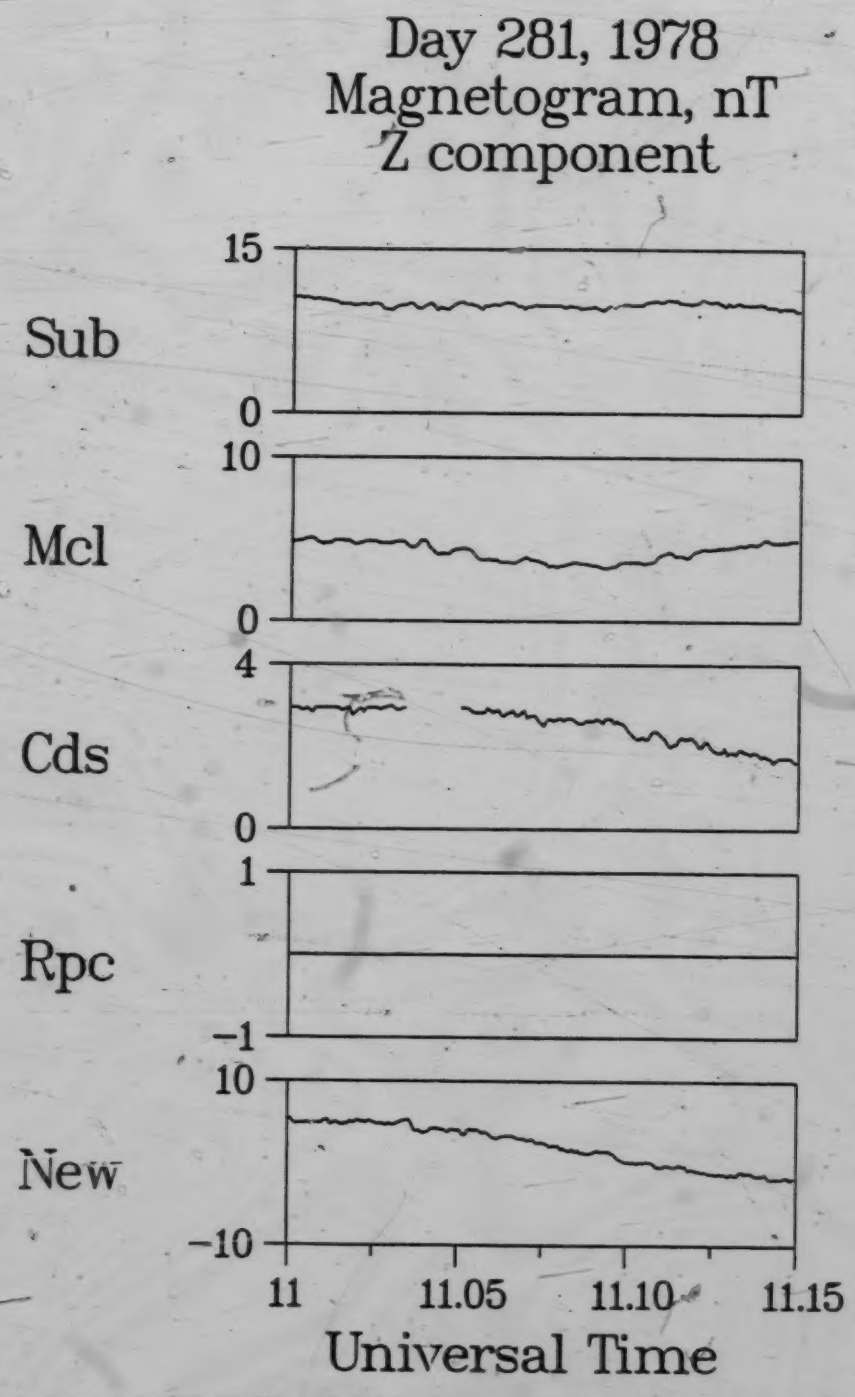

Figure 12c: Mid-latitude data from the AFGL array. (vertical component)

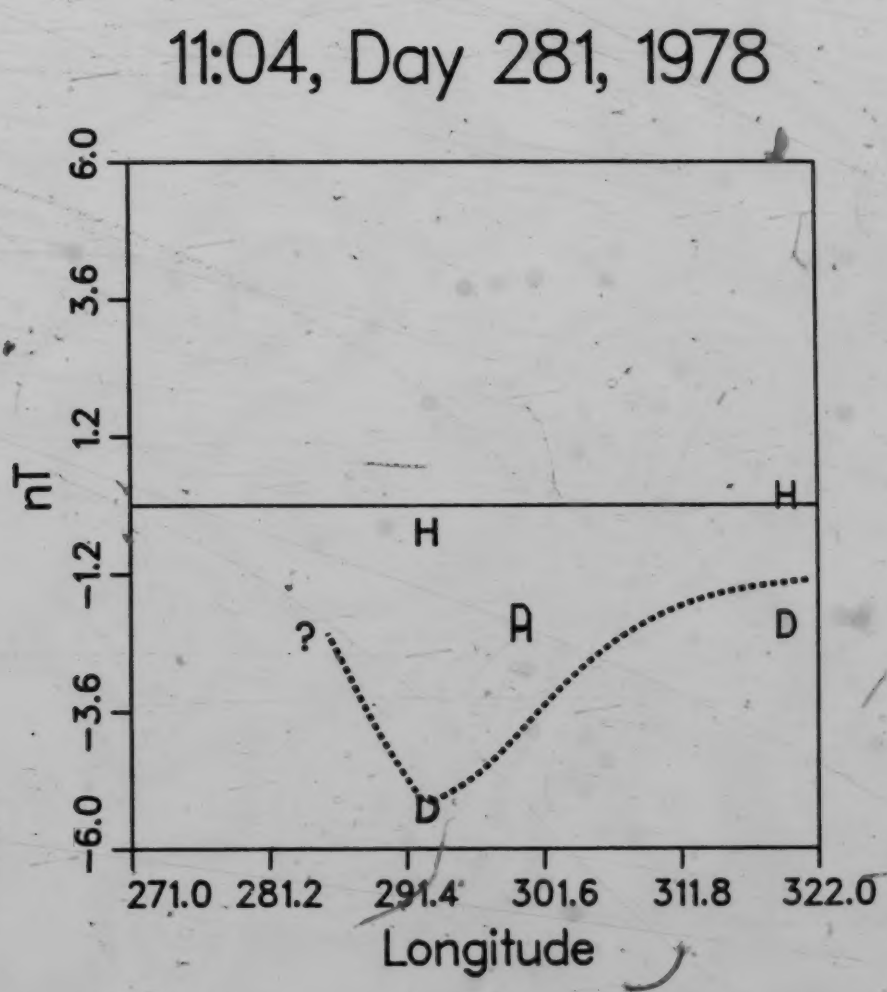

Figure 12d: Perturbation field at 11:04 Universal time for Vict, New, and Rpc. The curve represents an approximate fit to the D component data. The change of sign of the D component occurs to the west of the station coverage.

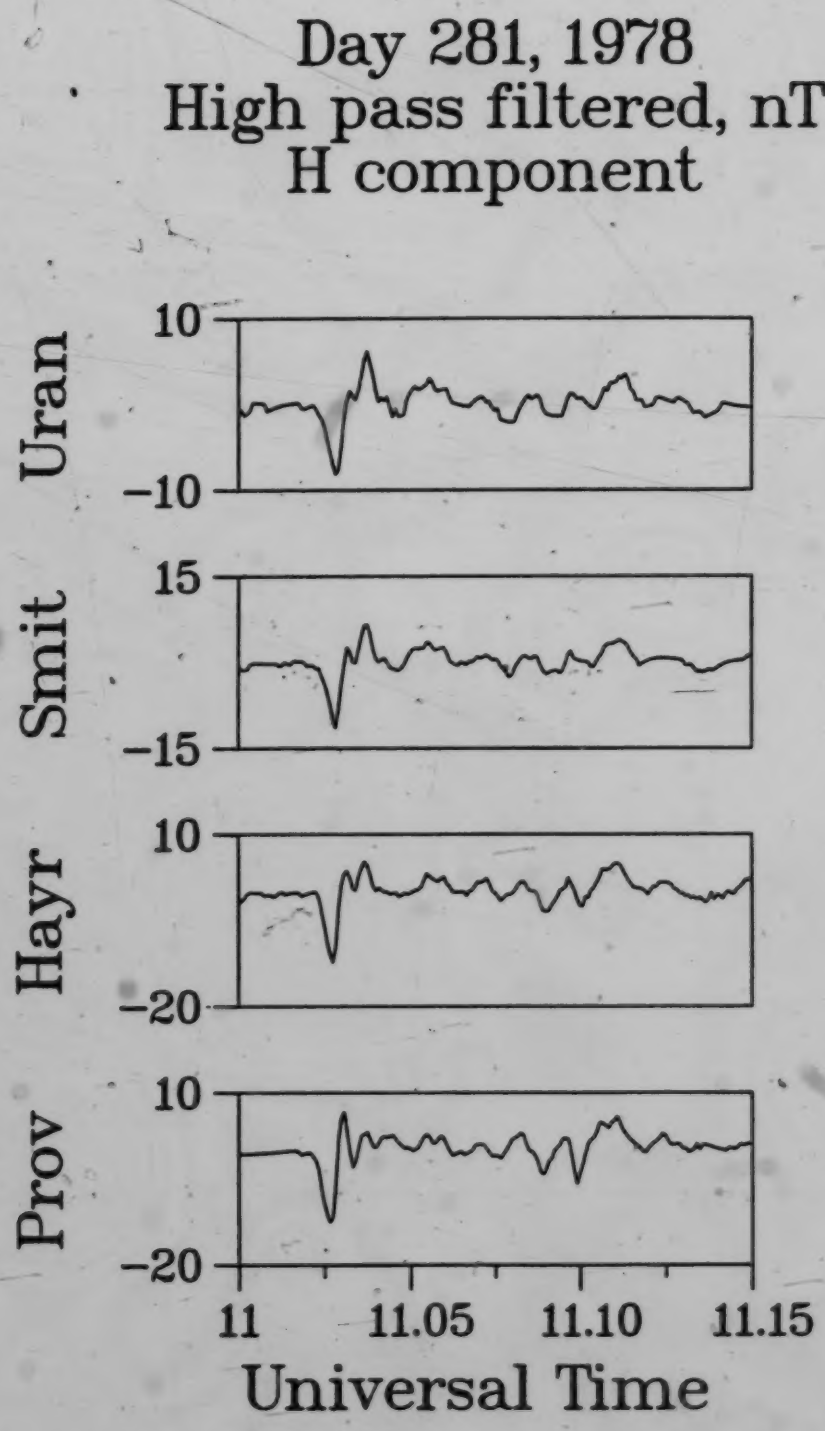

Figure 13a: High latitude filtered data from the U of A array.

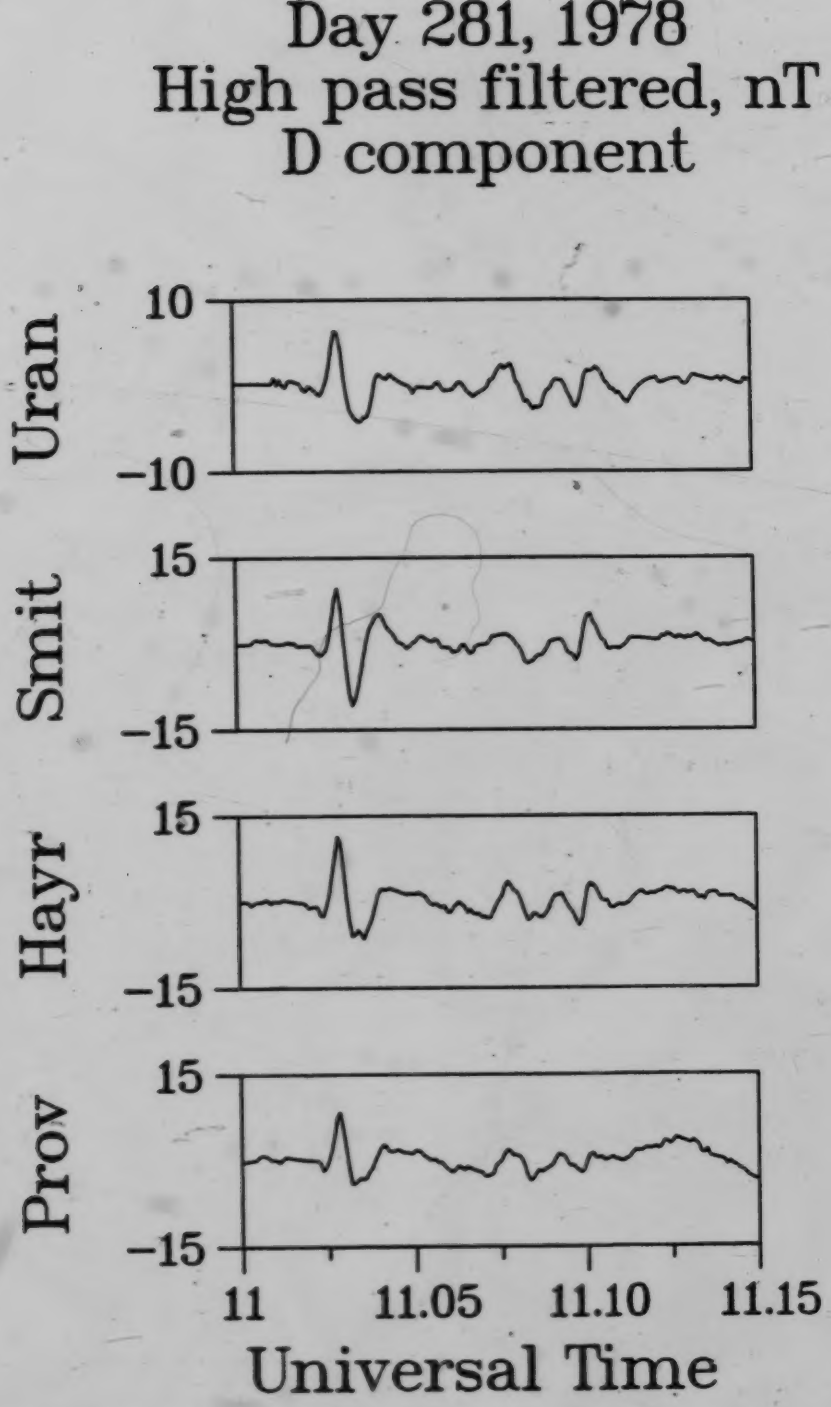

Figure 13b: High latitude filtered data from the U of A array.

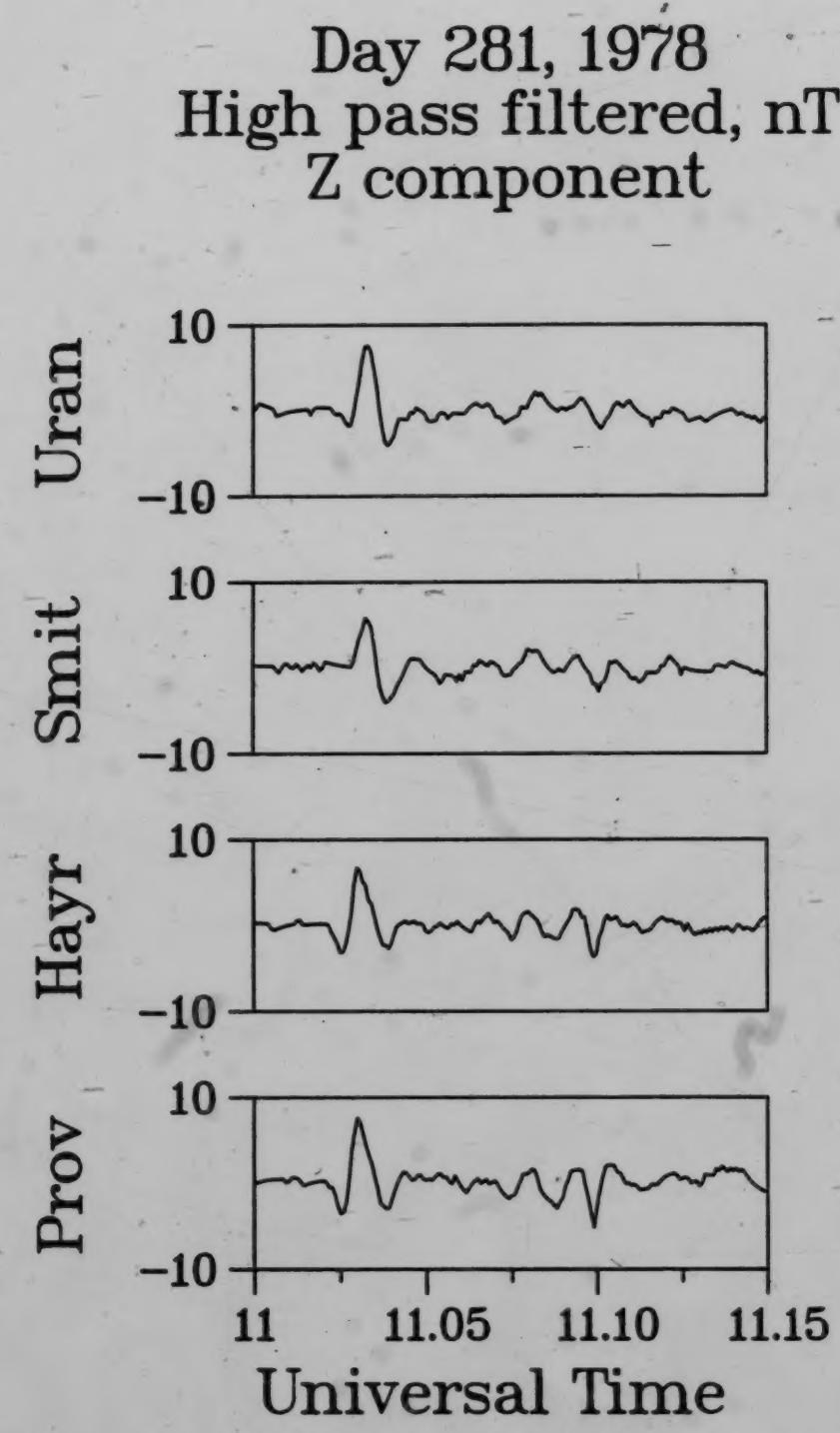

Figure 13c: High latitude filtered data from the U of A array.

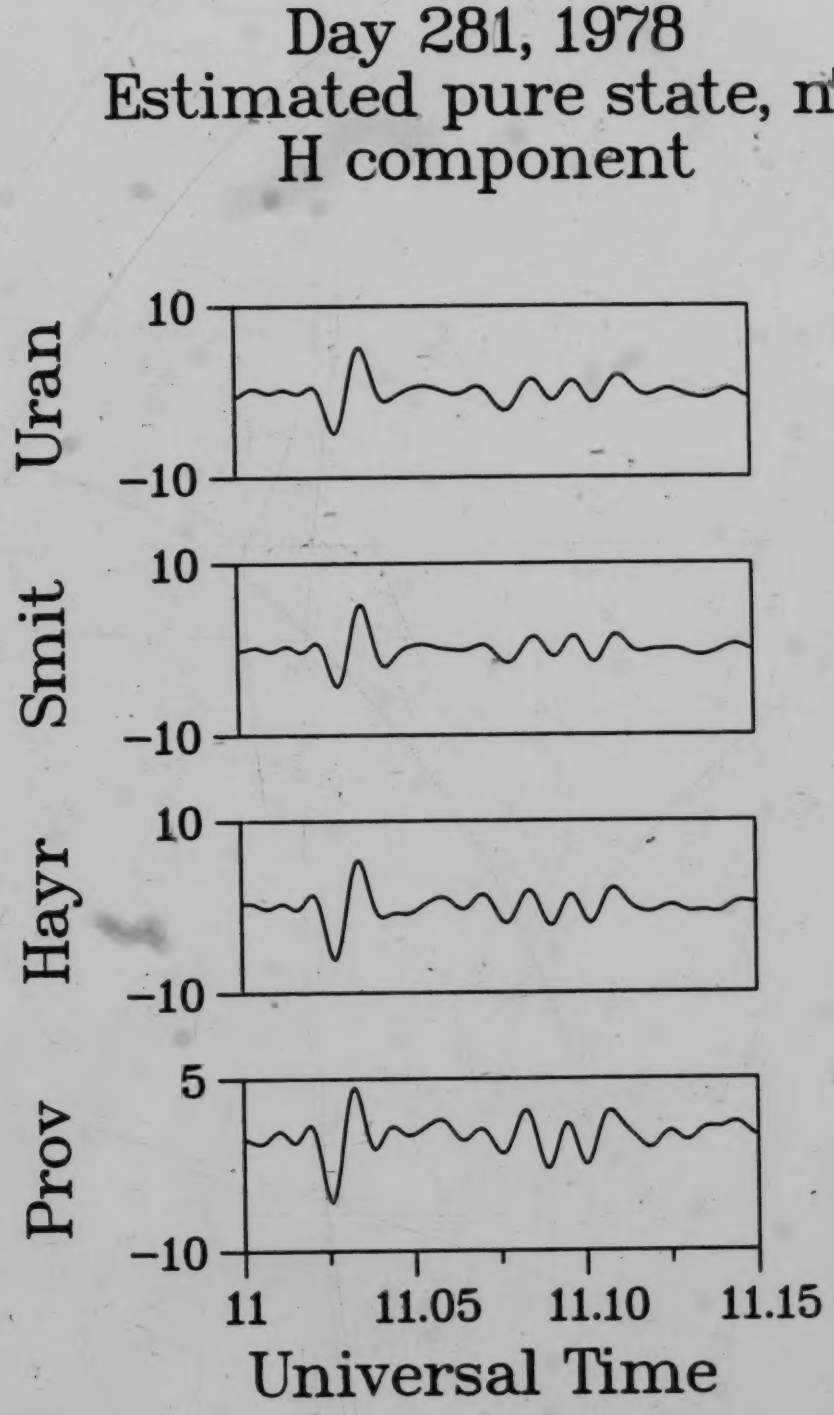
Day 281, 1978
Estimated pure state, nT
H component
Uran
Smit
Hayr
Prov
10
-10
10
-10
10
-10
5
-10
11
11.05
11.10
11.15
Universal Time

Figure 14

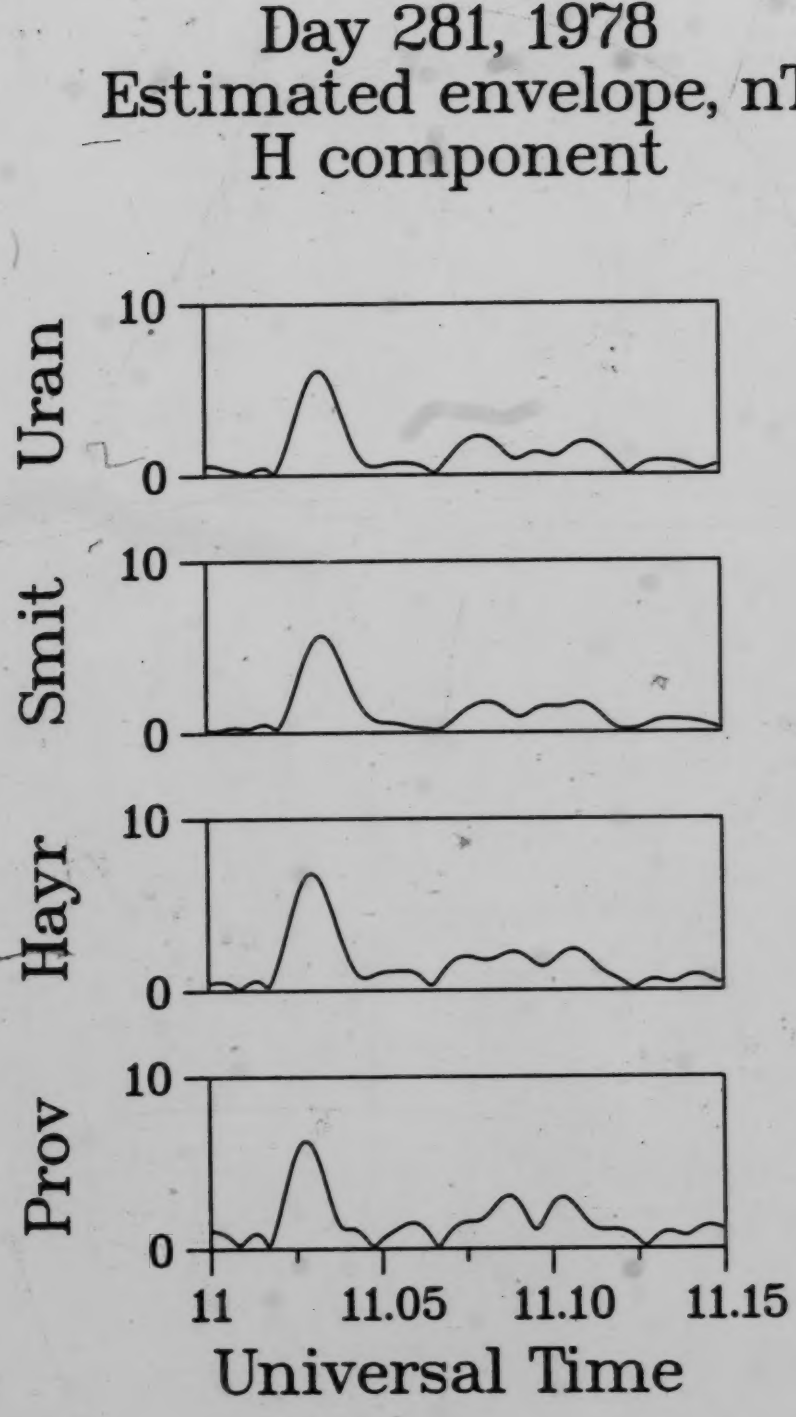
Day 281, 1978
Estimated envelope, nT
H component
Uran
Smit
Hayr
Prov
10
0
11
11.05
11.10
11.15
Universal Time

Figure 15

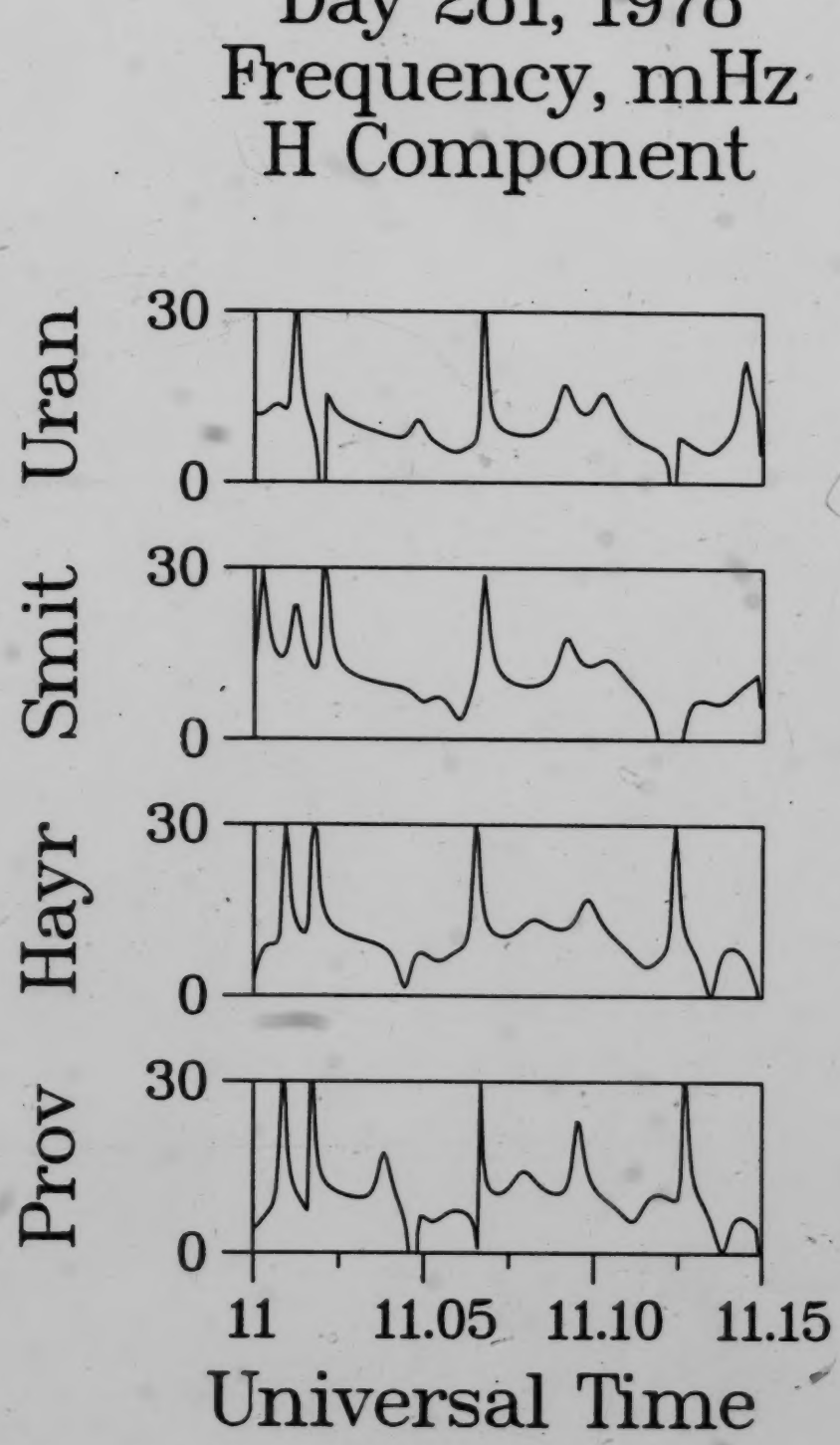
Day 281, 1978
Frequency, mHz
H Component
Uran
Smit
Hayr
Prov
30
0
11
11.05
11.10
11.15
Universal Time

Figure 16

Table 2: Results of Analysis of Day 281, 1978

Station	Rise time (sec)	Fall time (sec)	Freq. (mHz)	Phase delay sec/° long	Group delay sec/° long
Prov	52.9	52.6	10.4	3.7	4.0
Hayr	53.6	63.2	10.2	1.8	3.7
Smit	54.9	66.5	10.4	0.3	0.0
Uran	56.4	58.5	9.5	-	-

program illustrating the results of the various calculations. It is these values of phase delay, frequency, group delay , rise time, and fall time that are used in the statistical ensemble plots.

B. Phase Delay

We now turn to the analysis of the statistical data from the events listed in table 3 (satisfying the 5 selection criteria previously mentioned). The phase delay (k_y/ω) for Pi 2 type wave trains has been measured by Mier-Jedrzejowicz and Southwood (1979). These researchers found that both H and D components exhibited predominantly negative (westward) phase delays. These measurements were consistent with those of Baranskiy et al. (1980), Lester et al. (1983,1984), and Samson et al.(1985). Figures 17 and 18 show the phase delay (k/ω) results using the east - west high latitude chain of the U of A array. The results using the D component show a random scattering of data points to the west of the substorm center and a slight tendency toward

Table 3: Events used in the Phase study

Day	Year	Onset Time(UT)
82	1978	5:02
59	1979	8:07
252	1977	6:28
281	1978	11:02
114	1977	6:29
177	1977	9:15
43	1978	7:00
365	1977	8:11
364	1977	8:30
232	1976	5:52
243	1976	7:22
36	1979	5:18
39	1979	9:40
298	1978	7:37
351	1978	3:33
335	1977	4:13

eastward propagation to the east of center. The corresponding H component data shown in figure 18 illustrate a far more ordered picture. To the west of the substorm center there is a tendency toward westward propagation with a mean phase delay of about -1 second / degree longitude (that is, v_o = 42 km / sec westward). To the east of center, there is a strong tendency toward eastward propagation with a mean phase delay of about +1.2 seconds / degree longitude (i.e. v_o = 35 km / sec eastward).

The tendency of the D component data to exhibit a larger amount of scattering than the H component has also been observed at mid-latitudes by Lester et al. (1983) and Samson et al. (1985). It is possible that this observation may be due to how the Pi 2 power is distributed between the H, D, and Z components. If the H component has more of the

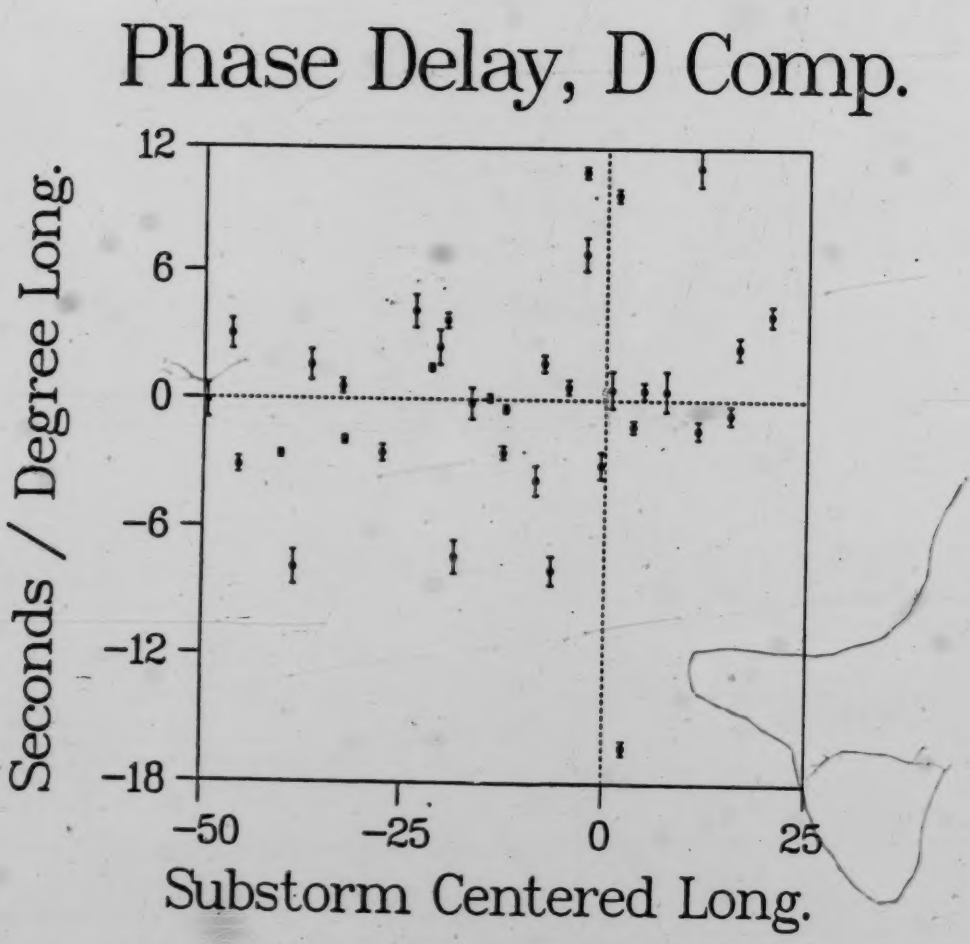

Figure 17: East-west phase delay obtained using the D component of the U of A array data.

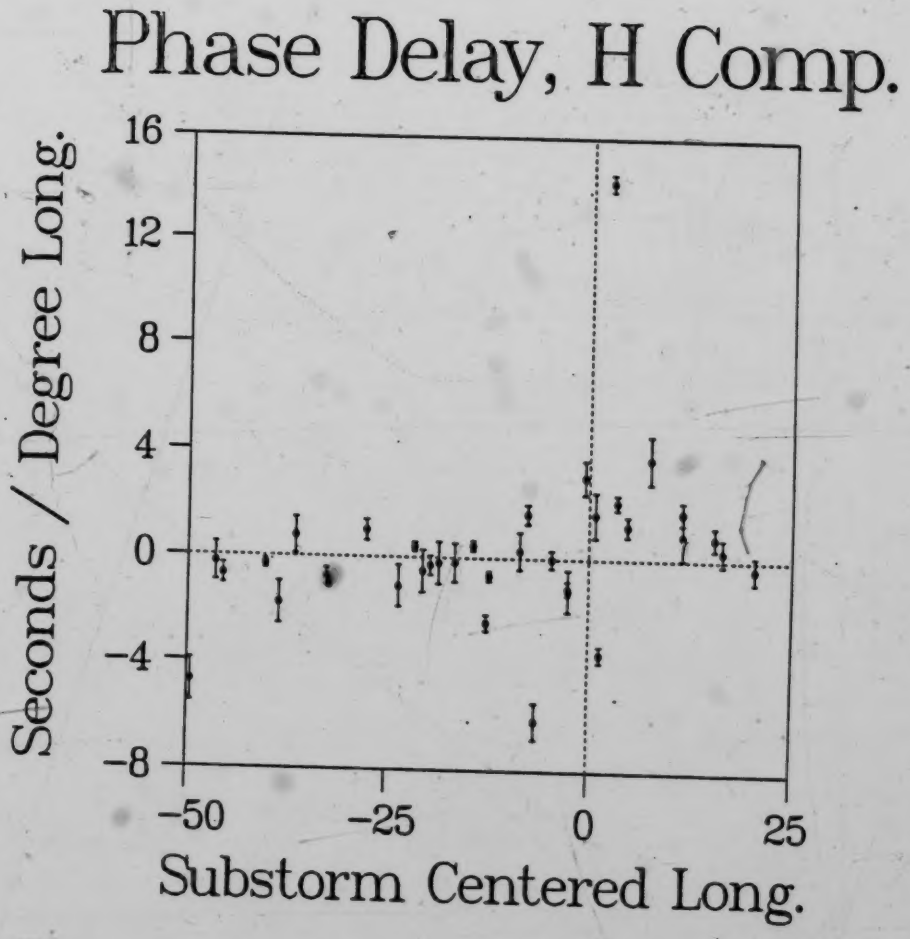

Figure 18: East-west phase delay obtained using the H component of the U of A array data.

Pi 2 signal then the D component, and if we consider the background noise to be isotropically distributed, then it is reasonable to expect that the component with the highest signal to noise ratio will yield the best filtering results and hence yield the most consistent phase delay results. To test this conjecture, the ratio of the maximum Pi 2 amplitude in the D component to that in the H component is calculated for each station (from the east-west part of the U of A array) of the 16 events used. The resulting 52 measurements are plotted in a histogram in figure 19. It is apparent that the D component Pi 2 amplitude is typically about 40% of that of the H component. Hence it is not surprising that H component yields more consistent phase delay results.

Figure 20 shows the phase delay results from Samson et al. (1985) using the east-west mid-latitude AFGL array. Unlike the high latitude results, there is no change of sign of the phase delay near the wedge center. However there may be evidence for an effective eastward propagation in the region from 25 to 50 degrees east of the wedge center. It is difficult to say whether or not this region is correlated with the eastward propagation region observed at high latitudes. More data are required in the intervening region in order to conclusively solve this question. Nevertheless, the lack of predominantly westward propagation at high latitudes suggests that there is a latitudinal dependence to the longitudinal wave number that must be taken into

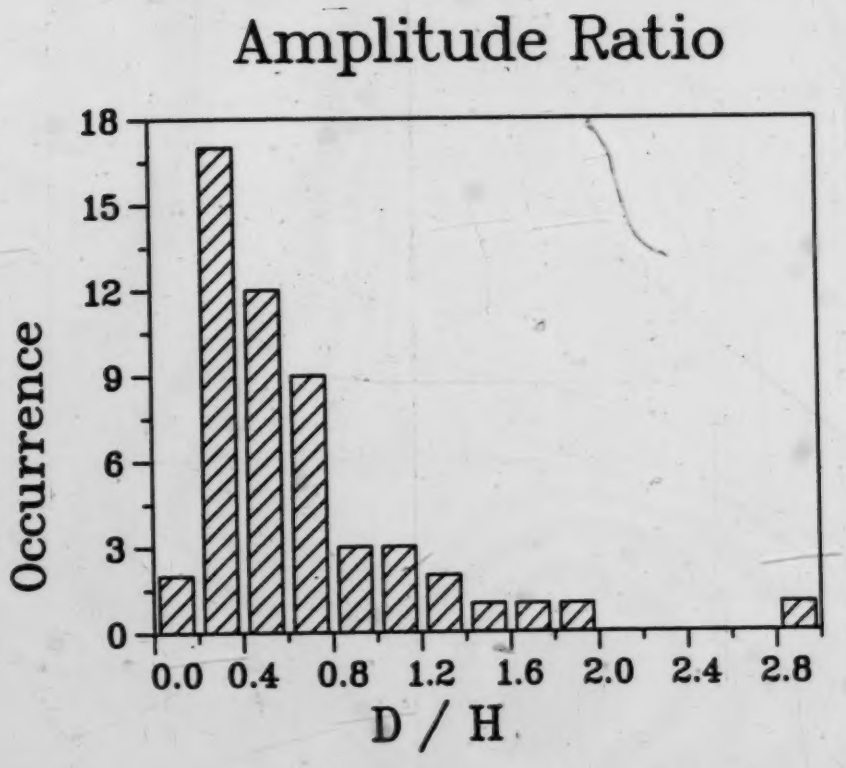

Figure 19: Ratio of the maximum amplitudes of the D and H components for all stations from the 16 events.

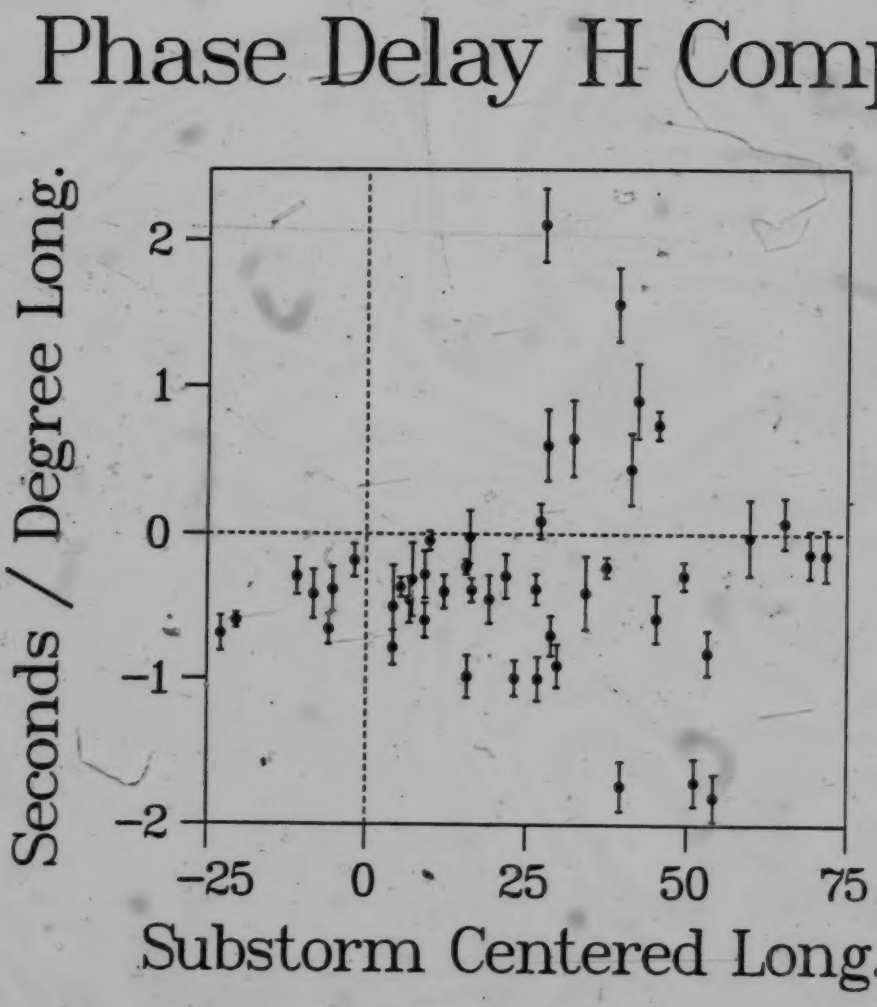

Figure 20: East-west phase delay obtained using the H component of the AFGL array data. From Samson, et al., 1985.

account. This aside, the effective phase delay observed at this latitude is approximately 0.5 seconds / degree longitude westward.

A comparison of figures 18 and 20 shows that at high latitude, there is more scatter in the data west of the breakup than east whereas at midlatitudes, this trend is reversed. At high latitudes, this could possibly be explained by the superposition of the westward travelling surge (for a description of this feature, see Tighe and Rostoker (1981)) on the magnetic perturbation measured by stations west of the breakup. The absence of a similar phenomena to the east of the breakup would yield an asymmetry in the scatter of the data. Also, it has been suggested by Samson (1982) that there may exist a low power eastward propagating Pi2 in the region south of the higher power westward propagating Pi2 and west of the breakup center. This would also explain the higher scatter and the few eastward phase velocity measurements in this region.

At midlatitudes, the observed signal attenuation with distance from the wedge center (see for example, fig. 18 in Samson, 1983a) implies that far to the east of the breakup, the signal power is very low. As a result it is difficult to accurately measure the phase difference of two signals. Hence far to the east, more scatter in the data is expected.

In figure 21 I have attempted to contour the longitudinal wave number k_y associated with the phase delay data of figure 18. I acknowledge that the data set is too

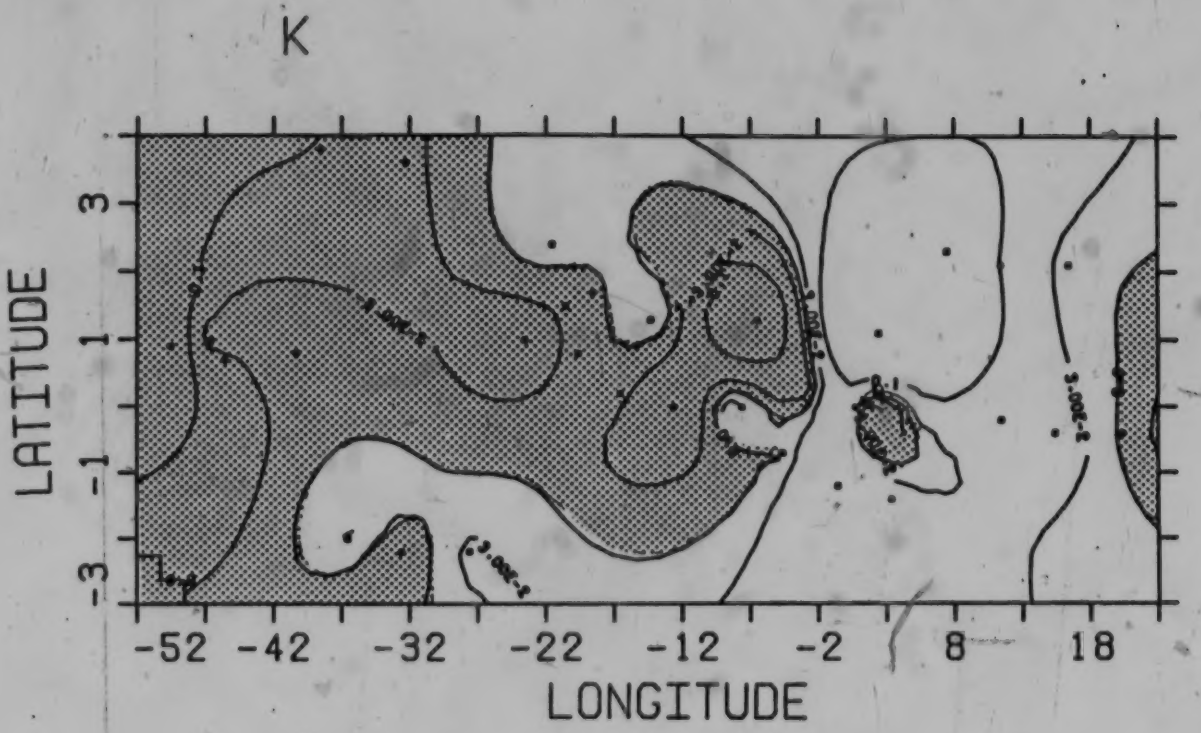

Figure 21: Contouring of the east-west component of the propagation vector K (radians/degree longitude) for the H component data. Shaded (clear) areas correspond to westward (eastward) regions of propagation.

small to draw any concrete conclusions, but there may be evidence of eastward propagation east of center and south of the power maximum. Samson (1983) acknowledges that there may indeed be an eastward propagating component to the west and south of the substorm center. Also there is evidence for westward propagation in the region around 0 degrees latitude and to the west of the longitudinal center.

C. Envelope Parameters

Figures 22 and 23 illustrate the envelope parameters for the high latitude data. The rise time refered to in figure 22 pertains to the time interval from the envelope peak to the point where the envelope falls to 1/e of its maximum on the rising part of the signal. It is apparent from this figure that for the events used in this study, there is a characteristic rise time of about 70 seconds. Since the period of oscillation of the Pi2's is generally greater than this characteristic time, any theory describing the Pi2 as a resonant phenomena is subject to question since it is doubtful that a resonance can be set up in less than one period of oscillation. This rise time is comparable to that observed at mid-latitudes (Samson et al., 1985). This correlation indicates that occurrences at high latitudes are strongly correlated to those at mid-latitudes and hence occur on the same time scale. This is not a trivial statement. It is strongly suggestive that the transient response model of figure 8 is the proper substorm current

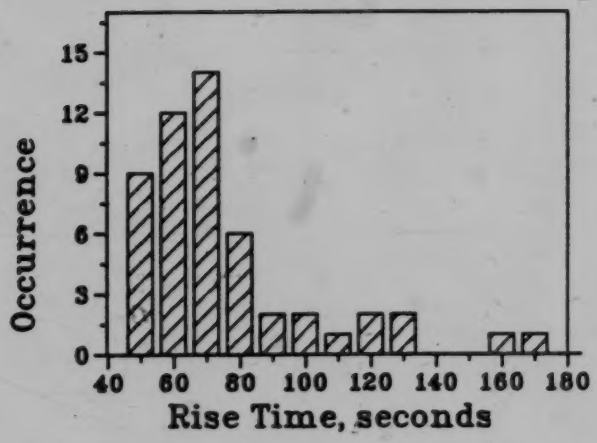

Figure 22: Histogram of envelope rise times for 16 events.

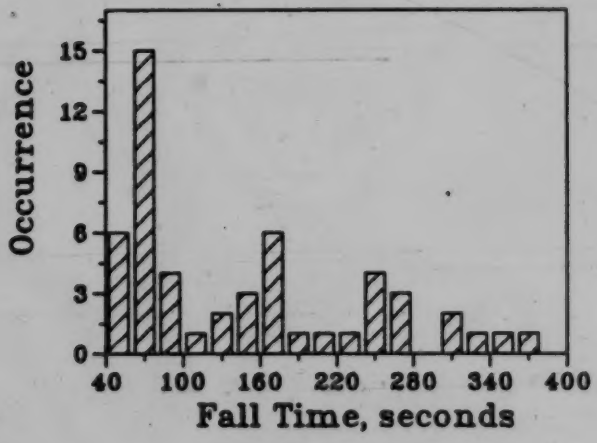

Figure 23: Histogram of envelope fall times for 16 events.

structure.

Figure 23 shows the corresponding fall times to accompany those of figure 22. Although the data is considerably more spread out than that of the previous figure, there does seem to be a peak at approximately 70 seconds. Rostoker (1967a) has previously noted the existence of such a short fall time for some Pi 2 events (which he has termed 'one pulse events'). Figure 24 is a histogram of the envelope width (= rise time + fall time). There seems to be a quasi-periodic structure with peaks at 140, 230, and 390 seconds. A second look at figure 23 indicates the source of this periodicity. The fall time histogram has peaks at 70, 170, and 250 seconds. This may imply that there exists prefered fall times which are roughly periodically spaced (at intervals of ~90 seconds). A reasonable explanation for this could not be found.

D. Group Delay

The analysis of the envelopes is continued in figures 25 and 26 with a comparison of envelopes of adjacent stations via the group delay. Figure 25 illustrates the results at high latitude from the events of the present study while figure 26 illustrates the observations at mid-latitudes from a study by Samson et al. (1985). Figure 26 indicates that there is little evidence for group propagation at midlatitudes. The same cannot be said at high latitudes. Figure 25 appears to indicate that west of the

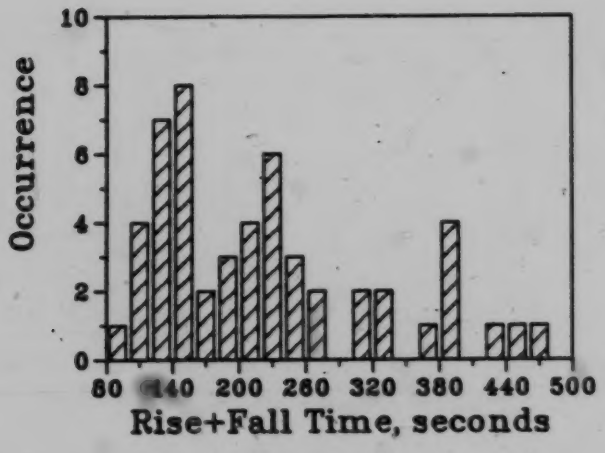

Figure 24: Histogram of envelope widths for 16 events.

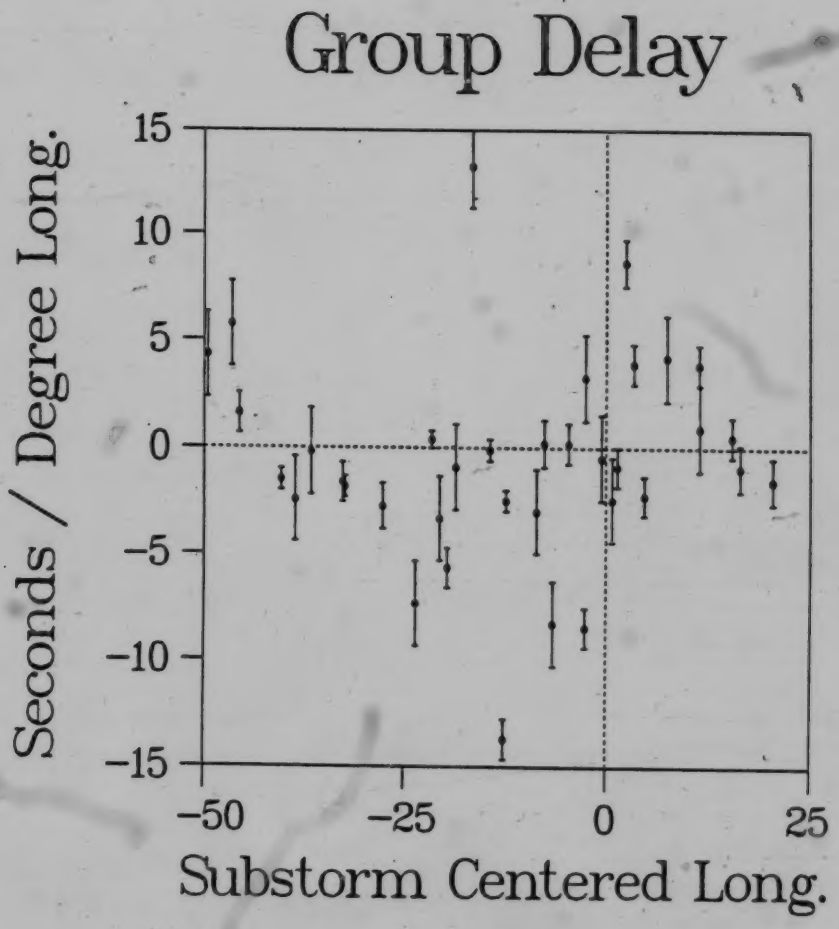

Figure 25: Measurement of the group delay obtained using the H component of the high latitude data from the U of A array.

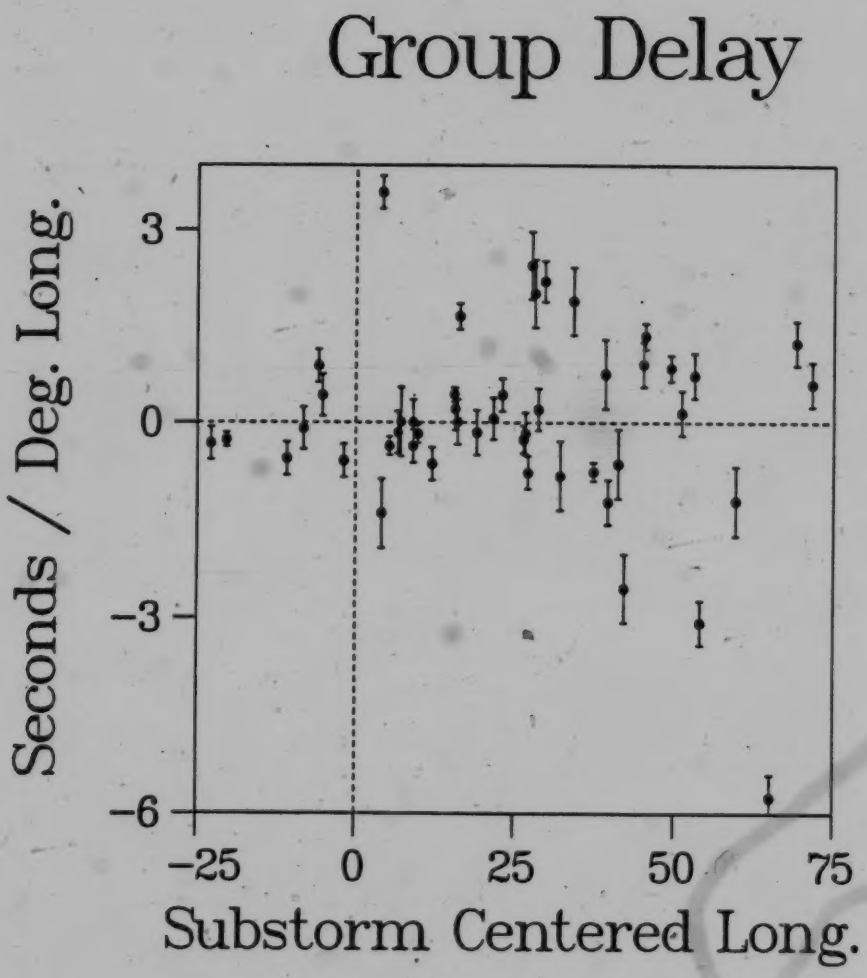

Figure 26: Group delay obtained using the H component of the mid-latitude data from the AFGL array. From Samson, et al., 1985.

wedge center, westward group propagation is observed and east of the wedge center eastward group propagation is recorded. This latitudinal dependence of group delay may be interpreted qualitatively using the transient response model of figure 8. It should be recalled that in the region of the auroral arc, an analogy was drawn between this current structure and a pair of magnetic solenoids. It was also mentioned that it is unlikely that the field perturbations associated with these solenoids would be recorded at midlatitudes. This is because the magnetic field signatures of the downward field aligned current north and south of the arc cancel the field signature of the upward field aligned current within the arc. This cancelation only occurs in areas sufficiently far north or south of the arc (of course, near the arc the magnetic field signatures of the upward and downward field aligned current reinforce one another).

In light of the group propagation data, it seems logical to associate the group propagation with the movement of the solenoid-like current structure. High latitude stations would thus see the propagation of this structure while the midlatitude stations (which see very little of the solenoid-like current signature compared to to the signature of the Hall closure current system) would not.

An analogy with the westward travelling surge (for a description of this phenomena see Tighe and Rostoker, 1981) should be apparent. The difficulty with this analogy is the following. From figure 25, west of the current wedge center,

the group delay is mainly greater than -5 sec/degree longitude (i.e. less than 5 in absolute value). This would imply a westward velocity of greater than 8 km/second. Tighe and Rostoker (1981) however, found that the maximum speed of this phenomena was about 3 km/second. This discrepancy indicates that our measurement of group delay is not a direct measurement of the velocity of the westward travelling surge, but includes some other phenomena. A logical explanation for, or description of, this phenomena could not be found.

There is one final observation worth noting in figure 25. It appears as though there is a periodic spatial variation in the group delay. Not only is there a change in sign near 0 degrees longitude, but there may also be evidence for another change in sign near -40 degrees. There is no apparent explanation as to why such a periodic dependence would be observed.

E. Frequency

The study of the spatial dependence of pulsation frequency is motivated by the predictions of both the transient response model (Kan et al., 1982) and the resonant field line model (Kuwashima and Saito, 1981) that the frequency should decrease with increasing breakup latitude. This correlation between frequency and breakup latitude has already been analyzed (Kuwashima and Saito, 1981). What I intend to examine is the variation of frequency from station

to station within a number of events.

The events used in this study were chosen using a slightly different criteria than those used in the first part of this analysis. In this section, events were required to have relatively small onsets at high latitudes in order that the error in the estimated frequency be about the same for each of the stations used (the error in the estimated frequency varies depending on the size of the onset -as discussed in the previous chapter). Table 4 shows the events used in the frequency-latitude study. Shown in figure 27 are the results from the individual events. It can be seen that in most events there is evidence for an increase in frequency with decreasing latitude. This trend is most evident in the events with the smallest onset - namely day 82, 1978 and day 90, 1979. Figure 28 shows these results assembled in a statistical manner. There is little evidence of a trend present in this figure because varying ionospheric and magnetospheric conditions makes some form of normalization necessary. The first normalization process used was to locate all the stations relative to the substorm electrojet. The results of this normalization are shown in figure 29. The frequency-latitude trend begins to become apparent but still more normalization is necessary. The second normalization process involves adjusting the measured frequency at each station to the mean frequency over all the stations used in the event. Hence the result of the two normalizations is shown in figure 30. This figure shows that

Table 4: Events used in the Frequency study

Day	Year	Onset Time(UT)
82	1978	5:02
59	1979	8:07
281	1978	11:02
114	1977	6:29
177	1977	9:15
364	1977	8:30
36	1979	5:18
90	1979	7:35
198	1978	9:40

the frequency increases slightly with distance south of the substorm enhanced electrojet. The frequency variation seems to be limited to a region within 4 degrees of the substorm enhanced electrojet.

Previous studies (Kuwashima and Saito, 1981; Olson and Rostoker, 1977; Rostoker, 1967a) examining the dependence of frequency on latitude have generally drawn two conclusions. The first is that the dominant frequency associated with an event varies inversely with the latitude of the breakup (i.e. the latitude of the substorm enhanced electrojet) (see for example, Kuwashima and Saito, 1981). This is logical in light of the fact that the field lines at higher latitudes are longer and hence the time that it takes a pulse of current to travel between the northern and southern ionospheres is longer (hence lower frequencies). The second conclusion is that for a single event, most of the recording stations observe the same pulsation frequency (i.e. negligible variation of frequency with latitude).

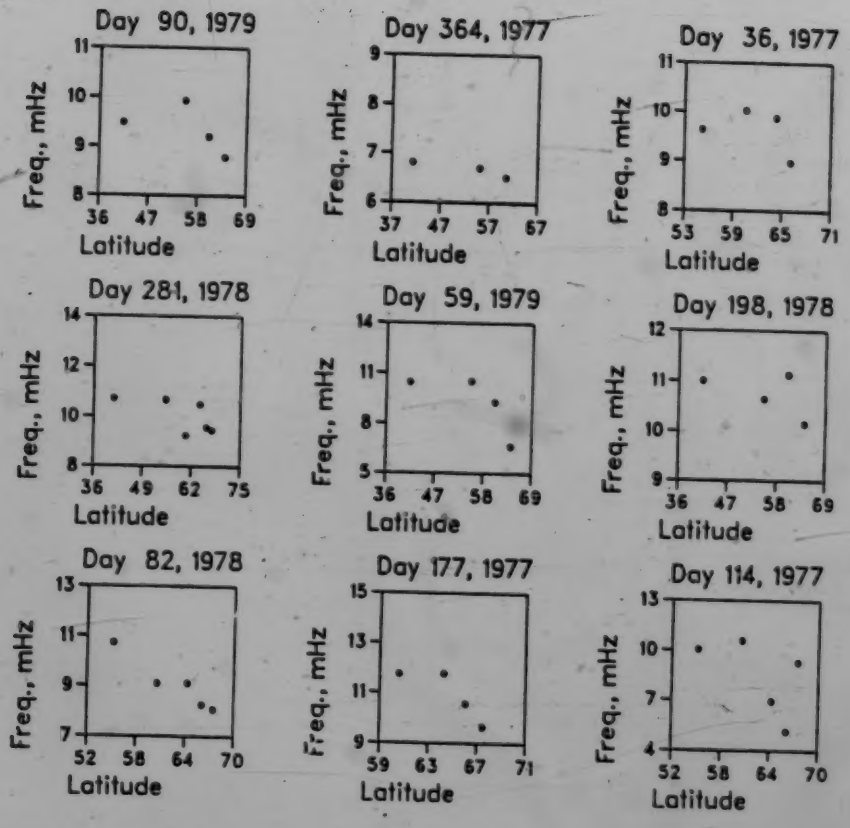

Figure 27: Estimated Pi 2 frequency plotted as a function of station location for each of the 9 events.

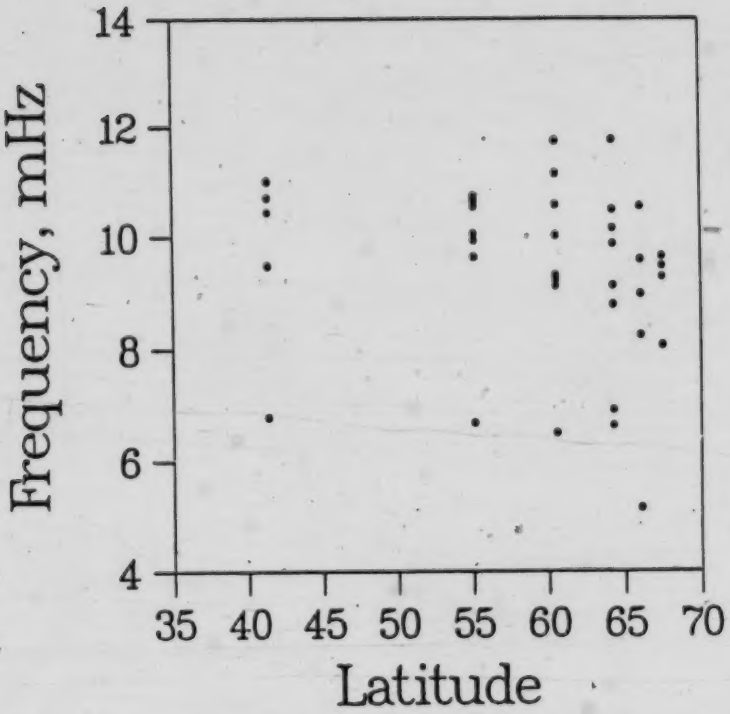

Figure 28: A composite plot of the data from figure 27.

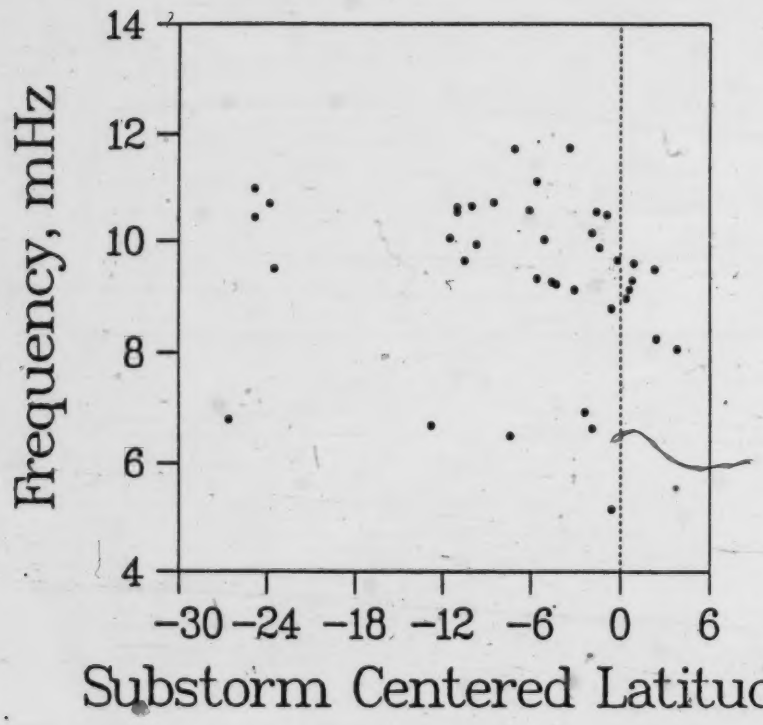

Figure 29: Pi 2 frequency plotted as a function of station location relative to the substorm enhanced electrojet.

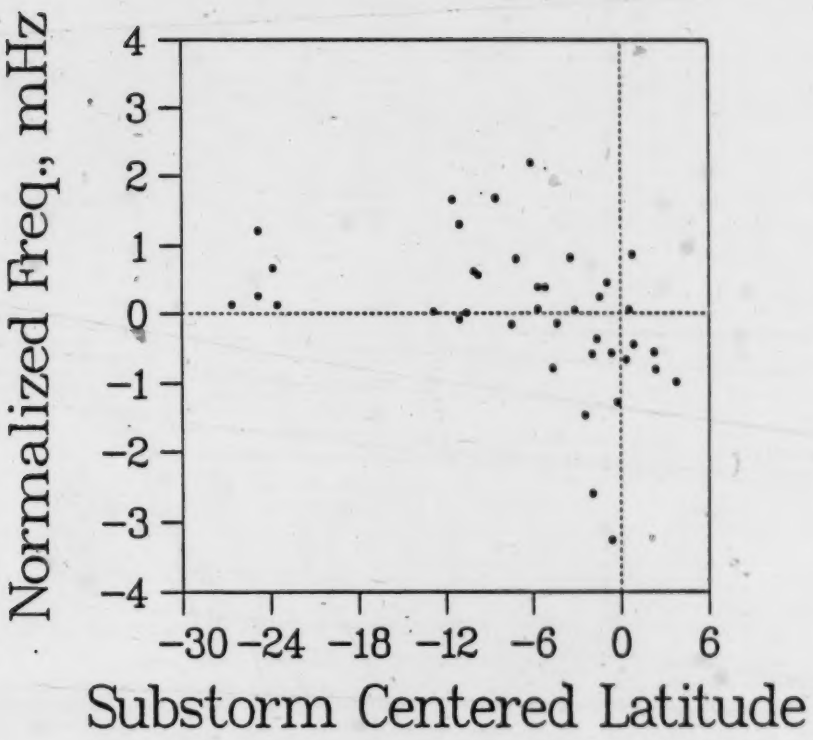

Figure 30: The mean frequency of each event is subtracted from each station's frequency estimate and plotted relative to the position of the substorm enhanced electrojet.

The explanation of these conclusions is straight forward. The current pulse propagates only in a localized latitudinal region. Thus observations at lower latitudes see the fields from the current pulse propagating on the high latitude field lines threading the source region. Thus the stations away from the source region see the integrated effect of waves passing through the source region and record the same frequency. For different events, a source region that maps to higher latitudes will yield lower bounce frequencies than events with a source region that maps to lower latitudes (Rostoker, 1967a).

The question that arises is "how can we reconcile this explanation with the data of figure 30?" Consider first the region south of -4 degrees in figure 30. In this region there appears to be no statistically significant variation of frequency with latitude. This observation agrees with the results of previous studies. However, within 4 degrees of the enhanced electrojet, spatial variation of frequency is observed. Recall that resonance model portrays Pi 2 pulsations as standing Alfvén waves confined to field lines passing through the source region. If these standing Alfvén waves are present within this region, then some variation of frequency with latitude might be expected. It is difficult, however, to correlate the results in figure 30 with the resonance model because of the normalization procedure and the coordinate system used. Qualitative examination of the theoretical relationship of Kuwashima and Saito (1981)

indicates that over an interval of 4 degrees, the frequency variation is about 6 mHz. The data of figure 30 indicates a frequency variation of considerably less than that. Thus the resonance model does not seem to adequately describe the frequency variation with distance relative to the enhanced electrojet.

F. Power

It is generally accepted that the spatial dependence of the Pi 2 power is of the following form: a) gradual decrease in longitude from the center of the main wedge current system (see for example Samson, 1983a). b) two peaked latitudinal dependence with a general decrease in power with decreasing latitude (Kuwashima, 1978; Kuwashima and Saito, 1981). Figures 31 and 32 illustrate a spatial analysis of the normalized power (using the data from Samson and Harrold, 1983). The location of the data points is shown in figure 31. Since the statistics in the region west of -25 degrees longitude are not very good, this region was not used in the analysis. The normalization process consisted of setting the station with the highest power for each event to one and scaling the other stations accordingly. The data were smoothed by taking the logarithmic average of the points in a rectangular region centered on each of the points plotted in the figure 32.

In the region extending from -20 degrees longitude to +15 degrees longitude the decrease in power with increasing

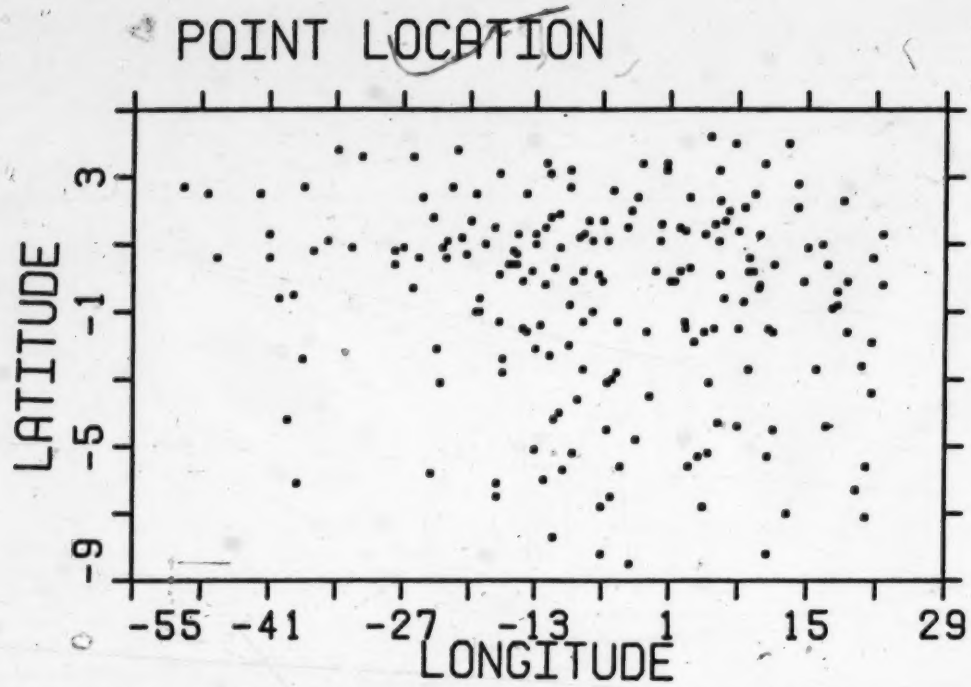

Figure 31: Distribution of stations relative to the substorm centered coordinates. The data is that of Samson and Harrold, 1983.

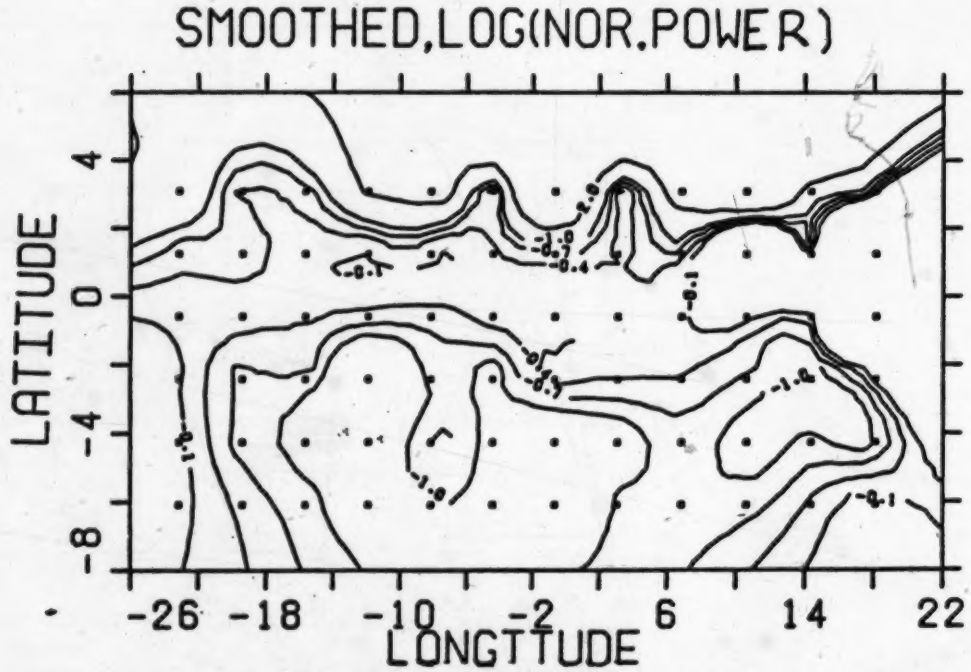

Figure 32: Spatial distribution of Pi 2 power which has been smoothed (about the array of points plotted) and normalized to the station in each event with the largest power.

latitudinal distance from the electrojet can clearly be seen. It should be noted that because of the normalization process and the fact that the array used in this study only spans 12.5 degrees of longitude, the general longitudinal variation of Pi 2 power cannot be seen in this representation.

In order to further investigate the latitudinal dependence of the Pi 2 power, the data set was subdivided into two groups. Group 1 consisted of all events in which the latitudinal location of the electrojet was south of Uranium City and group 2 consisted of all events in which the electrojet was located north of this station. This division is motivated by observations by Stuart et al. (1979) and Samson and Rostoker (1983) of a secondary peak in Pi 2 power south of that in figure 32. Using the same smoothing technique, the results are illustrated in figures 33, 34, and 35.

It is apparent from figure 33 that most of the events chosen were in group 1. As a result the contours of the smoothed, normalized log power are essentially the same as those of the original data set. Figure 35 shows the results for group 2. The relatively few data points available in this group rendered the smoothing operation ineffective and hence I have just contoured the normalized power directly. The failure to observe any secondary power peak suggests that either this feature is non-existent, that it is a rare occurrence, or that it is further south than our station

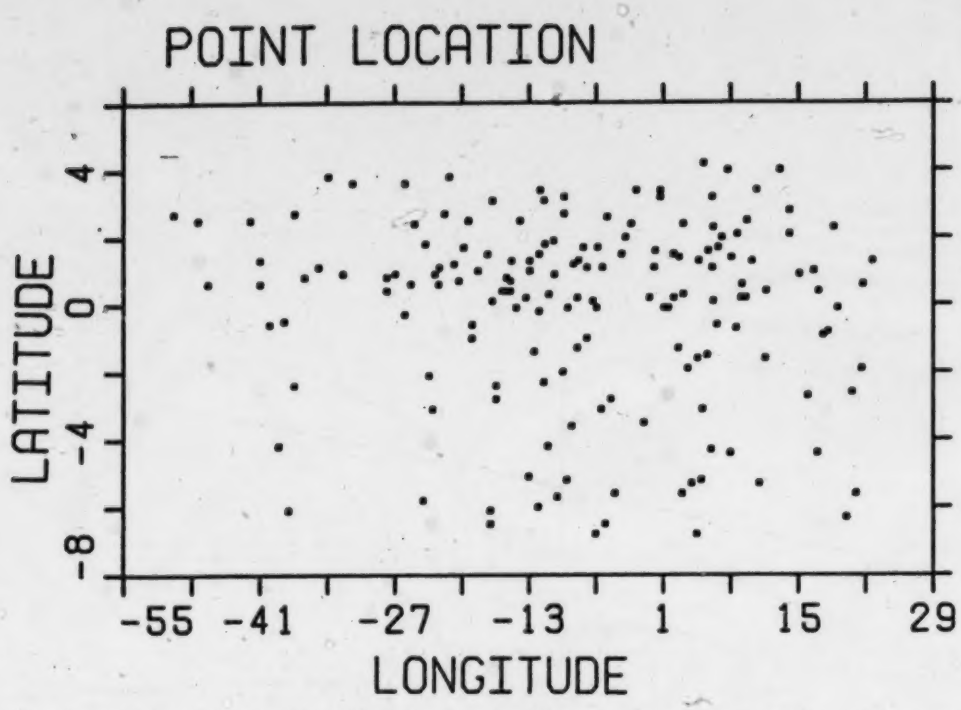

Figure 33: Distribution of stations for the data of group 1.

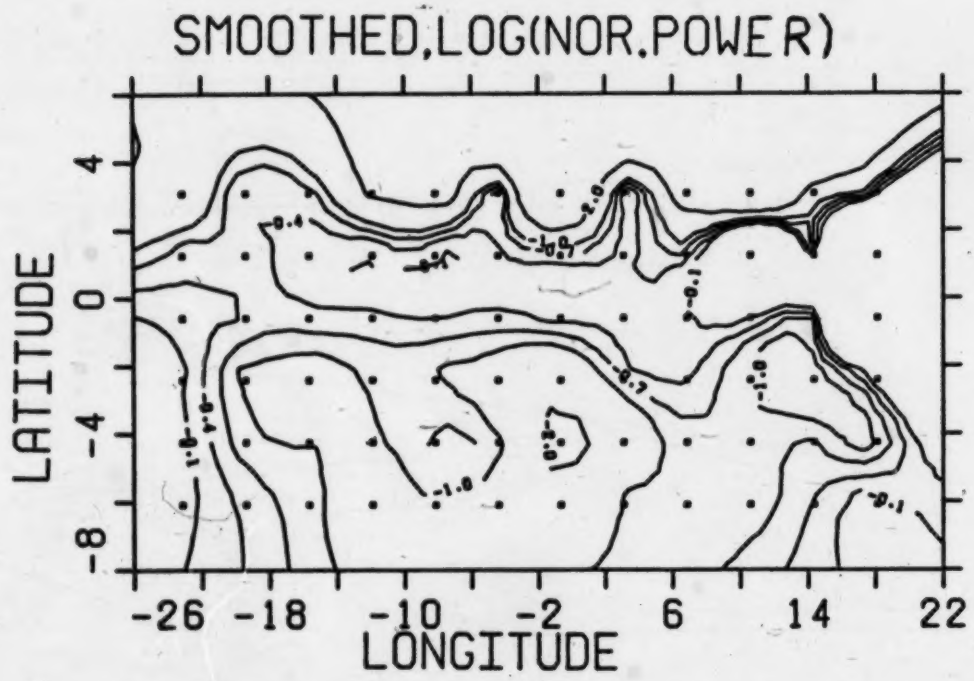

Figure 34: Spatial distribution of power for the data of group 1.

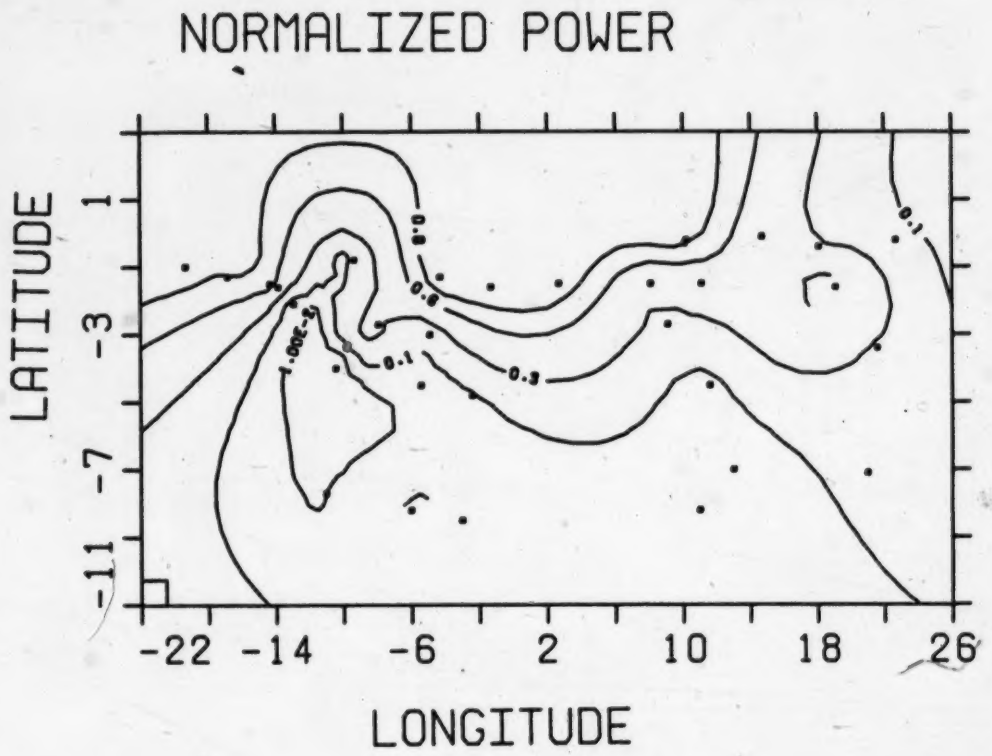

Figure 35: Spatial distribution of stations for the data of group 2 plus the distribution of normalized power.

coverage. The data presented here does not indicate an increase in power towards the the midlatitudes that one would expect from the latter conclusion. This observation conflicts with the conclusions of Samson and Rostoker (1983) and those of Stuart et al. (1979). Nevertheless, the high latitude localization is clearly seen.

In spite of the disagreement with the results of previous studies, the data of figure 32 can easily be interpreted in terms of the transient response model of figure 8. The large power gradients equatorward and poleward of 0 degrees latitude would correspond to regions of downward field-aligned current associated with the "solenoids" south and north of the auroral arc. We see that the equatorward region of downward field-aligned current corresponds to about 3 degrees south of the substorm enhanced electrojet. This estimate is not unlike that obtained from the frequency data (4 degrees).

G. Polarization Characteristics

The study of polarization characteristics of Pi 2's has predominantly involved the H and D components. Usage of the H and D components in the analysis occurs through the polarization ellipse which is parametrized by the ellipticity and angle that the major axis makes with the north-south meridian (the polarization angle or azimuth).

The ellipticity and polarization angles have been measured through statistical studies at midlatitudes by

Rostoker (1967), Bjornsson et al. (1971), Fukunishi (1975), Kuwashima (1978), and Lester et al. (1983, 1984). Fukunishi was able to correlate an observed latitudinal polarization reversal near L = 4 to the latitudinal location of the plasmapause. Further observations at conjugate points led to the conclusion that Pi 2 wave trains near L = 4 are odd mode standing Alfvén waves. Lester et al. showed that the polarization angles were consistent with a wedge model for the generating currents. The typical polarization ellipse pattern that is observed at these latitudes is illustrated in figure 3. Furthermore, Lester et al. (1983) concluded that the longitudinal extent of the current system was about 90 degrees (6 hours).

The picture at high latitudes is considerably more complicated. Samson and Harrold (1983) compiled the statistical pattern shown in figure 5. It can be seen that to the east of the main wedge current system the polarization angles were consistent with localized field aligned current but the pattern became progressively more random towards the west. This observation is not inconsistent with the transient response model of figure 8. Considering the complicated current structure near the arc, coupled with propagating current structures along the arc and the oscillations due to ionospheric reflection of the wave, it is to be expected that a statistical pattern of azimuthal angles be scattered. At high latitudes the ellipticity pattern observed by Samson and Harrold has 3

regions of clockwise sense separated by two areas of counterclockwise polarization as illustrated in figure 4.

An important correlation between the normalized power and a reversal of the sense of polarization is found by comparing figures 4 and 32. Close inspection reveals that there is a polarization reversal along a meridian wherever the gradient in Log(Normal power) is large. This is not surprising in light of the model in figure 8. This model correlates the large gradients in power with sheets of downward field aligned current. For two stations on opposite sides of this field aligned current, the D component of the perturbation field changes sign (noting of course it will be smaller in absolute value outside the "solenoid"). Because of edge effects, the H component will be the same sign. Thus for a current structure moving westward over the stations in a direction parallel to the alignment of the field aligned current, opposite senses of polarization will be observed for the two stations (see figures 36 and 37).

Rather than trying to explain the polarization reversals of the qualitative current model of figure 8, let us try to correlate the east-west component of the wave vector (k_y) to the observed distribution of power and the sense of polarization using the field line resonance model. Recall that equation I-15 predicts a clockwise (counterclockwise) sense of polarization when $\lambda d(\ln E_y)/dx$ ($\lambda = k_y$) is greater (less) than zero. (Note from Faraday's law that for the form of $\underline{E}$ in this model and for an $\exp(-i\omega t)$

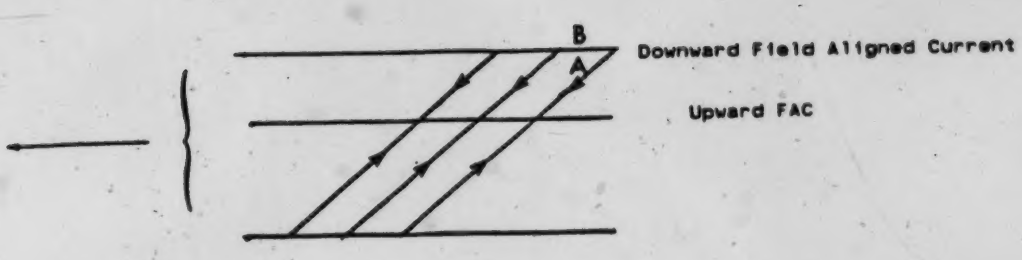

Figure 36: Currents associated with the "solenoid" structure near the arc. B sees effects from both upward and downward field aligned currents. A sees only the edge effects due to the downward field aligned current. Net effect is a change in sign of the D component perturbation. Ionospheric currents propagating westward yield a dc component + periodic component component in H. A and B have the "same" H component. Net result is a polarization reversal between A and B.

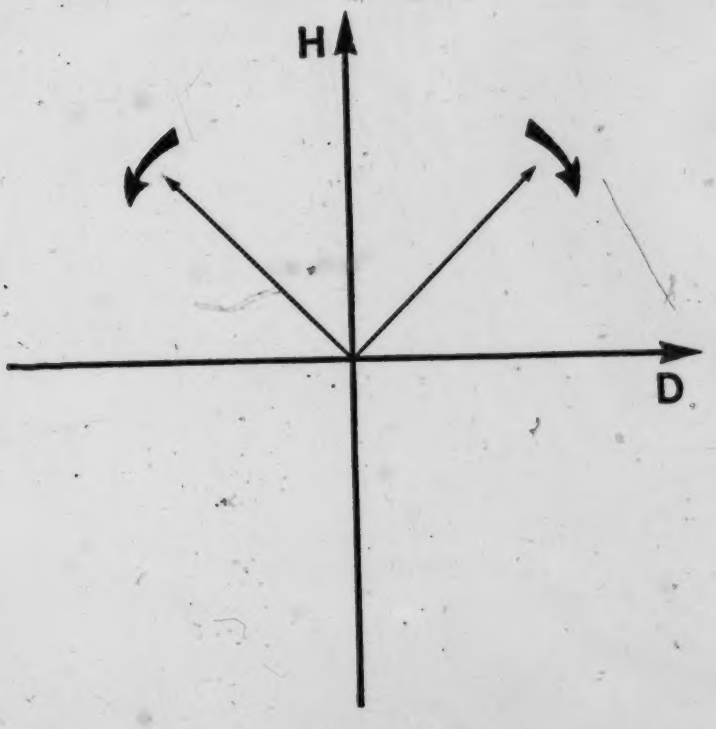

Figure 37: Illustration of how a reversal of the D component is associated with a reversal of the sense of polarization.

time dependence that the north south component of the perturbation magnetic field is: $b_x = (-kc/\omega)E_y$). Unfortunately, the Samson and Harrold (1983) data for b_x were not readily available so we shall use the power data for $|\underline{b}|$ (also from Samson and Harrold (1983)) presented earlier.

Using the power distribution of figure 32 (sketched in figure 38a) and the polarization data of figure 4 (sketched in figure 38b), the predicted sign of λ is shown in figure 38c. In the central region of this figure we have reversed the sign of both λ and $d(\ln E_y)/dx$ to maintain the sense of polarization as clockwise. Several points concerning these predictions are worth noting. The first is that at sufficient distances to the south, west and east of the substorm center, westward phase propagation is predicted. Samson et al. (1985) and Lester et al. (1983, 1984) have analyzed the midlatitude region (approximately 10 to 15 degrees south of the substorm enhanced electrojet) and have found predominantly westward phase propagation and counterclockwise polarization. Coupled with $d(\ln E_y)/dx > 0$, it would seem that this is in agreement with the prediction of equation I-15. However, Kuwashima and Saito (1981) have presented evidence that the Pi 2 perturbation fields may increase in strength near the plasmapause. This would imply a change in sign of $d(\ln E_y)/dx$ at midlatitudes. Thus, a simple extrapolation of the prediction in figure 38c cannot be made without detailed information of $d(\ln E_y)/dx$ at

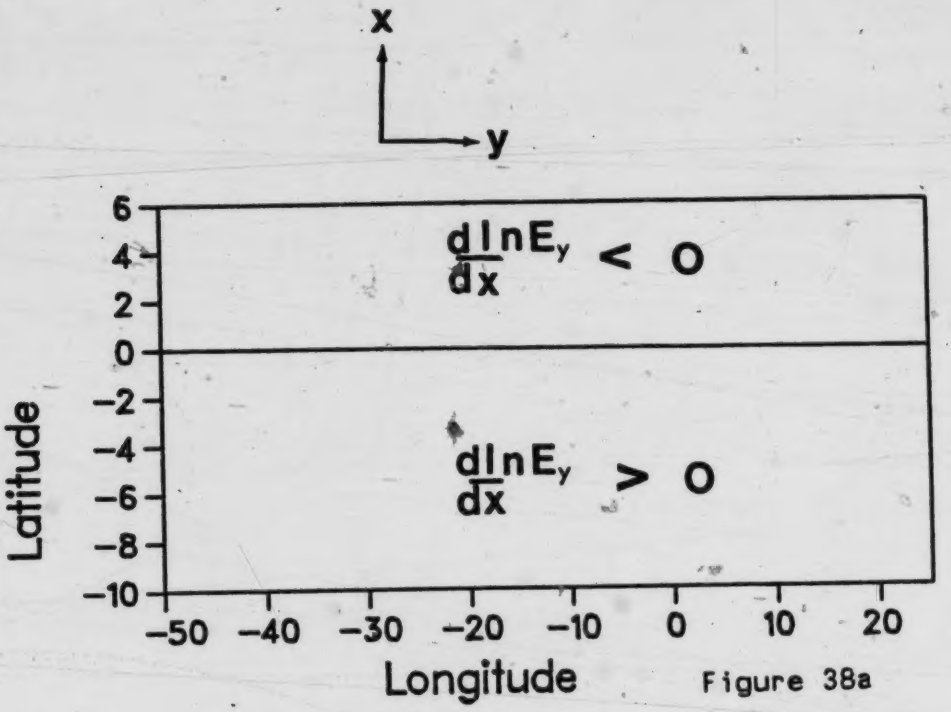

Figure 38a

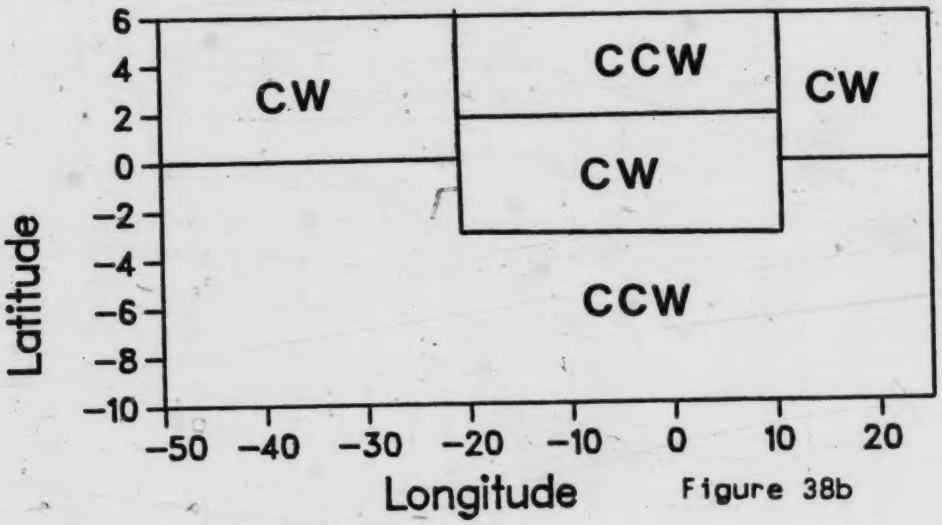

Figure 38b

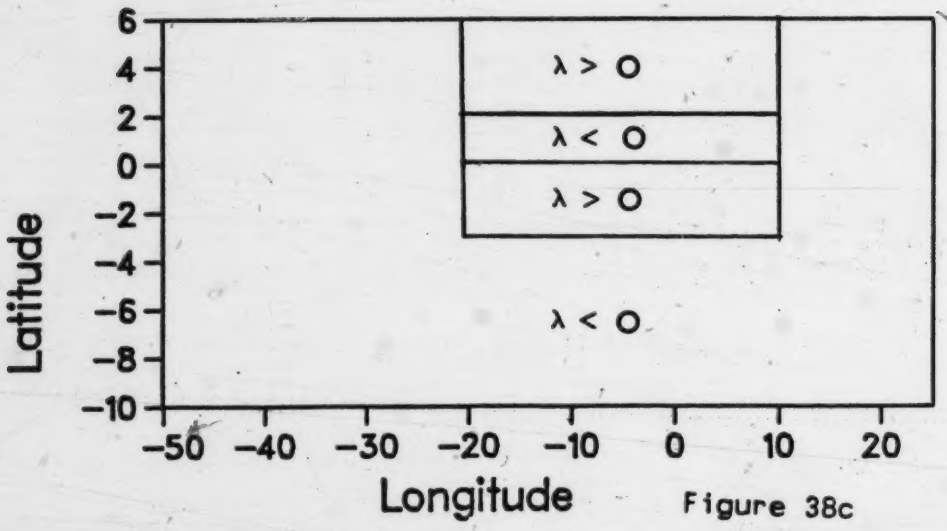

Figure 38c

Self-consistent relationship among power, sense of polarization, and phase propagation predicted by data and equation I-15.

midlatitudes.

The second point worth noting is that the resonant field line model was derived on the basis that λ was a constant. In the central region of figure 38c, it varies rapidly in space which violates the equation upon which figure 38 is based. Nevertheless, with these final two points noted, we tentatively compare the predictions of figure 38c to the data of figure 21.

To simplify the comparison, in figure 39 I have superposed figures 38c and 21. There seems to be some definite areas of agreement in spite of the smallness of the data set and hence the relatively poor statistics in all areas of the map. This correlation thus seems to support the resonant field line model of Pi 2 pulsations. However, recall that the original derivation of equation I-15 required only an electric field of the form $\underline{E}(\underline{r},t) = (E_x(x),E_y(x),0)\exp(i(\lambda y+kz-\omega t))$. Thus, in the interests of obtaining a somewhat similar phase propagation pattern for a three dimensional treatment of the transient response model, one might employ $\underline{E}(\underline{r},t) = \underline{E}(x,z,t)\exp(i\lambda y)$. Further exploration of this treatment is beyond the scope of this study.

H. Miscellaneous Interpretations

From the form of the time series recorded at high latitudes, we can obtain an idea of the field aligned extent of the wave front. The typical perturbation field (for say

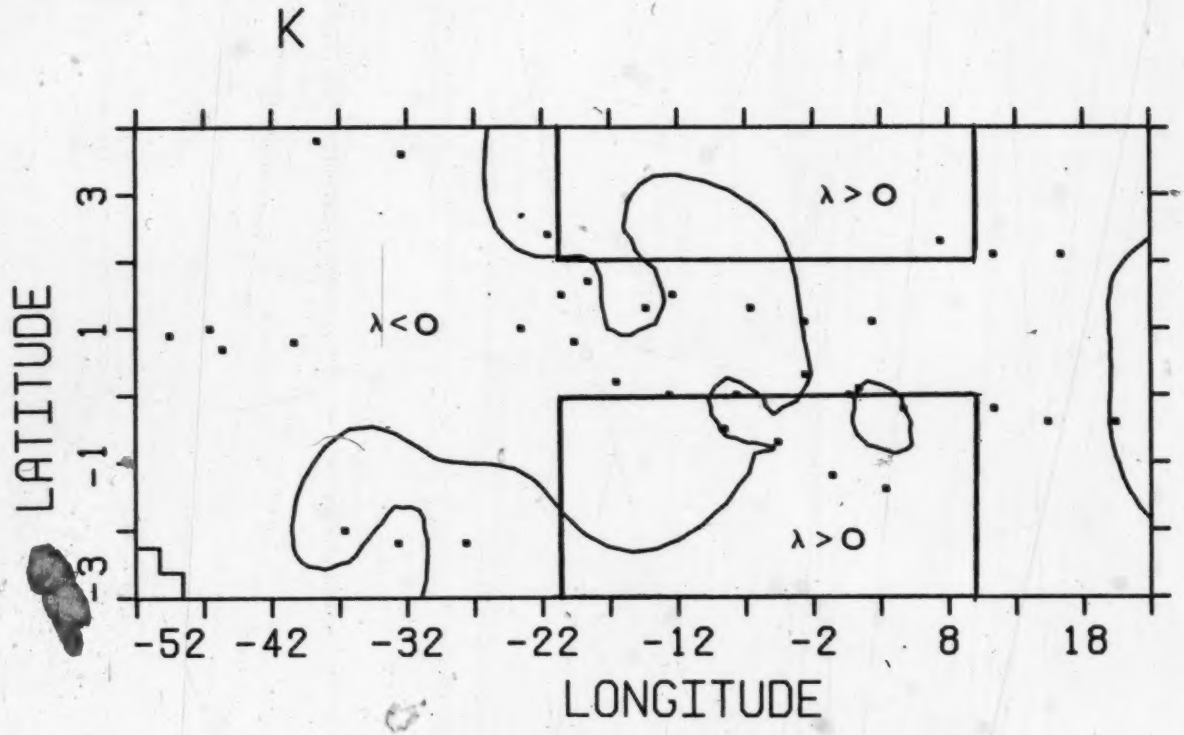

Figure 39: Correlation between the data of figure 21 and the prediction of figure 38c.

the Z component) associated with a geomagnetic substorm is shown in figure 40a. In figure 40b, is a wave propagating along the magnetic field. At point t_0, the portion of the wavefront "a" encounters the ionosphere and experiences reflection. At t_1, the portion of the wavefront "c" encounters the ionosphere. After the wavefront passes, ionospheric dissipation mechanisms reduce the strength of the perturbation electric field and so the ionospheric current strength decreases between times t_1 and t_3. At time t_2, the point "b" on the wavefront is reflected from the opposite ionosphere (assuming that the field lines have collapsed to a dipoar configuration). At time t_3, point "a" on the wave front once again encounters the ionosphere and the process repeats itself.

The field aligned extent of the wave front is indicated by the length $L_1 = (t_0 - t_1)/v$ (or equivalently $(t_3 - t_4)/v$). The length $L = (t_1 - t_4)/v$ represents the distance that the wavefront has travelled during one cycle (which is twice the length of a field line). The qualitative observation that $t_1 - t_2 \simeq (t_1 - t_4)/2$ provides a connection between the field aligned extent of the wavefront and the dimension of the magnetosphere. This may also serve to connect the resonant field line model to the transient response model.

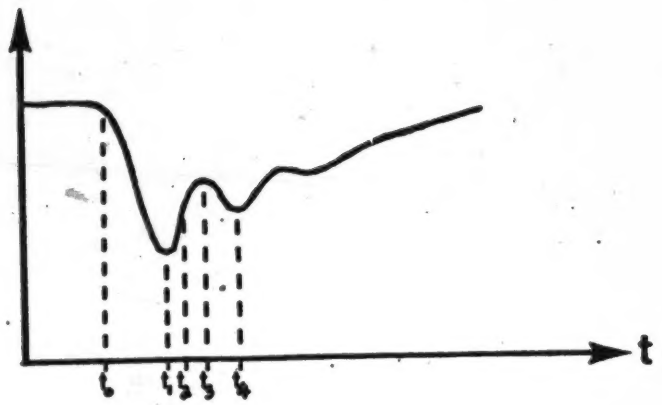

Figure 40a: A typical substorm perturbation field (simulated).

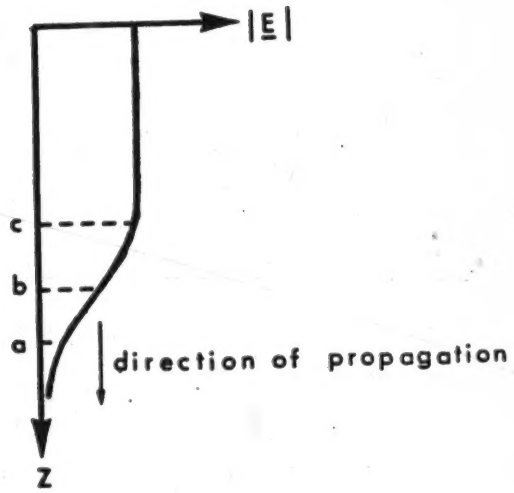

Figure 40b: Magnitude of the electric field for a propagating Alfven wave.

IV. Conclusions

This study has employed six types of measurements to examine Pi 2 type pulsations. The estimates of the envelope parameters indicate typical rise and fall times of 70 seconds. These short rise and fall times tend to dispute the concept of a Pi 2 pulsation as a resonance phenomena (Samson et al. (1985) have previously reached this conclusion).

The estimates of the group delay imply eastward group propagation to the east of the substorm center and predominantly westward group propagation to the west of center. The typical group propagation speed is greater than 8 km/sec. The discrepancy between this velocity and past estimates of the velocity of the westward travelling surge seem to indicate that group delay is not a direct measure of the azimuthal expansion of the substorm current system. Neither of the two Pi 2 models presented have provisions for group propagation. Such a provision would be an important addition to either theory.

Pi 2 frequency has been observed to slightly increase with latitudinal distance south of the substorm enhanced electrojet. This variation seems to be limited to a latitudinal region within about 4 degrees of this electrojet. This observation seems to support the resonance model.

The spatial dependence of Pi 2 power has confirmed the findings of previous studies, namely, that the Pi 2 is latitudinally localized in the region of the substorm

enhanced electrojet. The smoothing process masked out any longitudinal dependence of power, thus no conclusions as to this type of dependence could be made. The observed gradients of power with latitude could be explained in terms of sheets of field-aligned current and ionospheric currents using the qualitative transient response model of figure 8.

The phase propagation measurements indicate that to the west of the substorm center, westward propagation is recorded and to the east, eastward propagation is observed (typical speeds of about 40 km/sec). There is also evidence that phase propagation is dependent on latitude as well as longitude (relative to the substorm center). Correlations between the distribution of Pi 2 power, the sense of polarization and the direction of phase propagation have been attempted through the use of equation I-15. The data seems to be in agreement with this equation.

In spite of the variety of characteristics of Pi 2 pulsations discussed in this study, there remain several areas in need of further development. A map of k_y (λ) with better statistics is needed so that more concrete conclusions concerning equation I-15 can be drawn. It is important to develop a better understanding of what group delay means in the context of Pi 2 pulsations. Finally, a more quantitative correlation between the spatial dependence of frequency and the predictions of the resonance model needs to be made.

V. Bibliography

Atkinson, G., A theory of polar substorms, *J. Geophys. Res.*, *71*, 5157, 1966.

Arthur, C.W., R.L. McPherron, J.D. Means, A comparative study of 3 techniques for using the spectral matrix in wave analysis, *Radio Sci.*, *11*, 833, 1976.

Baranskiy, L.N., V.A. Troitskaya, I.V. Sterlikova, M.B. Gokhberg, N.A. Ivanov, I.P. Khartchenko, J.W. Munch, K. Wilhjeim, The analysis of simultaneous observations of nightime Pi pulsations on an east-west profile, *J. Geophys.*, *48*, 1, 1980.

Baumjohann, W., K.-H. Glassmeier, The transient response mechanism and Pi2 pulsations at substorm onset - Review and outlook, *Planet. Space Sci.*, 1984.

Baumjohann, W., H. Junginger, G. Haerendel, O.H. Bauer, Resonant Alfven waves excited by a sudden impulse, *J. Geophys. Res.*, *89*, 2765, 1984.

Beard, D.B., The interaction of the terrestrial magnetic field with the solar corpuscular radiation, *J. Geophys. Res.*, *65*, 3559, 1960.

Bjornsson, A., O. Hillebrand, H. Voelker, First observational results of geomagnetic Pi 2 and Pc 5 pulsations on a north-south profile through Europe, *Z. Geophys.*, *37*, 1031, 1971.

Bosinger, T. K. Alanko, J. Kangas, H. Opgenoorth, W. Baumjohann, Correlations between Pi B type magnetic micropulsatins, auroras and equivalent current sturctures during 2 isolated substorms, *J. Atmos. Terr. Phys.*, *43*, 933, 1981.

Chang, R.P.H., L.J. Lanzerotti, On the generation of magnetohydrodynamic waves at the onset of a substorm, *Geophys. Res. Lett.*, *2*, 489, 1975.

Chao, J.K., R.R. Heacock, Modulation of type Pi waves by temporal variations in ionospheric conductivity in a three-dimensional current system, *Planet. Space Sci.*, *28*, 475, 1980.

Chen, L., A. Hasegawa, A theory of long-period magnetic pulsations 1. Steady state excitation of field line resonance, *J. Geophys. Res.*, *79*, 1024, 1974.

Chen, L., A. Hasegawa, A theory of long-period magnetic pulsations 2. Immpulse excitation of surface eigenmode, *J. Geophys. Res.*, *79*, 1033, 1974.

Coroniti, F.V., C.F. Kennel, Auroral micropulsation instability, *J. Geophys. Res.*, *75*, 1863, 1970.

Dungey, J.W., The steady state of the Chapman-Ferraro problem in two dimensions, *J. Geophys. Res.*, *66*, 1043, 1961.

Eastman, T.E., L.A. Frank, W.K. Peterson, W. Lennartsson, The plasma sheet boundary layer, *J. Geophys. Res.*, *89*, 1553, 1984.

Ellis, P., D.J. Southwood, Reflection of Alfven waves by non-uniform ionospheres, *Planet. Space Sci.*, *31*, 107, 1983.

Fukunishi, H., Polarization changes of geomagnetic Pi 2 pulsations associatedd with the plasmapause, *J. Geophys. Res.*, *80*, 98, 1975.

Goertz, C.K., R.W. Boswell, Magnetosphere-ionnosphere coupling, *J. Geophys. Res.*, *84*, 7239, 1979.

Green, C.A., The longitudinal phase variation of midlatitude Pc 3-4 micropulsations, *Planet. Space Sci.*, *24*,79,1 1976.

Green, C.A., R.A. Hamilton, Polarization characteristics and phase differences of Pi 2 pulsations at conjugate stations, *J. Atmos. Terr. Phys.*, *40*, 1223, 1978.

Green, C.A., R.A. Hamilton, An ionospheric effect on the conjugate relationship of Pi 2 magnetic pulsations, *J. Atmos. Terr. Phys.*, *43*, 1133, 1981.

Goodman, N.R., Measuring Amplitude and Phase, *J. Franklin Inst.*, *270*, 437, 1960.

Hasegawa, A., L. Chen, Theory of magnetic pulsations, *Space Sci. Rev.*, *16*, 347, 1974.

Hasegawa, A. L.J. Lanzerotti, On the orientation of hydromagnetic waves in the magnetosphere, *Rev. Geoph. and Space Phys.*, *16*, 263, 1978.

Horwitz, J.L., J.R. Doupnik, P.M. Banks, Chatanika radar observations of the latitudinal distributions of auroral zone electric fields, conductivities, and currents, *J. Geophys. Res.*, *83*, 1463, 1978.

Hughes, W.J., R.L. McPherron, J.N. Barfield, Geomagnetic pulsations observed simultaneously on three geostationary spacecraft, *J. Geophys. Res.*, *83*, 1109, 1978.

Jacobs, J.A., Geomagnetic Micropulsations, 1970, Springer Verlag, New York.

Jenkens, G.M., D.G. Watts, Spectral Analysis and its Applications, Holden-Day, Inc., San Francisco, 1968.

Kan, J.R., R.R. Heacock, Generation of irregular (type Pi C) pulsations in the plasma sheet during substorms, *J. Geophys. Res.*, *81*, 1042, 1978.

Kan, J.R., L.C. Lee, Y.T. Chiu, D.U. Longenecker, Generation of Alfven waves by deceleration of magnetospheric convection and broadband Pi pulsations, *J. Geophys. Res.*, *87*, 3511, 1982.

Kan, J.R., D.U. Longenecker, J.V. Olson, A transient response model of Pi 2 pulsations, *J. Geophys. Res.*, *87*, 7483, 1982.

Kuwashima, M., Wave characteristics of magnetic Pi 2 pulsations in the auroral region=Conjugate relationships, *Mem. Nat. Inst. Polar Res. Spce. Issue Jpn.*, *no. 18*, 1980.

Kuwashima, M., T. Saito, A model of Pi 2 derived from

spectral and polarization studies, *Planet. Space Sci.*, 1980.

Kuwashima, M., Wave characteristics of Magnetic Pi 2 pulsations in the auroral region: spectral and polarization studies, *Mem. Nat. Inst. Polar Res., Japan, Series A*, 15, 1978.

Kuwashima, M., T. Saito, Spectral characteristics of magnetic Pi 2 pulsations in the aauroral region and lower latitudes, *J. Geophys. Res.*, *86*, 4686, 1981.

Lanzerotti, L.J., H. Fukunishi, Modes of MHD waves in the magnetospherre, *Rev. Geophys. Space Phys.*, *12*, 724, 1974.

Lanzerotti, L.J., H. Fukunishi, Relationships of the characteristics of magnetohydrodynamic waves to plasma density gradients in the vicinity of the plasmapause, *J. Geophys. Res.*, *80*,4627, 1975.

Lester, M., W.J. Hughes, H.J. Singer, Polarization Patterns of Pi 2 magnetic pulsations and the substorm current wedge, *J. Geophys. Res.*, *88*, 7958, 1983.

Lester, M., W.J. Hughes, H.J. Singer, Longitudinal structure in Pi 2 pulsations and the substorm current wedge, *J. Geophys. Res.*, *89*, 5489, 1984.

Lester, M., D. Orr, The spatio-temporal characteristics of Pi 2's, *J. Atmos. Terr. Phys*, *43*, 947, 1981.

Mallinckrodt, A.J., C.W. Carlson, Relations between transverse electric fields annd field aligned currents, *J. Geophys. Res.*, *83*, 1426, 1978.

Maltsev, Yu.P., S.V. Leontyev, W.B. Lyatsky, Pi 2 pulsations as a result of evolution of an Alfven impulse originating in the ionosphere during a brightening of aurora, *Planet. Space Sci.*, *22*, 1519, 1974.

Maltsev, Yu.P., W.B. Lyatsky, A.M. Lyatskaya, Currents over the auroral arc, *Planet. Space Sci.*, *25*, 53, 1977.

McPherron, R.L., C.T. Russell, M.P. Aubry, Satelite studies

of magnetospheric substorms on August 15, 1968, 9, Phenomenological model for substorms, *J. Geophys. Res.*, *78*, 3131, 1973.

Muira, A., T. Sato, Numerical simulation of global formation of auraral arcs, *J. Geophys. Res.*, *85*, 73, 1980.

Newton, R.S., D.J. Southwood, W.J. Hughes, Damping of geomagnetic pulsations by the ionosphere, *Planet. Space Sci.*, *26*, 201, 1978.

Nishida, A., Geomagnetic Diagnosis of the Magnetosphere, Springer-Verlag, New York, 1978.

Nishida, A., Possible origin of transient dusk to dawn electric field in the night side magnetosphere, *J. Geophys. Res.*, *84*, 3409, 1979.

Obayashi, J.A. Jacobs, Geomagnetic pulsations and the Earth's outer atmosphere, *Geophys. J.*, *1*, 53, 1958.

Obertz, P., O.M. Raspopov, Study of the spatial characteristics of type Pc 5 geomagnetic pulsations, *Geomag. Aeron.*, *8*, 424, 1968.

Ol', A.I., Long period gigantic geomagnetic field pulsations, *Geomag. Aeron.*, *3*, 90, 1963.

Olson, J.V., G. Rostoker, Latitude variation of the spectral components of auroral zone Pi 2, *Planet. Space Sci.*, *25*, 663, 1977.

Olson, J.V., G. Rostoker, Pi 2 pulsations and the auroral electrojet, *Planet. Space Sci.*, *23*, 1129, 1975.

Orr, D., A.D. Matthev, The variation of geomagnetic micropulsation periods with latitude and the plasmapause, *Planet. Space Sci.*, *19*, 897, 1971.

Pashin, A.B., K.-H. Glassmeier, W. Baumjohann, O.M. Raspopov, A.G. Yahnin, H.J. Opgenoorth, R.J. Pellinen, Pi2 magnetic pulsations, auroral breakups and the substorm current wedge: A case study, *J. Geophys.*, *51*, 223, 1982.

Pytte, T., R.L. McPherron, S. Kokubun, The ground signatures of the expansion phase during multiple onset substorms, *Planet. Space Sci.*, *24*, 1115, 1976.

Rostoker, G., The frequency spectrum of Pi 2 micropulsation activity and its relationship to planetary magnetic activity, *J. Geophys. Res.*, *72*, 2032, 1967a.

Rostoker, G., The polarization characteristics of Pi 2 micropulsations and their relation to the determination of possible source mechanisms for the production of nighttime impulsive micropulsation activity, *Canadian Journal of Phys.*, *45*, 1319, 1967.

Rostoker, G., S.-I. Akasofu, J. Foster, R.A. Greenwald, Y. Kamide, K. Kawasaki, A.T.Y. Lui, R.L. McPherron, C.T. Russel, Magnetospheric substorms - definition and signatures, *J. Geophys. Res.*, *85*, 1663, 1980.

Rostoker, G., T.J. Hughes, A comprehensive model current system for high-latitude magnetic activity-II. The substorm component, *Geophys. J. R. astr. Soc.*, *58*, 571, 1979.

Rostoker, G., J.C. Samson, Polarization characteristics of Pi 2 pulsations and implications for their source mechanisms: Location of source regions with respect to the auroral electrojets, *Planet. Space Sci.*, *29*, 225, 1981.

Saito, T., Geomagnetic pulsations, *Space Sci. Rev.*, *10*, 319, 1969.

Saito, T., T. Sakurai, Y. Koyama, Mechanism of association between Pi 2 pulsation and magnetopheric substorm, *J. Atmos. Terr. Phys.*, *38*, 1265, 1976.

Sakurai, T., T., Saito, Magnetic pulsation Pi 2 and substorm onset, *Planet. Space Sci.*, *24*, 573, 1976.

Samson, J.C., Pi 2 pulsations: High latitude results, *Planet. Space Sci.*, *30*, 1239, 1982.

Samson, J.C., Pi 2 micropulsations and prediction of localized intensifications of polar magnetic substorms, Final Report to the Boreal Institute for Northern Studies of

Alberta, 28 March, 1983a.

Samson, J.C., The spectral matrix, eigenvalues, and principal components in the analysis of multichannel geophysical data, *Annales Geophysicae*, *1*, 115, 1983b.

Samson, J.C., Pure states, polarized waves, and principal components in spectra of multiple, geophysical time-series, *Geophys. J. R. Astro. Soc.*, *72*, 647, 1983c.

Samson, J.C., B.G. Harrold, Maps of the polarizations of high latitude Pi 2's, *J. Geophys. Res.*, *88*, 5736, 1983.

Samson, J.C., B.G. Harrold, K.L. Yeung, Characteristic time constants and velocities of midlatitude Pi 2's, *J. Geophys. Res.*, *89*, 3448, 1985.

Samson, J.C., J.A. Jacobs, G. Rostoker, Latitude - dependent characteristics of long-period geomagnetic pulsations, *J. Geophys. Res.*, *77*, 1972.

Samson, J.C., G. Rostoker, Latitude - dependent characteristics of high-latitude Pc 4 and Pc 5 micropulsatioons, *J. Geophys. Res.*, *77*, 6133, 1972.

Samson, J.C., Rostoker, G., Polarization characteristics of Pi 2 pulsations and implications for their source mechanisms: influence of the westward travelling surge, *Planet. Space Sci.*, *31*, 435, 1983.

Scholer, M., On the motion of artificial ion clouds in the magnetosphere, *Planet. Space Sci.*, *18*, 977, 1970.

Singer, H.J., W.J. Hughes, P.F. Fougere, D.J. Knecht, The localization of Pi 2 pulsations: Ground-satelite observations, *J. Geophys. Res.*, 1982.

Singer, H.J., M. Lester, W.J. Hughes, The distinction between substorm and Pi 2 current systems (abstract), *Eos Trans. AGU*, *64*, 294, 1983.

Southwood, D.J., Some features of field line resonances in the magnetosphere, *Planet. Space Sci.*, *22*, 483, 1974.

Southwood, D.J., W.J. Hughes, Theory of hydrodynamic waves in the magnetosphere, *Space Sci. Rev.*, *35*, 301, 1983.

Spreiter, J.R., A.L. Summers A.Y. Alksne, Hydromagnetic flow around the magnetosphere, *Planet. Space Sci.*, *14*, 223, 1966.

Stuart, W.F., A special feature of impulsive pulsation (Pi2), *J. Atmos. Terr. Phys.*, *34*, 829, 1972.

Stuart, W.F., P.M. Brett, T.J. Harris, Mid-latitude secondary resonance in Pi2's, J. Atmos. Terr. Phys., 41, 65, 1979.

Stuart, W.F., C.A. Green, T.J. Harris, Correlation between modulation of the intensity of precipitating electrons in the auroral zone and a coincident Pi2, *J. Atmos. Terr. Phys.*, *39*, 631, 1977.

Sutcliffe, P.R., The association of harmonics in Pi 2 power spectra with the plasmapause, *Planet. Space Sci.*, *23*, 1581, 1977.

Sutcliffe, P.R., The longitudinal range of Pi 2 propagation at low latitudes, *Planet. Space Sci.*, *28*, 9, 1980.

Tighe, W.G., G. Rostoker, Characteristics of westward travelling surges during magnetospheric substorms, *J. Geophys.*, *50*, 51, 1981.

Voelker, H., Observations of geomagnetic pulsations: Pc 3, 4 and Pi 2 at different latitudes, *Ann. Geophys.*, *24*, 245, 1968.

VI. Appendix A

The following derivation uses the cold plasma equations to obtain a single expression for the electric field associated with plasma waves propagating in a uniform background magnetic field $\underline{B}_o$. The method of approach is to use the force equation and the expression for current to solve for the current in terms of the fields $\underline{E}$ and $\underline{B}$. It is assumed that the thermal motion of the particles ($\underline{v}_{ok}$) is neglible compared to the velocities induced by the wave fields ($\underline{v}_k$). For convenience, a time dependence of $\exp(-i\omega t)$ is employed. Thus:

(1) $m_k \frac{d\underline{v}_k}{dt} = q_k(\underline{E} + \underline{v}_k \times \underline{B}/c)$

(2) $\underline{J} = \sum_k n_k q_k \underline{v}_k$

(3) $\nabla . \underline{B} = 0$

(4) $\nabla . \underline{E} = 4\pi\rho$

(5) $\nabla \times \underline{E} = -c^{-1} \frac{\partial \underline{B}}{\partial t}$

(6) $\nabla \times \underline{B} = 4\pi c^{-1} \underline{J} + c^{-1} \frac{\partial \underline{E}}{\partial t}$

To lowest order, equation (1) becomes:

$$-i\omega m_k \underline{v}_k = q_k(\underline{E} + \underline{v}_k \times \underline{B}_o/c)$$

With the assumption that the ambient field, $\underline{B}_o$, is straight and parallel to the z axis, it is a simple matter to solve the above equation for the components of $\underline{v}_k$:

(8) $v_{kx} = iq_k\omega m_k^{-1}(E_x - i\Omega_k E_y/\omega) /(\omega^2 - \Omega_k^2)$

(9) $v_{ky} = iq_k\omega m_k^{-1}(E_y + i\Omega_k E_x/\omega) /(\omega^2 - \Omega_k^2)$

(10) $v_{kz} = iq_k m_k^{-1}\omega^{-1} E_z$

where $\Omega_k = q_k B_o/(m_k c)$.

Substituting equation (2) into equation (6) and using equation (5) yields:

$$(11)\quad \nabla x \nabla x \underline{E} = (4\pi i/\omega \Sigma_k n_k q_k \underline{v}_k + \omega^2 \underline{E})/c^2$$

Substituting equations (8), (9), and (10) into equation (11) yields:

$$(12)\quad \nabla x \nabla x \underline{E} = K.\underline{E}/c^2$$

where $K = \begin{pmatrix} S & -iD & O \\ iD & S & O \\ O & O & P \end{pmatrix}$

and $S = (R + L)/2$, $D = (R - L)/2$

with $R = \omega^2 - \omega \Sigma_k \Pi_k^2/(\omega + \Omega_k)$

$L = \omega^2 - \omega \Sigma_k \Pi_k^2/(\omega - \Omega_k)$

$P = \omega^2 \Sigma_k \Pi_k^2$

where $\Pi_k^2 = 4\pi n_k q_k^2/m_k$

If we assume that the plasma has only two components (ions and electrons) and that the plasma remains neutral ($q_i n_i = e n_o$, subscript 'o' denotes electrons) we find that in the low frequency limit ($\omega << \Omega_i$):

$$R \sim L \sim \omega^2 + \omega^2(\Pi_i^2 + \Pi_o^2)/(\Omega_i \Omega_o) = \omega^2(1 + c^2/V^2)$$

where $V^2 = B_o^2/(4\pi(n_o m_o + n_i m_i))$.

hence $D \sim 0$ and $S \sim \omega^2(1 + c^2/V^2)$.

Thus in this approximation, K is diagonal. We can now replace ω^2 by $-\partial^2/\partial t^2$. Noting that $\omega < \Omega_i$ corresponds to slowly varying fields, thus K =

$-\mathrm{diag}[(1+c^2/v^2)\partial^2/\partial t^2, (1+c^2/v^2)\partial^2/\partial t^2, (\partial^2/\partial t^2+\Pi^2)]$. Writing out the components of equation (12) explicitly:

$$\text{x comp: } \frac{\partial^2 E_y}{\partial x \partial y} + \frac{\partial^2 E_z}{\partial x \partial z} - \frac{\partial^2 E_x}{\partial y^2} - \frac{\partial^2 E_x}{\partial z^2} = -(1/c^2+1/v^2)\frac{\partial^2 E_x}{\partial t^2} \qquad (13)$$

$$\text{y comp: } \frac{\partial^2 E_x}{\partial y \partial x} + \frac{\partial^2 E_z}{\partial y \partial z} - \frac{\partial^2 E_y}{\partial x^2} - \frac{\partial^2 E_y}{\partial z^2} = -(1/c^2+1/v^2)\frac{\partial^2 E_y}{\partial t^2} \qquad (14)$$

$$\text{z comp: } \frac{\partial^2 E_x}{\partial z \partial x} + \frac{\partial^2 E_y}{\partial z \partial y} - \frac{\partial^2 E_z}{\partial x^2} - \frac{\partial^2 E_z}{\partial y^2} = -(\Pi^2 + \frac{\partial^2}{\partial t^2})E_z/c^2 \qquad (15)$$